THE UNIVERSITY
of EDINBURGH

MORPHOLOGICAL ASSESSMENT OF PARANASAL SINUSES AND TEETH IN THE HORSE

Tiziana Liuti

Prof. Padraic Dixon (supervisor)

Dr. Sionagh Smith (supervisor)

The University of Edinburgh

Royal (Dick) School of Veterinary Studies

Easter Bush Veterinary Centre

Midlothian, EH25 9RG Roslin

This study was approved by the Veterinary Ethical Research Committee (V.E.R.C.) of the Royal (Dick) School of Veterinary Studies on 16th February 2012. (VERC 2011-111)

Declaration

I declare that the contents of this thesis are my own work and that they have not been presented to any University other than the University of Edinburgh. The publications included in the thesis are my own work.

Tiziana Liuti

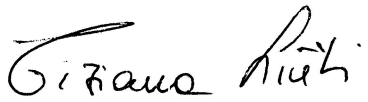

Edinburgh, March 2018

Acknowledgment

I would like to thank my primary supervisor Professor Padraic Dixon for his great support and expertise; his guidance and knowledge have been invaluable.

My thanks to Dr. Sionagh Smith who spent countless hours on helping me in reading the histological section and guiding me on the best sample staining to achieve good results.

A very big thank to Dr. Richard Reardon for his support and help with all the statistics.

I also would like to thanks Neil McIntyre for the histological processing of teeth section and Craig Pennycook for his technical assistance.

Dedication

I would like to dedicate this PhD to my husband Falco who has been always very supportive.

Abstract

Sinonasal and dental diseases can be a serious disorder in horses due to the persistence of the former and the common extension of the latter to the supporting bones of the skull. The diagnosis of equine sinonasal and dental disease can be challenging due to the complexity of these and adjacent anatomical structures, and therefore the use of advanced imaging, including computed tomography (CT) has greatly increased recently. A major aim of this study was to improve the morphological characterization of the sinuses and cheek teeth in normal horses of different ages. These studies defined the volumes of the 7 different sinus compartments; showed that the volume of the different compartments increase with age; that in contrast to accepted findings, the Triadan 09 alveoli is located in the caudal maxillary sinus (CMS) in 13% of the youngest group and the Triadan 10 alveoli is fully within the rostral maxillary sinus (RMS) in 53% of cases.

The infraorbital canal was found to be susceptible to apical infection-related damage in horses <2 years of age (<2 y.o.) due to the intimate relationship of this canal and the medial aspect of the maxillary cheek teeth alveoli. The mean positions of the clinical crowns and apices of the maxillary Triadan 11s were 2.48 cm (adjusted 5.2% of head height) and 2.83 cm (adjusted 6.2% of head height) more rostral, respectively in horses >16 y.o. compared to horses <6 y.o., consistent with rostral dental drift. Measurements of dental drift could provide further objective radiographic guidelines on ageing horses by dental imaging and also help our understanding of the aetiopathogenesis of cheek teeth diastemata.

This study also found that the reserve crown length decreased from a mean of 4.7 cm (adjusted 19.7% of head height) in the youngest (<6y.o.) group of horses to a mean of 2.9 cm (adjusted 10.5% of head height) in the oldest group (>15y.o.), with the 06s and 09s having the shortest reserve crowns. These data are useful reference information for clinicians and radiologists in the diagnosis and treatment of equine sinonasal and dental disease.

Morphological characterization of the ventral and dorsal conchal bullae in horses of different age using CT described the age-related difference in sizes of these structures (smaller in younger horses). In the ventral conchal bulla, this reduction in volume was probably related to protrusion of the large dental alveoli in young horses into the nasal cavity and bulla. Bullae linear measurements and volumes were also associated with head size. The anatomical position of both bullae was associated with specific maxillary cheek teeth, thus increasing the diagnostic value of conventional radiography in the investigation of bulla disease and providing landmarks for the surgical treatment of this disorder.

Skull shape analyzed with the use of Procrustes statistical analysis showed landmark variability between different age groups and in particular, high landmark variability between young (<5y.o.) and old (>16y.o.) horses and less landmark variability between adult (6-15y.o.) and old horses. Future studies could investigate changes in the equine skull in relation to genotype to characterize breed-related diseases affecting teeth and sinonasal compartments.

In the second part of the study, 32 infected maxillary cheek teeth extracted from clinical cases were evaluated grossly and histologically and these pathological results

were compared to the pre-extraction radiographic and CT imaging findings. This study showed a high sensitivity (97%) of CT in detecting changes in teeth affected by apical infection. In the third part of the study, 30 cheek teeth assessed as being abnormal based on oral, radiographic and CT examinations were extracted along with their alveoli from 27 cadaver heads. Gross and histological examination findings from these teeth and alveoli were compared to the pre-extraction imaging findings, again showed high sensitivity (96.4%) of CT in diagnosing cheek teeth apical infection. Additionally, CT showed a high correlation with histology in detecting dental infection related alveolar bone changes including alveolar bone lysis, sclerosis and bone thickening. This aspect of the study was also the second largest pathological study of equine apical infection published to date and thus has also improved our understanding of the pathogenesis of this disorder.

In conclusion, CT was shown to be an excellent imaging modality for improving the morphological characterization of the sinuses and teeth in normal horses of different ages, and thus also improving the value of this modality in diagnosis and treatment of disease affecting sinonasal and dental structures. This study also objectively showed the high sensitivity of CT in detecting cheek teeth apical infection in horses as compared to radiography, including by assessment of alveolar bone changes. Overall, the results of this project improve morphological knowledge of the equine skull and teeth and will have direct clinical benefits by improving the diagnosis and thus the treatment of equine sinonasal and dental disease.

Lay Summary

Sinonasal and dental disease are very significant problems in horses due to their typically chronic nature, the difficulties in establishing their precise cause and the poor response to treatment in many cases. The difficulty in establishing an accurate diagnosis is often due to the limitations of examining the affected horses by conventional radiography, due to the size and complexity of the equine skull, with myriads of superimposed structures. The current use of computed tomography (CT) allows effective, 3- dimensional imaging of suspect areas, including obtaining easily assessed "slices" in any direction. Until recently, equine CTs could only be obtained under general anesthesia, which is an expensive procedure and has a significant mortality rate in horses (up to 1% of healthy horses die from anaesthetic-related problems) and substantial additional non-fatal, anaesthetic-related problems. The acquisition of CT equipment by the Royal (Dick) School of Veterinary Studies in 2011 that allows CTs to be performed in standing sedated horses, has facilitated the increased use of CT in horses with sinonasal and dental disorders.

The first aim of this study was to characterize the morphology (shapes and sizes) of dental and sinus structures in normal equine cadaver heads of three different age groups using CT.

The first part of this study showed that the volumes of the different sinus compartment changed with age; and in contrast to previous descriptions, the sockets of the 4th cheek tooth (1st molar) were located in the caudal maxillary sinus in 13% of the youngest group and the alveoli of the 5th cheek tooth (2nd molars) were fully positioned in the rostral maxillary sinus in 53% of all cases; that the infraorbital

canal was susceptible to damage in horses under 2 years of age. due to the intimate relationship of this canal and the maxillary cheek teeth alveoli; that the mean positions of the clinical crowns (parts of tooth visible in mouth) and apices (root areas) of the 6th (last) cheek tooth were 2.48 cm (adjusted 5.2% of head height) and 2.83 cm (adjusted 6.2% of head height) more rostral (forward in head), respectively in the oldest (>16y.o.) than the youngest (<5y.o.) group, (<5y.o.) consistent with dental drift (movement). Measurements on this dental drift could provide further objective radiographic guidelines on ageing horses by dental imaging. The reserve crown (crown lying beneath the gum) length decreased (due to dental wear) from a mean of 4.7 cm in the youngest (<5y.o.) horses to a mean of 2.9 cm in the oldest group (>16y.o.), with the first and 4th cheek teeth having the shortest reserve crowns.

Anatomical studies of the ventral and dorsal conchal bullae in horses of different age was performed by CT imaging, adding important anatomical information to allow the diagnosis and thus treatment of disorders of this important, but poorly described anatomical region.

The shapes of equine skulls were evaluated using a new CT and computer generated statistical analysis called “Procrustes” to evaluate which anatomical structure within the skull showed most variation with age.

A further aim was to correlate the radiographic, CT and pathological findings of cheek teeth from horses presented to our referral hospital with sinonasal and dental disorders and also from cadaver heads with dental disorders that were euthanized on humane grounds for intercurrent disorders (such as long bone fractures or inoperable

colic). These two studies showed the very high sensitivity of CT (97%) in detecting changes in the teeth and alveolar bone affected by apical infection.

Overall, the results of this project has improved our anatomical knowledge of the equine skull and validated the use of CT for detecting dental infections. These findings will have direct clinical benefits by improving the diagnosis and hopefully the treatment of many equine sinonasal and dental diseases.

Table of Contents

CHAPTER 1: Literature Review

1.1 Introduction

The equine paranasal sinuses are seven air-filled cavities of uncertain function that vary greatly in morphology between different species (Sisson et al 1953, Dyce et al 2010) The ciliated respiratory mucosa of paranasal sinuses constantly produce mucus that is drained via long and narrow, mucosal-lined osti into the nasal cavity. Obstruction of this drainage pathway can occur with any type of sinus inflammation that can lead to a self- perpetuating disease (O'Leary and Dixon 2011). The presence of long crowned maxillary cheek teeth in horses, whose reserve crowns and apices lie in the maxillary sinuses is an additional predisposition to equine sinus disease (O'Leary and Dixon 2011).

Sinonasal disease is a very significant clinical problem in horses, due to its usual chronic nature, the difficulties in establishing the precise cause of the disorder and then in treating it (Tremaine and Dixon 2001a, Dixon et al 2012a). Several causes of equine sinus disease are recognised such as acute primary (bacterial or viral infection without recognised predisposing factors) sinusitis (< 2 months' duration), chronic primary sinusitis (> 2 months' duration), dental sinusitis, sinus cysts, traumatic sinusitis, dental-related oromaxillary fistula, sinus neoplasia, mycotic sinus disease and intra-sinus progressive ethmoid haematoma (PEH) (Dixon et al 2012a) and these are described in detail later inthis chapter. Clinical signs include unilateral mucopurulent to purulent, often malodorous nasal discharge, firm facial swelling, nasal airflow obstruction and ipsilateral submandibular lymphadenitis, the latter

more prominent in cases with active infections such as primary, dental or mycotic sinusitis (Dixon et al 2011).

Treatment of sinonasal disease depends on the nature of the underlying pathological changes and includes; removal of inspissated pus from cases of chronic primary sinusitis or extraction of infected cheek teeth and sinus lavage for cases of dental sinusitis (Dixon et al 2012).

The main differential diagnoses of cases of equine sinusitis are disorders of the nasal cavity itself, including nasal neoplasia, apical infection of the Triadan 06 and 07 cheek teeth with intra-nasal drainage, infection of the nasal conchal bullae, intra-nasal progressive ethmoid haematoma (PEH), nasal mycosis and nasal trauma.

The Equine Hospital at the Royal (Dick) School of Veterinary Studies R(D)SVS) has a high caseload of such disorders and is recognised as an international centre of excellence in both clinical and research aspects of equine sinonasal disease.

Radiography, nasal endoscopy and sinoscopy are currently important ancillary modalities in the diagnosis of sinonasal disease; however newer imaging modalities such as scintigraphy (Weller et al 2001, Barakzai et al 2006, Dixon et al 2012a), CT (Saunders and Windley 2011) and magnetic resonance imaging (MRI) (Arencibia et al 2000, Tessier et al 2013) are increasingly recognised as being of great value in improving the diagnosis of and identifying the cause of equine sinonasal disorders.

Due to the large size and complexity of the equine skull, and the myriad of superimposed structures, radiographic imaging of localized areas to help diagnose specific sinonasal disorders can be very difficult (Gibbs 1974, Wyn-Jones 1985).

In contrast, the use of CT allows effective three-dimensional imaging of the suspected area, including a detailed examination of selected thin slices in any plane

(Morrow et al 2000, Saunders and Windley 2011). Until recently, equine CTs could only be obtained with the horses under general anaesthesia that is an expensive procedure and also has a significant mortality rate (up to 1% of normal horses die from anesthetic-related problems) and with additional morbidity in other horses (Jones 2001, Wagner 2008).

The acquisition by R(D)SVS in 2011 of CT equipment that allows CTs to be performed in standing, sedated horses now permits this imaging modality to be more widely used in horses with sinonasal and dental disorders. The acquisition of this equipment has allowed significant advances to be made in the imaging of this complex 3-dimensional area and also allows in-depth correlation of radiographic and computed tomographic images with the actual anatomical structures of the equine sinonasal region, in both health and disease.

The increased use of CT imaging of the equine head and upper airway endoscopy over the past two decades has allowed recognition of new sinonasal disorders. In turn this has renewed interest in anatomical studies of the equine head. Anatomical studies of this area has been largely ignored for almost a century, since the demise of the importance of the horse following the mechanization of transport and agriculture in the early 20th century. Computed tomography is a useful tool for studying anatomy as it removes the need for physical dissection of tissues and the process does not damage the examined tissues. CT is particularly useful for imaging calcified structures, such bones and teeth and thus is ideal for studying the anatomy of the skull region.

The first aim of the study will comprise the morphological evaluation of various aspects of the paranasal sinuses, nasal cavity and maxillary cheek teeth in normal

horses with the use of CT in order to increase our anatomical knowledge of these complex anatomical structures and ultimately, to help provide a better diagnosis, treatment and prognosis in clinical cases

The second aim of this study is to compare radiographic and computed tomographic images with gross and histological anatomical sections of infected maxillary cheek teeth from clinical cases and cadaver heads in order to assess the accuracy of CT in detecting the pathological changes associated with dental disease, with the use of cadaver heads to allow assessment of alveolar bone changes.

1.2 Anatomy of the Paranasal Sinuses

Several publications have provided anatomical descriptions of the equine paranasal sinuses (Trotter 1993, Probst et al 2005, Tatarniuk et al 2010, O'Leary and Dixon 2011, Brinkschulte et al 2013).

There are 7 pairs of paranasal sinuses in horses: the caudal group consisting of the frontal and dorsal conchal, caudal maxillary sinus (CMS), ethmoidal (ES), sphenopalatine (SPS) that all interconnect and the separate rostral group comprising the rostral maxillary sinus (RMS) and ventral conchal sinus (VCS) that are also interconnected. The dorsal conchal sinus lies rostral to the frontal sinus with which it forms a single combined sinus (CFS). The CMS is the largest paranasal sinus in the horse and lies medial to the maxillary, lacrimal and zygomatic bones and caudal to the RMS.

The large oval fronto-maxillary opening provides communication from the conchofrontal sinus into the CMS and the location of this opening varies with age.

The ethmoidal sinus (termed the middle conchal sinus by some workers, including Brinkschulte et al 2013) consists of a small sinus that lies within the larger (number 2) of the ethmoturbinates (endoturbinates), that normally drain laterally into the CMS either directly or via the sphenopalatine sinus. The sphenopalatine opening located between the caudal origin of the infra-orbital canal and the ethmoturbinates connects the sphenopalatine sinus and the CMS (Probst et al 2005).

The sphenopalatine sinus also communicates with the ethmoidal sinus in most horses. The dorsal and lateral walls of the sphenopalatine sinus are very thin and are directly adjacent to cranial nerves II (optic), III (oculomotor), IV (trochlear), V (trigeminal) and VI (abducens) and also to major blood vessels.

The RMS is a small sinus compartment that is separated from the much larger CMS by a complete bony septum. This septum is usually angulated in a rostro-lateral to caudo-medial direction, and usually also slopes caudally. The VCS lies medial to the RMS, but extends caudal to the RMS, especially caudo-dorsally where it protrudes to the dorsal aspect of the CMS as a rounded, thin-walled diverticulum called the maxillary septal bulla (MSB), until recently mistermed the ventral conchal bulla. The concho-maxillary opening connects the ventral conchal sinus and the rostral maxillary sinus. This wide (but variably narrow in younger horses) entrance is located dorsal to the infraorbital canal at the level of the Triadan 08s and 09s (Dane et al 2010).

The secretions of both the VCS and RMS drain via the naso-maxillary ostia (opening) of the RMS into the caudal aspect of the middle meatus of the nasal cavity. This opening lies adjacent to, and sometimes joined to the naso-maxillary ostia of the caudal maxillary sinus; that drains the CMS and thus also the CFS, SPS and ES

that drain into the CMS. These ostia are located at the level of the upper Triadan 10s or 11s and are directed towards the middle nasal meatus. The above drainage pathways of the paranasal sinuses are very narrow (1-2 mm wide) and as noted, even a mild degree of inflammation of the sinonasal mucosa that lines these apertures may obstruct them.

1.3 Clinical signs and aetiopathogenesis of equine sinonasal disease

Sinonasal diseases are clinically significant disorders that as noted, have multiple causes. Horses with sinonasal disorders commonly present with unilateral, or less commonly bilateral nasal discharge, facial swellings, discharging facial tracts, epiphora, nasal obstruction, submandibular lymphadenopathy and abnormal respiratory noise (Tremaine and Dixon 2001a). Unilateral mucopurulent or purulent nasal discharge is less common with sinus cysts and neoplasms, where facial swelling is the most common presentation. A malodorous nasal discharge is more commonly associated with dental and mycotic sinusitis but is also often present with primary sinusitis. Hemorrhagic nasal discharge is more common with PEH or traumatic sinusitis (O'Leary and Dixon 2011).

1.4 Primary sinusitis

Horses with primary sinusitis have a bacterial sinus infection with no apparent predisposing factors other than a possible antecedent, generalized respiratory infection, that has been hypothesized to obstruct the normal sinonasal drainage. Affected horses usually present with a malodorous unilateral nasal discharge, unilateral submandibular lymphadenitis, slight or no facial swelling, that if present

may be painful on deep palpation due to localized inflammation of the soft tissue overlying the sinuses. Facial swelling can also be caused by osteitis with thickening and slight distension of the maxillary bone (Tremaine and Dixon 2001a).

Most cases of primary sinusitis resolve spontaneously, possibly when the respiratory infection and sinonasal mucosal swelling resolve, and antibiotic administration may be of value in some refractory cases. If the exudate within the sinuses inspissates (dries), or if permanent damage to the sinonasal drainage pathways occurs - then the sinusitis may become refractory and chronic (> 2 months duration). Histologically, primary sinusitis is characterized by increased mucosal fibroplasia with mucosal sections from cases of primary sinusitis containing granulation and mature fibrous tissue (Tremaine et al 1993). Hyperadrenocorticism due to pituitary adenoma is a predisposing factor for primary sinusitis as is prolonged trans-nasal catheterization such as an indwelling nasogastric tube.

Secondary sinusitis can be caused by a variety of lesions that are described in more detail below.

1.5 Dental sinusitis

Dental sinusitis is caused by infection of the caudal (08s-11s) maxillary dental apices that allows inoculation of bacteria across the alveolus into the sinuses. Dental sinusitis commonly causes a malodourous nasal discharge and granuloma formation may occur around the infected apex (O'Leary and Dixon 2011). Apical infection of cheek teeth (Dixon and Dacre 2005) is a significant problem in young horses where the infection invariably involves the supporting bones or paranasal sinuses.

Periapical maxillary cheek tooth infection was previously believed to be very commonly caused by food accumulation and deep fermentation within infundibular defects; however Dacre et al (2008d) found extension of infundibular caries to cause apical infection in 16% of infected maxillary cheek tooth, but Suske et al (2016b) later found infundibular disease to be associated with a higher (26%) proportion of maxillary cheek teeth apical infections.

It was also previously believed that an imbalance between wear and formation of subocclusal secondary dentine could lead to exposure and infection of the dental pulp cavity (Dixon and Dacre 2005), thus causing apical infection of both lower and upper cheek teeth. More recent studies have indicated that pulpar exposure is actually secondary to pulpar death rather than being its cause (Dacre et all 2008c,d).

Apical infections are currently believed to be mainly caused by anachoretic (blood or lymph born) bacterial infection, and less commonly due to periodontal spread, gross, or fissure fractures, dysplasia and, as noted, for a proportion of maxillary cheek teeth cases, an extension of infundibular caries. A high percentage of apical tooth infections diagnosed with anachoresis have a decreased thickness of regular secondary dentine indicating great chronicity (Dacre et al 2008b).

Fissure fractures extending from the periphery of the crown into an infected pulp (usually in bucco-palatal/lingual plane) have been suspected as cause of apical infection. However, Simhofer et al (2008) and Ramzan and Palmer (2010) found such fractures in about 50% of all horses, with no direct relationship to apical infection found.

The loss of the periodontal membrane from gingiva to apex along with the presence of peripheral cemental changes such as discoloration along such tracts, indicates that

periodontal disease was a possible route of apical infection (termed a periodontal - apical lesion), but it is also possible that such tracts are secondary to drainage into the oral cavity of an apical infection, for example of anachoretic origin.

1.6 Maxillary cheek teeth anatomy

Examination of the endodontic anatomy of the maxillary cheek teeth found five pulp horns for the Triadan 07-10 positions; six pulps for 06s and lower 11s and seven pulps in mature upper 11s (Dacre et al 2008a). A thorough knowledge of equine cheek teeth anatomy is necessary in order to recognize the pathological features of diseased cheek teeth, such as the presence of occlusal pulpar exposure in apically infected teeth.

Moreover, knowledge of pulpar anatomy is essential for endodontic treatment of cheek teeth (Dacre et al 2008a). Additionally, in routine clinical dentistry it is important to know how much pulp has been replaced by subocclusal dentine as this indicates how much crown may be therapeutically removed, for example in an overgrown tooth, before vital pulp is exposed (Dacre et al 2008a).

Histologically, dentine can be classified as primary, secondary or tertiary. Dacre et al (2008b) proposed that the type of secondary dentine always present towards the centre of the pulp should be termed irregular secondary dentine and not as previously termed, tertiary dentine that technically should only occur in the presence of dental disease. Dacre et al (2008b) proposed that the term tertiary dentine should be fully reserved for the focal areas of irregular dentine laid down following insult to dentine or pulp. Histological studies of apically infected cheek teeth have shown that there is reduced thickness of regular and irregular secondary dentine indicating the great

chronicity of many of these infections. Due to the reduced thickness of secondary dentine deposition, the pulp horns were much wider than normal in the apically infected cheek teeth (Shaw et al 2008, Dacre et al 2008b). However primary dentine thickness did not differ between apically infected and control teeth indicating that abnormal development, or alternatively later destruction of primary dentine are not features of cheek tooth apical infection (Shaw et al 2008, Dacre et al 2008b).

1.7 Oro-maxillary fistula

The presence of oro-maxillary fistulas is a less common dental cause of equine sinusitis (Hawkes et al 2008). These are usually caused by deep diastemata between the caudal upper cheek teeth and subsequent food impaction in these spaces that eventually enters the sinuses allowing ascending bacterial penetration into the sinus lumen. Oro-maxillary (or or-nasal) fistulae can also occur following dental extractions, especially by repulsions (Dixon et al 2008, Hawkes et al 2008).

1.8 Sinus cysts

Sinus cysts are common benign lesions of all age groups that cause obstruction by occluding sinus drainage and compressing the adjacent structures with subsequent facial distortion and airflow restriction. They are often accompanied by secondary infection of the affected or adjacent sinus. In a report of 15 cases of sinus cysts; nasal airway obstruction, facial swelling, and nasal discharge were the main clinical signs (Lane et al 1987). Sinus opacification was a consistent radiographic feature and in several cases the sinus bones had increased thickness. On ventro-dorsal radiographic projections, the nasal septum was sometimes displaced due to increased intra-sinus

pressure. Other less common radiographic feature included free fluid accumulation within the affected sinuses, dental distortion and displacement. The most common site for sinus cysts was the caudal maxillary sinus and less commonly the frontal and rostral maxillary compartments (Lane et al 1987).

In a more recent study, 52 horses with sinus cysts presented with facial swelling, mucopurulent nasal discharge, nasal airflow obstruction and abnormal respiratory noise (Woodford and Lane 2006). No biphasic age distribution was identified unlike, a previous report that suggested a biphasic age predisposition, with peaks between 1 and 9 years of age (Lane et al 1987).

A histological study of equine sinus cysts (Tremaine et al 1993) showed the cyst walls to vary in thickness, and the underlying bone had areas of osteoclastic remodeling in conjunction with oedema of adjacent connective tissue. Some cysts had a thin mucoperiosteal layer between the epithelium and the underlying bony capsule, while in others, a thick layer of fibrous tissue was present. An epithelial layer was present on both sides of the bony cyst capsule. The presence of fibrous tissue and chronic, inflammatory cell infiltrate in sinus cyst walls, suggests that low-grade inflammation is a consistent feature of these lesions, as compared with other inflammatory sinus disorders.

In the study of Tremaine et al (1993), seven horses had pus filled cystic type lesions within the maxillary sinuses of which two were classified as inflamed sinus cysts, two as intra-sinus abscess and 3 of uncertain classification More recent studies indicate that some of these lesions may have been pus-filled ventral conchal sinuses with distension of the maxillary septal bullae (Dixon et al 2012a, Perkins et al 2009).

1.9 Sinus neoplasia

A review of the literature on equine sinonasal tumors (Head and Dixon 1999, Dixon and Head 1999) suggest that equine sinonasal tumours are relatively uncommon, with benign neoplastic growths such as sinus cyst, PEH, and inflammatory nasal polyps more commonly recorded in the sinonasal region. Sinonasal neoplasms usually affect older horses with squamous cell carcinoma, undifferentiated carcinomas and adenocarcinoma the most commonly identified types. Tumours of other cell types such as fibroblasts (fibrosarcoma, fibro-osseous myxoma and myxosarcoma), endothelial cell (haemangioma and haemangiosarcoma), round cell (lymphoma, mast cell neoplasia) and osteoblast (osteosarcoma) have been less commonly described in these areas (Dixon and Head 1999). In a study of 28 horses with sinonasal neoplasia, most cases presented with a unilateral purulent or mucopurulent nasal discharge and gross facial swelling (Dixon and Head 1999). Benign tumours originating in the nasal cavity can extend rostrally to the nostril and caudally to the nasopharynx. Tumors of the fronto- conchal sinus can extend via the frontomaxillary opening to the caudal maxillary sinus. Tumors of the rostral maxillary sinus can extend medially over the infraorbital canal into the ventral conchal sinus. Overall, the caudal maxillary sinuses are the most common sites for sinonasal tumors (Head and Dixon 1999; Dixon and Head 1999).

Metastases of equine sinonasal tumor are rarely recorded, both because of the nature of these tumors and because affected animals are often destroyed soon after a diagnosis is established. However, local metastasis to the mandibular and retropharyngeal lymph node has been recorded, although swelling of these lymph

nodes is more usually secondary to inflammation and infection caused by the neoplasms (Dixon and Head 1999).

1.10 Mycotic sinusitis

Mycotic sinusitis is a poorly recorded and uncommon disorder whose prevalence andaetiology can vary in different geographical regions. Aspergillus fumigatus is the usual isolate in the UK (Greet 1981; McGorum et al 1992). In warmer climates, mycotic nasal granulomas caused by a wide range of other fungal organism are common (Tremaine et al 1993). The most common clinical signs are chronic, malodorous, unilateral nasal discharge, and low-grade epistaxis. No radiographic features were attributable to mycotic sinusitis, however mycotic plaques were endoscopically visible in the affected sino-nasal regions in all affected horses (McGorum et al 1992). A histological study of mycotic sinonasal disease (Tremaine et all 1993), showed inflammatory changes and necrotic plaques overlying areas of ulcerated, necrotic epithelium. Branching fungal hyphae with sporulating bodies were also observed.

1.11 Progressive ethmoid haematoma (PEH)

PEH lesions cause low-grade, chronic unilateral epistaxis, and rarely facial swelling or purulent nasal discharge. Head and Dixon (1999) suggest that these lesions are best pathologically described as haemorrhagic polyps originating from the ethmoturbinate mucosa. These lesions most commonly grow rostrally down the nasal cavity and less commonly dorsally into the conchofrontal sinus or laterally into the caudal maxillary sinus.

1.12 Traumatic sinusitis

Trauma to the facial bones due to external injury, such as kicks, can cause haemorrhage into the sinuses and bone damage may not be apparent in all cases. Even in the absence of detectable bony damage, insult to the facial bone suture lines may cause later remodeling at these sites, with suturitis and bony exostoses of the fronto-nasal and lacrimal- nasal bones.

1.13 DIAGNOSTIC IMAGING REVIEW OF SINONASAL AND DENTAL DISEASE

1.13.1 Radiology

The equine head is difficult to evaluate radiographically because of its large size, the large number of superimposed structures, including thick bones, and its relatively complex anatomy. However, despite these limitations, radiography is currently the standard imaging modality and provides diagnostic information for the majority of equine head disorders (Trotter 1993, Pease 2007). Nasal discharge, (unilateral or less commonly bilateral), facial swelling, nasal airway obstruction, discharging purulent tracts, are the most common reasons for performing equine skull radiography. Other signs, such as quidding, epiphora, facial deformity following trauma are less common reasons (Gibbs 1974, Gibbs and Lane 1987, Lane et al 1987)

Many different projections are required to properly evaluate the equine head

Lateral projection

Dorsoventral projection

Latero30°dorsal-lateroventral oblique (left and right maxillary cheek teeth apices and sinuses)

Latero35°-45°ventro-laterodorsal obliques (left and right mandibular cheek teeth apices and hemimandible)

These projections, adequately image the reserve crown, dental apices, lamina dura and alveolar bone, as well as associated mandible, maxilla and sinonasal structures (O'Leary and Dixon 2011). Additional projections, including open-mouthed dorsolateral-lateral oblique and open mouthed ventrolateral-lateral oblique, have

been described to evaluate the erupted (clinical) crowns of the mandibular and maxillary equine cheek teeth (Barakzai and Dixon 2003) and intra-oral radiographs to assess the incisors.

In cases of unilateral nasal discharge suspected to be due to sinusitis, a lateral projection is useful to show the degree and distribution of opacification of the paranasal sinuses, especially for showing fluid lines; for distinguishing between solid and fluid sinus contents and for estimating the quantity of fluid (Gibbs 1974, Gibbs and Lane 1987, Lane et al 1987). Lateral projections can also be used to detect expansion and opacification of the maxillary septal bulla, , gross dental defects and for showing distortion of the frontal sinus and nasal bones in cases of head trauma (with secondary sinusitis) and later showing fronto-nasal and other suture exostoses (Gibbs 1974, Gibbs and Lane 1987, Lane et al 1987).

Oblique projections cause separation and thus allow more effective assessment of dental apices and reserve crowns. This projection can provide additional information about the paranasal sinus contents, although fluid lines will not be apparent (Gibbs 1974, Gibbs and Lane 1987, Lane et al 1987).

In cases of suspect dental sinusitis, lateral-oblique radiographs may show dental apical changes such as widening of periodontal space, loss of lamina dura and blunting or lysis of the roots (O'Leary and Dixon 2011)

A dorso ventral projection is useful for showing nasal septal deviation and expansion of the sinuses, in particular expansion of the VCS into the nasal chambers (Gibbs 1974, Gibbs and Lane 1987, Lane et al 1987).Radiographic studies have good specificity but poor sensitivity for detecting periapical infection, however a recent study showed that the use of computed radiography (CR) improves the sensitivity of

radiography in detecting periapical infection (Weller et al 2001, Townsend et al 2011).

1.13.2 Ultrasonography

Ultrasonography is useful for evaluation of superficial soft tissue structures but a major limitation of its use in detecting sinonasal disease are the overlying head bones, which prevent penetration of sound waves. However ultrasonography has been used to evaluate skull fracture, temporo-mandibular joints, retrobulbar masses, and jugular vein thrombosis. Guttural pouches and lymph nodes can also easily be evaluated ultrasonographically (Pease 2007).

1.13.3 Computed Tomography (CT)

The use of cross-sectional imaging such as CT eliminates the problem of superimposition of overlying structures. CT allows the evaluation of thin slices of tissues in different planes and also allows the three-dimensional reconstruction of the imaged area for lesion evaluation and possible surgical planning. However, this advance modality requires expensive, specialized equipment, and purpose-built buildings to accommodate the size of the horse (Pease 2007), in addition to specialized staff training to allow both the safe acquisition and accurate interpretation of imaging findings.

CT allows excellent visualization of bony structures and therefore is currently the optimal imaging modality to evaluate the equine paranasal sinuses and nasal cavity. CT imaging studies of the normal anatomy of adult equine and foal heads has been described (Morrow et al 2000, Smallwood et al 2002, Tucker et al 2015). Over the

last decade studies on the use of CT for detecting dental disease and sinusitis in horses have been published by Henninger et al 2003, Veraa et al 2009 and Buhler et al 2014. A recent study comparing radiography and CT imaging in 19 horses presented with non-neoplastic mandibular disease showed the advantage of CT in identifying diseased teeth which were normal radiographically. The detected dental changes included identification of dental pulp changes, lamina dura loss, the presence of intra-alveolar bone fragments, alveolar periosteal reaction, and cortical bone destruction (Huggons et al 2011).

More detailed specific, dental-related studies on the two- and three-dimensional CT anatomy of the enamel, infundibulae and pulp in normal and affected cheek teeth have recently added greatly to the literature on this topic (Windley et al 2009a,b, Saunders and Windley 2011, Kopke et al 2012). In particular, these studies highlight the value of CT reconstruction to enable detailed imaging of pulpar anatomy in different aged teeth, allowing the variable interpulpar communication between the different pulp horns and the pulpar volume of each tooth to be appreciated.

Micro-CT, is an ex-vivo technique that images very thin slices of tissues , but can only examine small volume of tissue such as extracted teeth. This technique has been used to evaluate in great detail the three-dimensional configuration of the infundibulum and in particular to examine infundibular vasculature and infundibular cementogenesis (Suske et al 2016a). CT has more recently been used in clinical cases to evaluate cheek teeth in horses with suspect apical infections (Veraa et al 2009, Buhler et al 2014). However, these studies gave minimal or no pathological details about the extracted teeth to allow a correlation of imaging and anatomical findings. A recent CT study on diseased teeth extracted from horses on clinical

grounds along with pathological examination of some of these teeth (Suske et al 2016b) have improved our knowledge of infundibular disorders). CT features related to changes in the infundibulum, pulp, tooth root, lamina dura, periapical bone and periodontal space and presence of dental fracture have been described in many of these CT clinical studies. Semi-automated segmentation of CT dataset has been used to provide three- dimensional visualization and volume measurements of equine sinuses that has improved our understanding of this anatomically challenging area, in particular for treatment planning and surgery (Brinkschulte et al 2013).

1.13.4 Magnetic Resonance Imaging

MRI has infrequently been used for evaluation of the normal equine head and for detection of sinonasal disease (Arencibia et al 2000, Tessier et al 2013, Manso-Diaz et al 2015). These studies include a cadaver study highlighting the anatomical structures of the equine head visible on MRI by Arencibia et al (2000) who found that MRI provided good details of the oral and nasal cavity, paranasal sinuses and associated structures. A more recent publication described the use of MRI in imaging 14 horses with sinonasal disease (Tessier et al 2013). Lesions identified included primary or secondary sinusitis, paranasal sinus cysts, progressive ethmoid haematoma, and sinus neoplasia. The most useful sequences were FAST SPIN ECHO T2 transverse and sagittal, STIR dorsal and FE3D MPR. Mucosal thickening, presence of encapsulated contents, fluid accumulation, bone deformation and thickening were common features (Tessier et al 2013, Manso-Diaz et al 2015). MRI appears to be a potentially useful head imaging modality but always requires general anesthesia, with its inherent high costs and high morbidity and mortality risks

(Arencibia et al 2000). Additionally, its restricted ability to image calcified structures greatly limits its use for investigating equine sinonasal and dental disorders.

1.13.5 Scintigraphy

Nuclear medicine has been used to identify localized sites of increased bone activity and remodeling in horses (Pease 2007). The most common radiopharmaceutical used in scintigraphy is Technetium-99 labelled with methylene diphosphonate. Radioactive tracer labeling of white blood cells has also been used in horses, but with poor results (Weller et al 2001). In the equine head, the main use for scintigraphy is for evaluating dental disease and differentiating primary sinusitis from dental sinusitis (Barakzai et al 2006). In addition, scintigraphy is useful for identifying bone remodeling caused by degenerative joint disease of the temporomandibular and temporohyoid joints, which might not be evident on radiographs (Pease 2007).

There is a focal markedly increased uptake in the region of an apically infected tooth, with moderate diffuse uptake over the affected sinus. However, cases of primary sinusitis also show diffuse increased radiopharmaceutical uptake over the affected region, with unexplained focal areas of increased uptake, likely caused by focal areas of facial bone osteitis, (that have more recently been recognised on CT; (Liuti T and Dixon PM 2017, unpublished observations). Scintigraphy has high sensitivity (95%) but moderate specificity (86%) for apical infection (Weller et al 2001, Barakzai et al 2006). The sensitivity of conventional radiography for equine dental disease is approximately 50% but when used in combination with scintigraphy can reach up to 97% sensitivity and 100% specificity (Pease 2007).

1.14 Nasal endoscopy, Sinoscopy and Oral Endoscopy

Nasal endoscopy is usually performed to evaluate the ventral and middle meati for evidence of exudate, especially for the presence of purulent/mucopurulent exudate draining from the sinonasal ostium at caudal aspect of the middle meatus ("drainage angle"). It can also

detect evidence of nasal trauma, sinonasal fistulae, mycotic lesions and sinus tracts from apically infected rostral cheek teeth. More recently with the recognition of sinonasal fistulas (Dixon et al 2011) and nasal conchal bulla disease (Dixon et al 2015), endoscopy of the middle meatus is routinely performed to detect these lesions. The presence of food material within the nasal cavity usually indicates the presence of an oronasal fistula, unless food is detected originating from the sinonasal ostium (or a sinonasal fistula).

Sinoscopy is a simple and inexpensive technique to help to investigate cases of sinusitis (Tremaine and Dixon 2001a,b). Sinoscopy allows examination of most of the intra-sinus structures, and allows biopsy collection and intrasinus treatment (O'Leary and Dixon 2011). Sinoscopy can detect the presence of intra-sinus fluid and inspissated exudate, PEH lesions, small cysts or tumours, mycotic plaques and intrasinus food in cases of oro-maxillary fistula (O'Leary and Dixon 2011).

Oral endoscopy is increasingly used to clinically evaluate the cheek teeth (Simhofer et al 2008, Ramzan 2009, Ramzan et al 2011). The most commonly detected abnormalities include sharp enamel edges, focal dental overgrowths, fissure fractures, gross fractures, maxillary cheek teeth infundibular cemental hypoplasia

(which can be difficult to differentiate from infundibular caries); and diastemata (Simhofer et al 2008).

We hypothesise that the use of CT will allow new and clinically relevant anatomical information on the linear and volumetric dimensions of equine sinonasal structures and maxillary cheek teeth to be obtained. Likewise, clinically important information on the eruption and rostral drift of maxillary cheek teeth will be obtained by CT examination of these structures in groups of horse of different ages. The relatively recent use of CT in the diagnosis of equine maxillary cheek teeth apical infection appears to be a major diagnostic imaging improvement over radiography, but this apparent advantage of CT over radiography has not been validated. A further aim of this study is to attempt to validate the accuracy of CT in the diagnosis of maxillary cheek teeth apical infections.

CHAPTER 2: Computed tomographic assessment of equine maxillary cheek teeth anatomical relationships, and paranasal sinus volumes

Paper published in Veterinary Record (2017) DOI: 10.1136/vr.15

2.1 Introduction

This chapter describes the use of CT in the morphological evaluation of normal equine skulls in different age groups. The use of CT is increasing in the investigation of sinonasal and dental disease in horses (Morrow et al 2000, Henninger et al 2003, Solano and Brawers 2004, Veraa et al 2009, Windley et al 2009a,b, Buhler et al 2014). In particular, the development of mobile platforms that allow CT imaging in standing sedated horses has been a major improvement, with reduced costs and morbidity/mortality risks when compared to general anaesthesia, as previously noted (Jones 2001, Wagner 2008). Moreover, new sinonasal disorders such as infections of the nasal conchal bullae have now been recognised with the use of CT (Dixon et al 2015).

CT is also an effective and non-invasive method to perform anatomical studies of the skull structures, including allowing two and three dimensional measurements to be readily obtained.

Although there are multiple publications on equine sinonasal and dental anatomy, including classical anatomical texts such as Sisson and Grossman (1953) and Dyce et al (2010), none describe the position of maxillary cheek teeth alveoli in relation to individual sinus compartments; the length of the reserve crown in relation to age; age-related rostral drift of cheek teeth; or the position of the infraorbital canal in

relation to cheek teeth alveoli. Such information would be clinically valuable for investigating and treating sinonasal and dental disorders. Sinus volume has been previously assessed by semi-automated segmentation of CT data sets (Brinkschulte et al 2013), which showed major age-related changes in sinus compartment shapes and dimensions in Warmblood horses

The use of CT in this study has been shown to provide detailed information on the anatomical localisation of the cheek teeth alveoli in relation to the sinus compartments: rostral dental drift; position of the infraorbital canal; the length of the reserve crown and on the measurement of sinus volume in horses of different age. The advantage of CT imaging for anatomical studies is facilitated by the use of thin slices, multiplanar reconstruction and the high resolution of the bone window used for this study. The results of this study provide objective measurements of the above parameters and offer clearer guidelines for diagnostic imagers and clinicians and will help to improve the diagnosis and treatment of sinonasal and dental disease in horses, whilst also serving as a basis for further research projects.

Conception and design of the study was by Tiziana Liuti and Prof. P.M Dixon

Data acquisition was by Tiziana Liuti

Analysis and data interpretation was by Tiziana Liuti with the assistance of Dr. Richard Reardon

Drafting of the article was by Tiziana Liuti

Revision of the article for intellectual content was by Prof. P.M Dixon, Richard Reardon and Tiziana Liuti

Final approval of the completed article was by Tiziana Liuti and Prof. P.M Dixon

Paper

Computed tomographic assessment of equine maxillary cheek teeth anatomical relationships, and paranasal sinus volumes

Tiziana Liuti, Richard Reardon, Paddy M Dixon

Disorders affecting the equine maxillary cheek teeth and paranasal sinuses are relatively common, but limited objective information is available on the dimensions and relationships of these structures in horses of different ages. The aims of this study were to assess age-related changes in the positioning and anatomical relationships of the individual maxillary cheek teeth with the infraorbital canal and maxillary septum and the volumes of the individual sinus compartments. CT and gross examination were performed on 60 normal equine cadaver heads that were aged by their dentition. The intrasinus position of cheek teeth, length of reserve crowns, relationship to the infraorbital canal and measurements of rostral drift and sinus compartment volumes were assessed from CT images. The findings included that Triadan 10 alveoli lay fully or partially in the rostral maxillary sinus (RMS) in 60% of cases. The infraorbital canal lay directly on the medial aspect of the alveolar apex in younger horses. The Triadan 11'sclinical crowns and apices drifted a mean of 2.48 and 2.83 cm more rostral to the orbit, respectively, in the >15 years old vs the <6 years old age group. The mean volumes of sinus compartments ranged from 175 cm³ for the caudal maxillary sinus (CMS) to 4 cm³ for the ethmoidal sinus (ES). This information should be of value in the diagnosis and treatment of equine dental and sinus disorders and as reference values for further studies.

Introduction

The growing use of CT has allowed a reassessment of the very complex and variable sinonasal and dental anatomy of the horse, which additionally becomes altered with disease. This three-dimensional imaging modality is increasingly used in the diagnosis of equine sinonasal[1–3] and dental disorders,[4–6] where it has been shown superior to conventional radiography in which superimposition of adjacent structures is problematic. The use of CT has also enabled new sinonasal disorders to be recognised.[7]

Limited objective information is available on the position of maxillary cheek teeth alveoli in relation to individual sinus compartments[8 9]; on age-related eruption and rostral drift of cheek teeth and on the position of the infraorbital canal (IOC) in relation to the cheek teeth alveoli, although such information would be of clinical value for investigating and treating sinus and dental disorders. The volumes and relationships of the individual paranasal sinus compartments, as assessed by semi-automated segmentation of CT data sets, has recently been reported,[10 11] and a study of three-dimensional anatomy of Arabian foal paranasal sinuses[12] showed major age-related changes in sinus shapes and dimensions.

The purpose of this study was to quantify the position of the cheek teeth alveoli in relation to individual sinus compartments; the poorly described, age-related rostral drift of cheek teeth; the eruption-related changes in the reserve crown length and the position of the IOC in relation to the alveoli and conchomaxillary ostium. An additional aim was to measure the volumes of the individual compartments in a large number of horses of different ages, using a different image processing software (Osirix, http://www.osirix-viewer.com/)[1] and breeds from previous equine studies[10,12] to provide further objective information, including the relationship between sinus and head volumes, and age-related changes in these complex and variable structures.

Veterinary Record (2017) doi: 10.1136/vr.104185

Tiziana Liuti, DVM, DipECVDI, Pg.CAP, MRCVS, FHEA,
Paddy M Dixon, MVB, PhD, FRCVS, DipEVDC (Equine),
Veterinary Clinical Sciences, Diagnostic Imaging, Royal (Dick) School of Veterinary Studies, University of Edinburgh, Edinburgh, Midlothian, UK
Richard Reardon, BVetMed(Hons), MVM, PhD, CertES(Orth), DipECVS, MRCVS,
Veterinary Clinical Sciences, Royal (Dick) School of Veterinary Studies, University of Edinburgh, Edinburgh, Midlothian, UK
Paddy M Dixon is also at Veterinary Clinical Science, Royal (Dick) School of Veterinary Studies, University of Edinburgh, Edinburgh, Midlothian, UK
E-mail for correspondence: tiziana.liuti@ed.ac.uk

Provenance and peer review Not commissioned; externally peer reviewed.

Received October 26, 2016
Revised June 9, 2017
Accepted July 29, 2017

Materials and methods

Specimens

Head were available from two sources:

Group A

The heads of 54 horses freshly obtained from an abattoir, with unknown histories but similar in size to Thoroughbred heads had transverse CT images obtained, with the heads positioned on their mandibles, using a multislice CT scanner (Multislice CT scanner Siemens Volume Zoom, Munich, Germany) in a helical scan mode using a 512×512 Matrix, 120 kV, 300 mA, at a slice thickness of 1.5 mm. After image acquisition, the heads were frozen (−20°C) and then sectioned transversely (48 heads) and sagittally (5 heads) at 5 cm intervals with a band saw. After thawing out, both sides of all transverse sections were visually examined for the presence of sinonasal or significant dental abnormalities.

Group B

Anatomical and CT images of a further 36 equine heads with unknown histories that had been freshly obtained from an abattoir were also included in this study. CT images were acquired using a fourth-generation, Universal Medical System CT scanner, GE light speed ultras, Highland Heights, Ohio, USA, at 1.25 mm slice thickness, 120 kV, 300 mA. The CT images were examined for the presence of sinonasal disease or significant dental abnormalities.

Twenty-six of 54 heads (48%) in group A had gross and/or imaging evidence of dental or sinonasal disease and were excluded from the study, leaving 28 heads in this group. Four of the 36 heads in group B with imaging evidence of dental or sinonasal disease were also excluded, leaving 32 heads in this group (total of 60 normal heads).

These 60 heads were aged by clinical incisor examination using standard guidelines,[13] along with CT examinations of cheek teeth reserve crown and root lengths and were placed into one of three age groups: <6 years old (group 1: n=15), 6–15 years old (group 2: n=21) and >15 years old (group 3: n=24).

Image manipulation

Bone window CT data of the 60 heads were transferred as DICOM images to Osirix imaging software, which was used to perform multiplanar image reconstructions to allow identification and measurements of the sinuses and adjacent structures and 30 heads, including 10 randomly selected from each age group, were used for sinus and head volume measurements.

Sinus volume

Sinus compartment volumes were calculated using three-dimensional regions of interest/volume (Osirix) by outlining the internal boundary of each sinus on transverse images using every image slice (1.5 mm slice thickness) of that compartment as previously described,[14] using a bone window (70 algorithm), which accurately differentiated bone from mucosa: 15–90 slices were used per sinus compartment.

Head volume

The 'volume' of each skull was calculated as described.[14] To allow comparison of the head sizes in the study population with head sizes of known breed, CT measurements were compared with equivalent measurements from CT images of the heads of 12 Thoroughbreds of known age (<6 years old (n=4); 6–15 years old (n=4); >15 years old (n=4)) without identified head disorders.

Position of cheek teeth in relation to maxillary sinus compartments

Transverse and sagittal CT slices were used to identify the location of each maxillary cheek tooth alveolus in relation to the RMS and CMS compartments; the maxillary septum and orbital bone.

Rostral drift of the maxillary cheek teeth

Sagittal CT slices were used to assess the distance between a reference line drawn at the most rostral aspect of the orbital rim (fig 1, line C) that was perpendicular to the line of best fit on the maxillary cheek teeth occlusal surfaces—which have a variable dorsal slope at the level of the caudal cheek teeth (Curve of Spee) (fig 1, line D) and the caudolateral (buccal) aspect of the occlusal surface of the caudal maxillary cheek teeth (Triadan 11) (hereafter termed the 'caudal aspect of the Triadan 11 clinical crown') (fig 1, line Y) and the caudal aspect of the lateral root of the Triadan 11 (termed the 'caudal aspect of the Triadan 11 apex') (fig 1, line X) to the reference line C. The reference line C was considered point '0' and the distances rostral to it (left side of the line) were considered negative and the ones caudal to it (right side of the line) positive.

Length of reserve dental crown

Transverse CT slices were used to assess the length of the reserve crown (unerupted, enamel-containing areas of teeth) on both palatal and buccal aspects of all maxillary cheek teeth. The occlusal surface is angulated palato-bucally (transversely), and this angle also varies between the different Triadan positions.[15] Consequently, the mean of buccal and palatal measurements was used to measure the length of each reserve crown using an 'open polygon' tool, that is, a linear measurement composed of a series of straight-line segments; if the surface to be measured was curved, multiple-line segments were drawn adjacent to each other until the desired end point was reached (fig 2). The reserve crown length was calculated as the mean of the palatal and buccal lengths.

Position of the IOC in relation to the cheek teeth alveoli; and ventral and conchal sinus walls (conchomaxillary ostium)

Transverse CT slices were used to document the anatomical position of the IOC in relation to the 08–11 maxillary cheek teeth alveoli bilaterally, including its height above the rostral and caudal roots of these teeth (fig 3).

The width of the conchomaxillary ostium at the rostral aspect of Triadan 10 and middle of Triadan 11 were also measured at sites both horizontal and vertical to the IOC (fig 4).

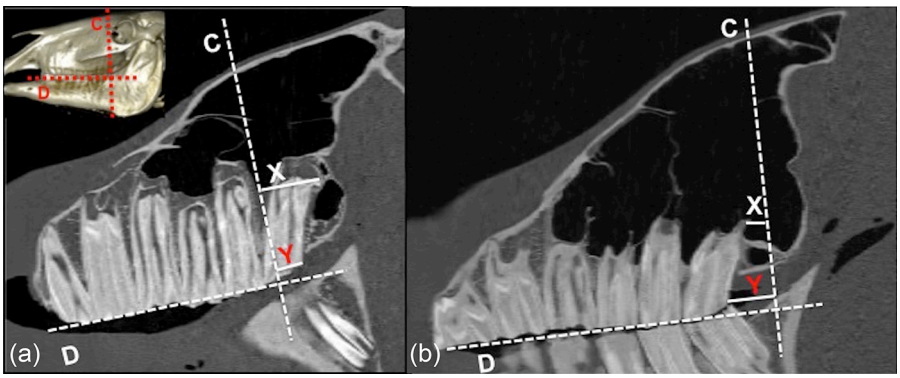

FIG 1: Sagittal CT image of a horse aged 4 years (A) and a horse aged 16 years (B). Note the fixed orbital reference line (C) and the line parallel to the maxillary cheek teeth occlusal surface (D). The distance between the caudolateral aspect of the Triadan 11s occlusal surface to the orbital reference line (Y) and the distance between the caudolateral aspect of the caudal tooth root of Triadan 11 and the orbital reference line (X) were measured. Almost all of the Triadan 11 in the younger horse is caudal to the orbital reference line, while all of the Triadan 11 is rostral to this reference line in the older horse. Note the three-dimensional volume rendering image of the skull in figure 1A, showing the reference line C and D.

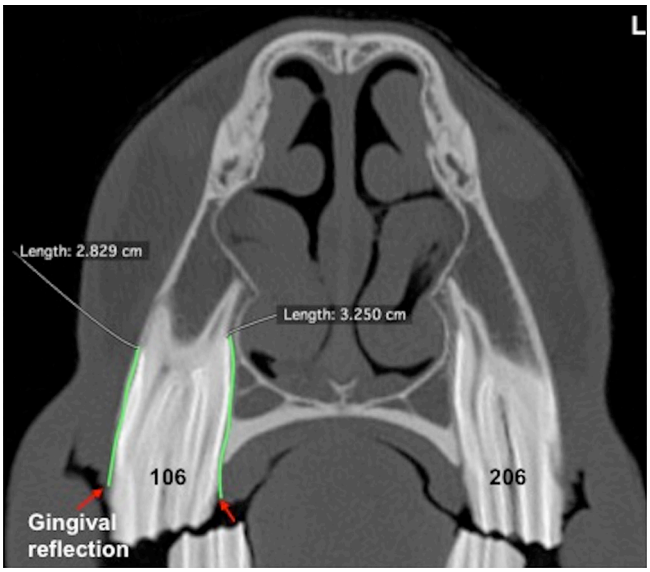

FIG 2: Transverse CT image of an adult horse at the level of Triadan 09. Note the difference in the lengths of the palatal and buccal aspects of the reserve crown, due to occlusal angulation. The green lines on the buccal and palatal aspects of the tooth represent joined points created by an open polygon tool that was used to measure these curved structures. The sites of gingival reflection (boundary between clinical and reserve crown) on the palatal and buccal aspect of this tooth has been indicated with red arrows *L, left*.

Statistical analyses

Sinus and head volume and linear measurements were assessed for normality using Shapiro-Wilk tests, the results of which were used to guide appropriate statistical test choice.

Paired T-tests were used to examine for significant differences in volume of the seven sinus compartments, and in length measurements between the left and right sides of each head.

To assess the relationships between mean sinus compartment and head volumes, scatter plots with lines of best fit were produced. Linear regression was performed to assess whether the mean volumes of individual sinus compartments and total head volumes were significantly associated.

To assess for significant differences in sinus compartment volumes, Triadan 11 positions relative to the orbital bone and crown length between age groups, measurements adjusted to head size were calculated as follows:

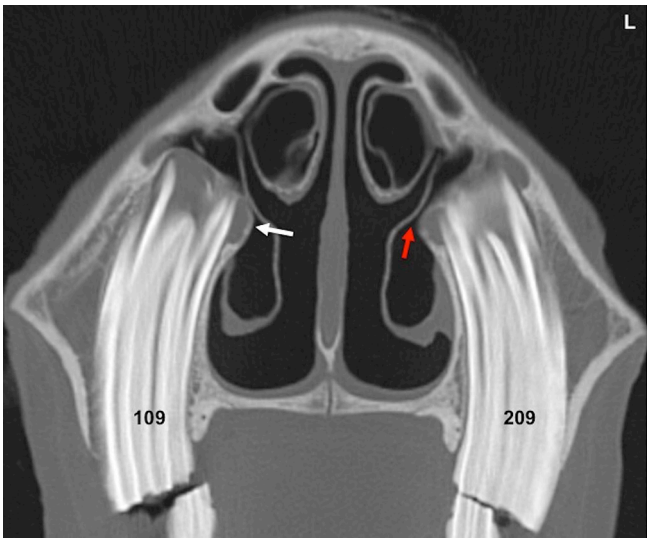

FIG 3: Transverse CT image of a horse aged one year at the level of 09. Note the mediodorsal location and the intimate relationship of the infraorbital canals (white arrows) with the dental apex. Note also the restricted conchomaxillary drainage in this young horse (red arrow). *L, left*.

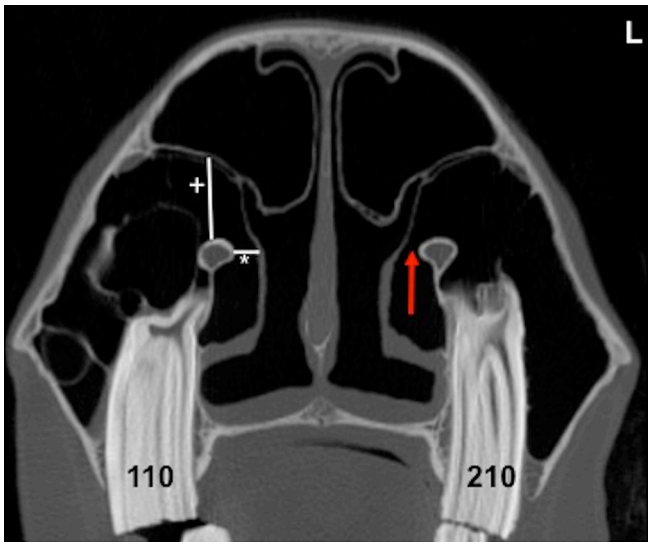

FIG 4: Transverse CT image of a horse aged 12 years at the level of Triadan 10. Note the distance between the infraorbital canal (IOC) and the medial (*) or dorsal (+) ventral conchal sinus wall; note the conchomaxillary aperture (red arrow). The horizontal and vertical line to the IOC represent the size of the conchomaxillary ostium. *L, left*.

Adjusted sinus volume = (mean measured sinus volume/measured head volume) × 100.

Adjusted Triadan 11 position (both apical and occlusal) = (mean measured length/measured head length) × 100.

Adjusted crown length = (mean measured crown length/measured head height) × 100.

Box and whisker plots were produced to visualise the spread of adjusted sinus volumes between the three age groups (fig 5).

Analysis of variances were performed to determine whether adjusted sinus volumes, Triadan 11 positions and reserve crown lengths differed significantly between age groups.

Results

Gross observations

All 90 heads, including the 26 with sinonasal or significant maxillary cheek teeth disorders, had grossly intact maxillary septae, including the dorsally situated maxillary septal bulla (previously misnamed 'ventral conchal bulla') that was often not fully detectable on CT imaging. There was much variation in the overall size and shape of this bulla, that is, in how far caudally, dorsally and lateromedially it protruded into the caudal maxillary sinus.

Position of cheek teeth in relation to the maxillary sinuses

The alveoli of the maxillary: 06s and 07s were not in contact with any sinus lumen in any age group; All 08s were partly or fully within the RMS; 09s were fully within the RMS in all, except two young (aged 1.5 and 2 years) cases where they were fully in the CMS; 10s were variably in the RMS or CMS; and 11s were consistently within the CMS (table 1).

Position of the IOC in relation to cheek teeth alveoli

In the nine youngest horses (aged one to two years), the IOC lay in direct contact with the mediodorsal aspect of the alveolus (fig 3), appearing to share a common bony wall initially. In the 51 horses older than two years, the IOC ran dorsomedial to the maxillary cheek teeth alveoli, connected only by a bony septum that increased in height with age and dental eruption. There was no significant difference in the distance between the dental apices and the IOC: between left and right sides; rostral and caudal roots and Triadan positions. As expected, the distance between the dental apices and the IOC increased with age (table 2).

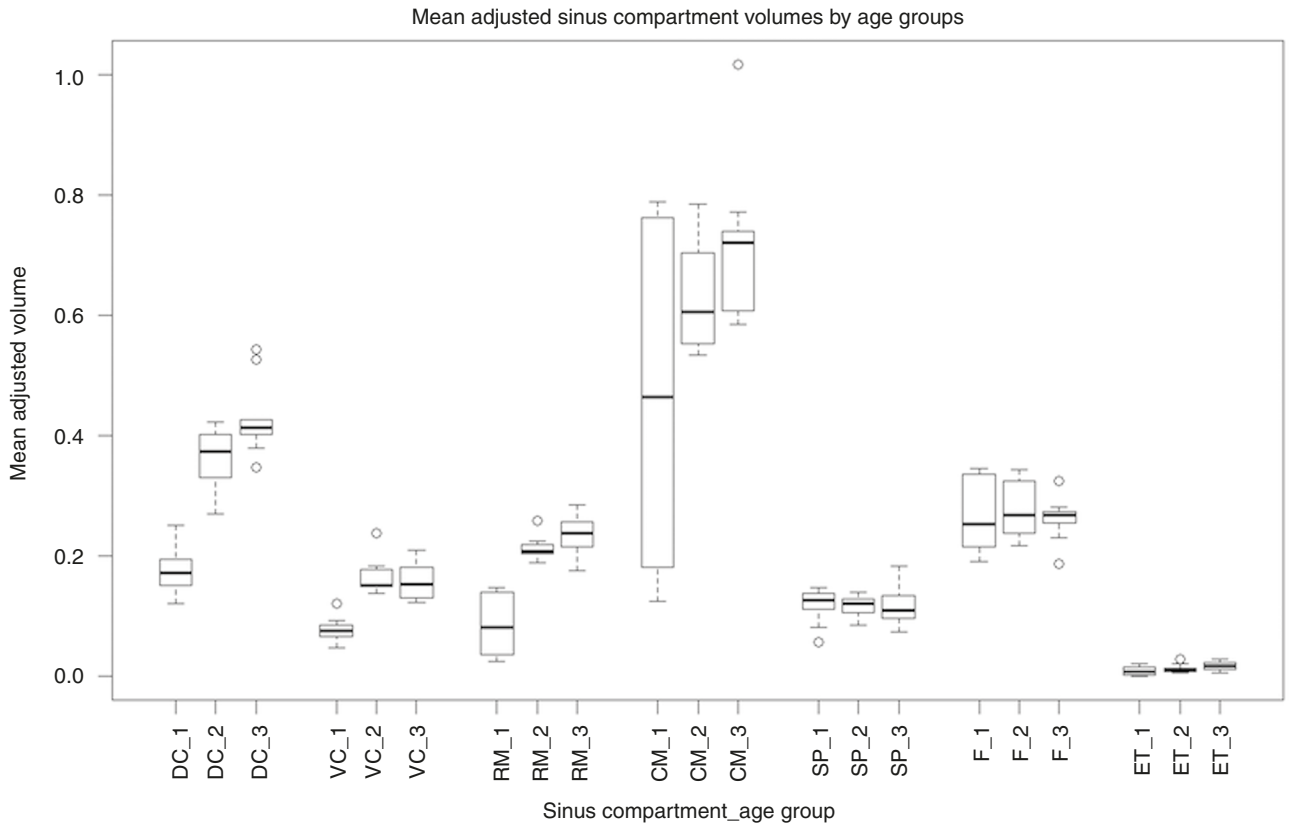

FIG 5: Mean adjusted sinus compartment volumes subdivided by age groups. Sinus compartments: DC, dorsal conchal; VC ventral conchal; RM rostral maxillary; CM, caudal maxillary; SP, sphenopalatine; F, frontal; ET, ethmoidal. Age groups: 1=<6 years old; 2=6–15 years old; 3=>15 years old. Lower and upper box lines=25th and 75th percentiles, respectively; middle box line in bold=median; lower and upper whiskers=lower and upper adjacent values, respectively; open circles=outliers.

The distance between the IOC and the medial (horizontal measurement) or dorsal (vertical measurement) wall of the ventral conchal sinus (VCS) (fig 4), that is, the narrowest and widest aspects of the conchomaxillary ostium showed no significance difference between left and right side ($P>0.8$) and mean values are given in table 3.

Rostral migration of maxillary cheek teeth

The distances between the caudal aspects of the Triadan 11 clinical crowns and apices and the reference site (orbital rim) were measured in the 53/60 heads where the Triadan 11 teeth had erupted. There was no significant difference between the left and right side measurements, and means of these values were subsequently used for statistical analyses.

TABLE 1: Location of dental alveoli in relation to the maxillary sinuses in 60 heads.

Triadan	Group 1 (<6 yo) (n=15)	Group 2 (6–15 yo) (n=21)	Group 3 (>15 yo) (n=24)
106/206	N/A	N/A	N/A
107/207	N/A	N/A	N/A
108/208	RMS (7) p RMS (8)	RMS (18) p RMS (3)	RMS (22) p RMS (2)
109/209	RMS (13) CMS (2)	RMS (21)	RMS (24)
110/210	RMS (6) CMS (9)	RMS (15) CMS (6)	RMS (11) CMS (9) R/CMS (4)
111/211	CMS (8) N/A (7)	CMS (21)	CMS (24)

yo, years old; N/A, not in any sinus; RMS, rostral maxillary sinus; CMS, caudal maxillary sinus; R/CMS, partly in rostral and caudal maxillary sinuses; p, alveolus partly in sinus

In 5/8 heads in group 1 (aged <6 years) and in 6/21 heads of group 2 (aged 6–15 years), the caudal aspect of the clinical crown of the Triadan 11 s lay caudal to the orbital reference line. Because of the caudally directed curvature of the Triadan 11 s, the caudal aspect of the apices in all (8/8) heads in group 1 and 10/21 heads in group 2 lay caudal to the orbital rim.

In all other heads, both dental landmarks were rostral to the orbital rim. The mean absolute (and adjusted) distances between the orbital landmark and the caudal clinical crown; and the apices of the Triadan 11 s are shown in table 4. The adjusted mean distances were significantly different between age groups for both the caudal clinical crown ($F[2,50]=17.15$, $P<0.001$) and apices ($F[2,50]=15.85$, $P<0.001$), with the mean absolute (and adjusted) distance of the clinical crowns and apices of the Triadan 11 s in group 3 (aged >16 years) being 2.48 cm (5.2%) and 2.83 cm (6.2%) more rostral, respectively, than those in group 1 (aged <6 years).

Length of reserve crown in maxillary cheek teeth

Mean absolute (and adjusted) reserve crown lengths, for each Triadan position and age group are shown in table 5. There was no statistical difference between left and right side reserve

TABLE 2: Mean distances (cm) between the dental apices and the infraorbital canal (IOC) in horses of different ages

Triadan position	Age group 1 <6 yo	Age group 2 6-15 yo	Age group 3 >15 yo
08	0.8	1.5	2.6
09	1.7	2.5	4
10	0.6	1.5	3.6
11	0.5	1.3	3.4
Mean of all teeth	0.9	1.7	3.4

yo, years old.

TABLE 3: Mean distance (cm) between the infraorbital canal and the medial and dorsal walls of ventral conchal sinus (conchomaxillary opening) level with Triadan 10 and 11 positions.

Plane of measurement	Age group	1	2	3
Horizontal	At Triadan 10	0.3	0.6	0.6
Horizontal	At Triadan 11	0.4	0.9	0.8
Vertical	At Triadan 10	1.7	3.1	2.2
Vertical	At Triadan 11	1.9	2.9	2.4

crown lengths, and mean values were used for comparison between age groups. Mean adjusted reserve crown lengths differed significantly between age groups for each Triadan position: 06 ($F[2,57]=29.13$, $P<0.001$); 07 ($F[2,57]=23.53$, $P<0.001$); 08 ($F[2,57]=14.58$, $P<0.001$); 09 ($F[2,57]=47.56$, $P<0.001$); 10 ($F[2,57]=59.06$, $P<0.001$) and 11 ($F[2,57]=8.25$, $P<0.001$) with length decreasing with age.

Sinus volumes

There were no significant differences in individual sinus compartment volumes between left and right sides; consequently all further analyses used the mean of left and right measurements. The mean volumes of sinus compartments from the 30 measured skulls and the details of sinus volumes, subdivided by age group are shown in table 6. When accounting for age group, the dorsal choncal sinus (DCS) was larger than the frontal sinus (FS) in group 2 (aged 6–15 years) horses—(121.1 vs 85.1 cm^3) and group 3 (aged >15 years) horses (126.6 vs 79.7 cm^3) but not in group 1 (aged <6 years) horses (37.3 vs 56.7 cm^3) where these compartments were incompletely developed.

The volumes of the two intraconchal sinuses greatly differed, with the DCS approximately two to three times larger than the VCS in all age groups; group 1 (37.3 vs 15.5 cm^3), group 2 (112.1 vs 49.3 cm^3) and group 3 (126.6 vs 46.5 cm^3). Details of sinus volumes, subdivided by compartment and age group are shown in table 6.

The mean 'head' volume from the 30 measured skulls was 27,175 cm^3 (range 9405–37,758 cm^3) in comparison to a mean volume of 31,777 cm^3 (range 25,194–37,076 cm^3) in the known Thoroughbred group (n=12). All individual sinus compartment volumes were significantly positively associated with head volume. The results of the linear regression analyses are shown in table 7.

The adjusted sinus compartment volumes differed significantly between age groups for all except the sphenopalatine sinus (SPS) and the FS (table 6). Graphical representation of the spread

TABLE 6: Average sinus volumes measured by computed tomography in 30 horses subdivided by compartment, average sinus volume subdivided by age group and results of analysis of variance (ANOVA) comparisons of sinus volumes (adjusted to head size) between age groups.

		Mean (SD) sinus volumes (cm^3) by age group			
Paranasal sinus	Mean (SD) sinus volume (cm^3)	Group 1 (aged <6 years)	Group 2 (aged 6–15 years)	Group 3 (aged >15 years)	ANOVA comparisons of adjusted sinus volumes between age groups
Dorsal conchal	92 (43)	37.3 (15.4)	112.1 (24.6)	126.6 (8.7)	F[2,27]=70.94, P<0.001
Ventral conchal	37 (17)	15.5 (5.2)	49.3 (8.7)	46.5 (4.4)	F[2,27]=31.8, P<0.001
Rostral maxillary	52 (27)	20.8 (17.0)	64.5 (12.7)	70.3 (15.0)	F[2,27]=43.63, P<0.001
Caudal maxillary	175 (82)	112.4 (87.2)	193.9 (49.4)	219.7 (67.9)	F[2,27]=5.05, P=0.0137
Sphenopalatine	31 (9)	25.3 (10.8)	35.5 (7.3)	33.4 (6.1)	F[2,27]=0.07 P=0.9343
Frontal	73 (24)	56.7 (22.4)	85.1 (24.0)	79.7 (18.6)	F[2,27]=0.30 P=0.7445
Ethmoidal	4 (3)	2.4 (2.2)	4.0 (2.3)	5.6 (2.7)	F[2,27]=3.38, P=0.0491

F, F value, figures in square brackets refer to the degrees of freedom for the effect and the degrees of freedom for the error term, respectively; significant P values in bold.

TABLE 4: The mean absolute (and adjusted) distances between the rostral orbital landmark and the caudal clinical crown; and the apices of the Triadan 11s

	Group 1 (aged <6 years)		Group 2 (aged 6–15 years)		Group 3 (aged >15 years)	
Orbital landmark to:	Mean (SD) absolute distance (cm)	Mean (SD) adjusted distance (%)	Mean (SD) absolute distance (cm)	Mean (SD) adjusted distance (%)	Mean (SD) absolute distance (cm)	Mean (SD) adjusted distance (%)
Caudal clinical crown	0.28 (1.3)	0.8 (2.7)	−0.7 (1.2)	1.4 (2.5)	−2.2 (1.2)	−4.4 (2.2)
Apices of Triadan 11	2.3 (1.4)	5.1 (3.4)	0.5 (1.6)	1.1 (3.3)	−0.53 (0.9)	−1.1 (1.8)

TABLE 5: Mean (of left and right sides) absolute and adjusted reserve crown lengths, subdivided by Triadan position and age group.

	Group 1 (aged <6 years)		Group 2 (aged 6–15 years)		Group 3 (aged >15 years)	
Triadan tooth	Mean (SD) absolute length (cm)	Mean (SD) adjusted length (%)	Mean (SD) absolute length (cm)	Mean (SD) adjusted length (%)	Mean (SD) absolute length (cm)	Mean (SD) adjusted length (%)
06	4.1 (1.3)	17.0 (5.3)	3.3 (0.7)	11.9 (2.4)	2.3 (0.7)	8.4 (2.6)
07	4.8 (1.5)	19.9 (6.0)	4.5 (0.7)	16.0 (3.3)	3.0 (0.9)	10.8 (3.4)
08	4.5 (1.8)	18.5 (6.6)	5.1 (0.9)	18.4 (3.9)	3.3 (1.0)	11.8 (3.8)
09	5.5 (1.0)	23.5 (6.1)	4.3 (0.8)	15.4 (3.3)	2.8 (1.0)	9.9 (3.5)
10	6.1 (0.8)	25.6 (4.3)	5.0 (1.0)	17.7 (3.9)	3.2 (1.0)	11.4 (3.8)
11	3.5 (2.4)	13.9 (9.2)	4.8 (0.9)	17.2 (3.9)	2.9 (1.0)	10.4 (3.7)

Adjusted reserve crown length calculated as a percentage of measured head height.

TABLE 7: Results of linear regression analysis of sinus compartment volumes compared with head volumes, measured in 30 equine heads

Sinus	Coefficient	Lower 95% CI	Upper 95% CI	se	P value
Dorsal conchal	0.0047	0.0033	0.0060	0.0007	<0.001
Ventral conchal	0.0016	0.0010	0.0022	0.0003	<0.001
Rostral maxillary	0.0032	0.0025	0.0038	0.0003	<0.001
Caudal maxillary	0.0100	0.0082	0.0119	0.0009	<0.001
Sphenopalatine	0.0009	0.0006	0.0012	0.0002	<0.001
Frontal	0.0029	0.0022	0.0035	0.0003	<0.001
Ethmoidal	0.0002	0.0001	0.0003	0.0000	<0.001

of adjusted sinus compartment volumes for the different age groups is shown in fig 5.

Discussion

It is commonly stated that the alveoli of the maxillary Triadan: 06–07 lie in the maxillary bone; 08–09 lie within the RMS/VCS and 10–11 lie within the CMS, in young-adult horses,[16] but little objective information on the intrasinus disposition of these alveoli is available. The current study found the Triadan 09 alveoli to be located in the CMS in only 2/15 (13%) of the youngest group and the Triadan 10 alveoli to be fully positioned in the RMS in 53% of all cases (32/60 heads). The difference between this finding and conventionally accepted information is difficult to explain, but may be related to variation in the site and in the degree of caudomedial obliquity of the maxillary septum. The rostral aspect of the maxillary septum was reported to be rostral to the 09 s in 47% of cases and to the 10 s in 44% of cases in a previous study.[10] However, the variation in the obliquity of the maxillary septum means that assessment of the intrasinus position of each tooth has to be assessed over the full width of each alveolus.

Knowledge of the position of the IOC in relation to the cheek teeth apices is important to understand its susceptibility to damage from apical infection, and to avoid its damage during dental repulsion or sinus surgery.[16 17] The intimate relationship of this canal and the medial aspect of the maxillary cheek teeth alveoli in horses aged less than two years also makes the IOC susceptible to damage from extension of apical infection.[18] In this study, all horses older than two years had complete separation of the IOC and the apices of all the maxillary cheek teeth, despite root elongation with cementum following eruption.[9 19] In horses aged <6 years (group 1), the IOC was closer (mean distance 0.9 cm) to the dental apices than in older horses (1.7 cm in group aged 6–15 years and 3.4 cm in the group aged >15 years) making sinus surgery (particularly of the RMS) in younger horses more challenging. These findings also indicate that drainage of the VCS into the RMS by fenestrating the septum between IOC and dental apex is only practical in horses aged 15 years and older.

Probst and others[20] reported the conchomaxillary opening to be 1–8 mm wide, but did not describe age-related differences in this parameter. In this study, both the narrowest and widest sites were measured and younger horses were found to have a smaller conchomaxillary opening than older horses, likely due to the large reserve crown within the VCS narrowing of this ostium (fig 6). The small dimensions of the conchomaxillary ostium (mean of 6 mm in adults) readily explains why with sinus inflammation and mucosal thickening, it will become sealed such that the VCS loses its drainage into the RMS.

Equine cheek teeth normally drift in a rostral (mesial) direction with age,[9] which is likely contributed to by the continued eruption of the rostrally angulated clinical crowns (caudally angulated reserve crowns) of the caudal cheek teeth, especially the 11 s (equivalent to the 'wisdom tooth' in humans).[19] Posteruptive dental movement in brachydont teeth compensates for interproximal wear and the rostrally (mesially) directed brachydont dental drift is mainly caused by normal occlusal forces and by trans-septal ligament contraction.[8] Such rostral drift is additionally needed by equine teeth because they taper in towards their apices, thus making the clinical crown smaller with age,[19] but in contrast to some brachydont species, equine dental drift is restricted by the caudally angulated Triadan 06.

The presence of effective rostral dental drift can bring and also keep the occlusal aspects of cheek teeth in tight contact and thus can resolve cheek teeth diastemata in younger horses and continually prevent it in adults. Rostral drift also influences the degree and speed of postextraction site closure.

In the current study, the mean positions of the clinical crowns and apices of the Triadan 11 s were 2.48 cm (adjusted 5.2%) and 2.83 cm (adjusted 6.2%) more rostral, respectively in the oldest than the youngest group, consistent with dental drift. The caudal aspect of the 11 s can demonstrate more dramatic changes in position as the more horizontal aspect of this curved tooth erupts and thus shortens the tooth. However, the variable laying down of root cementum that elongated the apical aspect of some teeth, made the apex a less reliable landmark than the crown to assess dental drift. These measurements on dental drift could provide further objective radiographic guidelines on ageing horses by dental imaging.

Equine dental reserve crown length decreases with age, but this prolonged eruption has not been well quantified. The reserve crown length decreased from a mean of 4.7 cm (adjusted length 19.7%) of all 12 teeth in the youngest (aged <6 years) horses to a mean of 2.9 cm (adjusted length 10.5%) in the oldest group (aged >15 years), with the 06 s and 09 s having the shortest reserve crowns. The horse heads in this study were all aged by their dentition into five-year groupings. Due to the limitations of these dental ageing techniques, it is possible that some heads could have been placed into an incorrect age group. A study where the exact age of each horse was known would provide more valuable information in this regard. A small number of horses were borderline for placement in the group aged 6-15 years or alternatively the group aged >15 years, but following further examinations a consensus was reached to allow them to be placed in one group. The use of CT images of clinical cases without identifiable cheek teeth abnormalities would allow a more precise

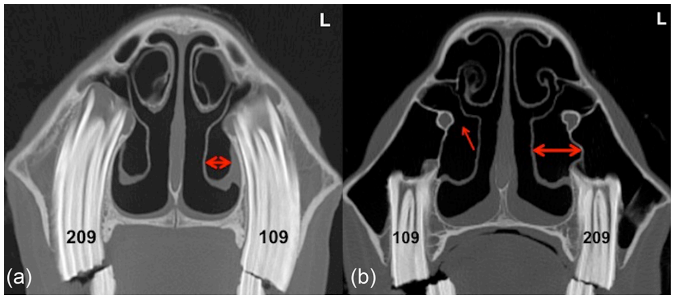

FIG 6: Transverse CT image of a horse aged 1 year (A) and a horse aged 10 years (B) at the level of Triadan 09. Note the compression of the ventral conchal sinus (VCS) (double arrow head) by the tall reserve crowns in the young horse as compared with the adult horse, and the height of the septum beneath the infraorbital canal that separates the VCS and the RMS (red arrow) in the mature horse. *L, left*.

ageing of cases, but would not allow the anatomical head dissections that were performed on most of these heads to verify the imaging findings.

The concept of two functional sinus compartments termed the rostral and caudal sinus systems[10 21] was supported in this study by the presence of an intact maxillary septum on gross examinations in all 90 heads originally examined, including those with sinonasal or significant dental disease, where the maxillary septum was sometimes thickened but never perforated, as was found in 2.5% of sinusitis cases in one clinical study.[22]

No significant differences were found between left and right individual sinus compartment volumes as previously noted.[10] Significant age-related increases in sinus compartment volumes were observed for the DCS, VCS, CMS, RMS, SP, but not for the small ES and large FS. Brinkschulte and others[10] also found that most age-related differences in volume occurred in the RMS, VCS and CMS compartments,[10] all which contain dental alveoli and so would be expected to increase in volume with dental eruption.[8 9] The volume of the other sinus compartments are unaffected by dental eruption, but growth in head size would influence the dimensions of all sinus compartments in the younger group. Similar to previous findings,[10] the current study identified a significant positive association between head volume and the individual sinus compartment volumes.

The sinus compartment volumes found in this study (table 6) were similar to those of the Brinkschulte and others[10] study, where 14/18 examined horses were Warmbloods, of a similar age distribution to the current study. The main difference between the current findings and those of the previous study[10] were the much smaller FS and larger DCS volumes found in the current study, that is, means of 73.8 and 92 cm^3, respectively vs means of 186.0 cm^3 for FS vs 41.7 cm^3 for DCS by Brinkschulte and others.[10] While different methodologies were used to assess volumes in these two studies, the above discrepancy is most likely due to differences in the convoluted boundary used to separate the DCS and FS in these two studies, because the combined values of the FS and DCS (ie, the conchofrontal sinus) was very similar between studies, that is, 204.7 cm^3 in the current vs 227.8 cm^3 in the previous study.[10] Interstudy differences in results may also reflect breed differences between the two studies as no breed information was available for the 30 heads used in the current study, although as shown, they were similar to the size of Thoroughbreds to that are somewhat smaller than the Warmbloods used by Brinkschulte and others,[10] but overall, this larger study validates the former study. The small size of the VCS (mean volume 37 cm^3; SD=17 cm^3) can explain the difficulty in performing sinoscopy on this compartment in some, especially in younger horses.

Multiple studies have reported the use of three-dimensional CT to assess: normal human sinus anatomy during development,[23 24] sinus fractures[25] and to develop a staging system to correlate symptoms with radiological imaging results in patients with chronic rhinosinusitis.[26] Potentially, future equine CT studies could provide a similar grading system to guide treatment in cases of primary sinusitis.

Acknowledgements

The authors would like to thank Justin Perkins from the Royal Veterinary College in London for his contribution of CT data from 36 horses.

Competing interests None decared.

Ethics approval This study was approved by the Royal (Dick) School of Veterinary Studies and the Royal Veterinary College Ethical Review Committees.

References

1 MORROW KL, PARK RD, SPURGEON TL, *et al*. Computed tomographic imaging of the equine head. *Vet Radiol Ultrasound* 2000;41:491–7.
2 HENNINGER W, FRAME EM, WILLMANN M, *et al*. CT features of alveolitis and sinusitis in horses. *Vet Radiol Ultrasound* 2003;44:269–76.
3 SOLANO M, BRAWER RS. CT of the Equine Head: Technical Considerations, Anatomical Guide, and Selected Diseases. *Clin Tech Equine Prac* 2004;3:374–88.
4 VERAA S, VOORHOUT G, KLEIN WR. Computed tomography of the upper cheek teeth in horses with infundibular changes and apical infection. *Equine Vet J* 2009;41:872–6.
5 WINDLEY Z, WELLER R, TREMAINE WH, *et al*. Two- and three-dimensional computed tomographic anatomy of the enamel, infundibulae and pulp of 126 equine cheek teeth. Part 1: Findings in teeth without macroscopic occlusal or computed tomographic lesions. *Equine Vet J* 2009;41:433–40.
6 BÜHLER M, FÜRST A, LEWIS FI, *et al*. Computed tomographic features of apical infection of equine maxillary cheek teeth: a retrospective study of 49 horses. *Equine Vet J* 2014;46:468–73.
7 DIXON PM, FROYDENLUND T, LUITI T, *et al*. Empyema of the nasal conchal bulla as a cause of chronic unilateral nasal discharge in the horse: 10 cases (2013-2014). *Equine Vet J* 2015;47:445–9.
8 DYCE KM, SACK OW, WENSING CJG. The head and ventral neck of the horse In. *Textbook of veterinary anatomy*. 4th edn. Edinburgh: Elsevier, Saunders, 2010:479–509.
9 SISSON S, GROSSMAN JD. The digestive system In. *The anatomy of the domestic animals*. 4th edn revised. Philadelphia: WB Saunders Co, 1953:463–87.
10 BRINKSCHULTE M, BIENERT-ZEIT A, LÜPKE M, *et al*. Using semi-automated segmentation of computed tomography datasets for three-dimensional visualization and volume measurements of equine paranasal sinuses. *Vet Radiol Ultrasound* 2013;54:n/a–90.
11 BRINKSCHULTE M, BIENERT-ZEIT A, LÜPKE M, *et al*. The sinonasal communication in the horse: examinations using computerized three-dimensional reformatted renderings of computed-tomography datasets. *BMC Vet Res* 2014;10:72.
12 BAHAR S, BOLAT D, DAYAN MO, *et al*. Two- and three-dimensional anatomy of paranasal sinuses in Arabian foals. *J Vet Med Sci* 2014;76:37–44.
13 MUYLLE S. Ageing. In: EASLEY J, DIXON PM, SCHUMACHER J, eds. *Equine dentistry*. 3rd edn. St Louis: Elsevier, Saunders:85–96.
14 LIUTI T, REARDON R, SMITH S, *et al*. An anatomical study of the dorsal and ventral nasal conchal bullae in normal horses: Computed tomographic anatomical and morphometric findings. *Equine Vet J* 2016;48:749–55.
15 BROWN SL, ARKINS S, SHAW DJ, *et al*. Occlusal angles of cheek teeth in normal horses and horses with dental disease. *Vet Rec* 2008;162:807–10.
16 DIXON PM, HAWKES C, TOWNSEND N. Complications of equine oral surgery. *Vet Clin North Am Equine Pract* 2008;24:499–514.
17 TREMAINE WH. *Complications associated with dental and paranasal sinus surgery*: Published in IVIS with the permission of the AAEP, 2006.
18 EASLEY JT, FREEMAN DE. New ways to diagnose and treat equine dental-related sinus disease In. *The Veterinary clinics of North America. Equine practice*. , 2013:29, 467–85.
19 DIXON PM, DU TOIT N. Dental Anatomy. In: EASLEY J, DIXON PM, SCHUMACHER J, eds. *Equine dentistry*. 3rd edn: Elsevier, Saunders, 2011:p51–76.
20 PROBST A, HENNINGER W, WILLMANN M. Communications of normal nasal and paranasal cavities in computed tomography of horses. *Vet Radiol Ultrasound* 2005;46:44–8.
21 O'LEARY JM, DIXON PM. A review of equine paranasal sinusitis. Aetiopathogenesis, clinical signs and ancillary diagnostic techniques. *Equine Vet Educ* 2011;23:148–59.
22 DIXON PM, PARKIN TD, COLLINS N, *et al*. Equine paranasal sinus disease: a long-term study of 200 cases (1997-2009): treatments and long-term results of treatments. *Equine Vet J* 2012;44:272–6.
23 KAWARAI Y, FUKUSHIMA K, OGAWA T, *et al*. Volume quantification of healthy paranasal cavity by three-dimensional CT imaging. *Acta Otolaryngol Suppl* 1999;540:45–9.
24 PARK IH, SONG JS, CHOI H, *et al*. Volumetric study in the development of paranasal sinuses by CT imaging in Asian: a pilot study. *Int J Pediatr Otorhinolaryngol* 2010;74:1347–50.
25 BELINA S, CUK V, KLAPAN I. Virtual endoscopy and 3D volume rendering in the management of frontal sinus fractures. *Coll Antropol* 2009;33:43–51.
26 DEEB R, MALANI PN, GILL B, *et al*. Three-dimensional volumetric measurements and analysis of the maxillary sinus. *Am J Rhinol Allergy* 2011;25:152–6.

2.2 Conclusion

The current study found that the Triadan 09 alveoli, that are stated in the literature to lie in the RMS, were located in the CMS in 2/15 (13%) of the youngest group and that the Triadan 10 alveoli, that are stated in the literature to lie within the CMS, were fully positioned in the RMS in 53% of all cases (32/60 heads). These findings could be due to variation in the site and degree of caudo-medial obliquity of the maxillary septum. The variation in the obliquity of the maxillary septum also means that assessment of the intra-sinus position of each tooth must be conducted over the full width of each alveolus.

These new findings will need to be considered by imagers and surgeons, when determining which sinus compartments will be affected by apical infections. For example, lavage of the CMS was believed to be an effective treatment for sinusitis related to maxillary Triadan10 dental infections. However, this study showed that over 50% of Triadan 10s are, in fact, fully or partially within the RMS, indicating that the rostral sinus compartments must also be accessed in order to adequately treat many of these cases.

The rostral drift is of equine cheek teeth has been almost fully ignored to date although it is of great clinical importance. Currently, the common procedure of open mouth oblique radiography in cheek teeth diastemata cases is usually performed to assess the angulation of reserve crowns, to prognosticate on the case, and often to decide on treatment. Horses with poor cheek teeth angulation will not achieve enough dental drift to close diastemata and will consequently have a poor long-term prognosis for dental disease, whilst those with good angulation have a much better drift and thus prognosis.

The presence of effective rostral dental drift can not only brings the occlusal aspects of cheek teeth into tight contact, but it can also maintain this tight relationship. As a result, it can resolve cheek teeth diastemata in younger horses and continually prevent it in adults. The degree of rostral drift found in this study (2.48cm and 2.83cm respectively in the >15 years old vs <6 years old age group) would be more than adequate to close multiple diastemata, that are often just 2mm wide occlusally indicating that horses with normal dental drift should not develop diastemata. This study only examined rostral dental drift caused by the angulation of the Triadan 11 and 10, but not the caudally directed drift caused by the angulated Triadan 06. Additionally, horses were placed in 5 year age groups. A further study on horses of precisely known ages that examined both rostral and caudal drift would be of even greater value.

Knowledge of the position of the IOC in relation to the cheek teeth apices is important to understand its susceptibility to damage from apical infection, and to avoid its damage during dental repulsion or sinus surgery (Tremaine et al 2006, Dixon et al 2008). In this study, the IOC of all horses older than two years of age was completely separate from the apices of all the maxillary cheek teeth.

This study also demonstrated that younger horses have a smaller conchomaxillary opening compared to older horses, possibly due to their large reserve crowns compressing the VCS and thus narrowing this ostium. The small dimensions of the conchomaxillary ostium readily explain why, with sinus inflammation and mucosal thickening, it can become occluded, such that the VCS loses its drainage into the RMS and develops chronic sinusitis.

The width of the conchomaxillary opening was measured at the level of Triadan 10s and 11s, although measurements from the level of Triadan 08 caudally would have given additional clinically relevant anatomical information.

Drainage of the VCS into the RMS by fenestrating the septum between the IOC and dental apex is possible in adult horses. Because over 10mm of distance is present between the IOC and alveoli by 10 years of age, this age rather 15 years of age as was cited in this article is more correct.

Equine dental reserve crown length decreases with age. The mean length of all 12 cheek teeth reserve crowns decreased from 4.7 cm (19.7% of tooth length) in the youngest horses (<6y.o.) to a mean of 2.9 cm (adjusted length 10.5% of its length) in the oldest group (>15y.o.), with the 06s and 09s having the shortest reserve crowns.

The current study found no significant differences between left and right individual sinus compartment volumes as previously noted (Brinkschulte et al 2013).

Significant age-related increases in sinus compartment volumes were observed for the DCS, VCS, CMS, RMS and SP but not for the small ES and large FS. Dental eruption and growth in head size are the main influence on the dimensions of the sinus compartment in horses of different age. Similar to the findings of Brinkschulte et al (2013) the current study identified a significant positive relationship between head volume and the individual sinus compartment volumes.

The information provided in this chapter provides valuable, clinically relevant information on the anatomical characterization of the equine skull; especially on the relationships of the maxillary cheek teeth to other head structures and also in some age-related changes in these relationships. The use of 3D printing or advanced

software could provide a more tangible experience to undergraduate students who should be aware of the anatomical difference between different aged equine heads and also knowledgeable of important anatomical structure including the infraorbital canal, dental reserve crowns and physiological changes including dental eruption and drift.

CHAPTER 3: An anatomical study of the dorsal and ventral nasal conchal bullae in normal horses: Computed tomographic anatomical and morphometric findings

Paper published in Equine Veterinary Journal 2016 (48), 749-755

3.1 Introduction

This chapter describes the use of CT in the anatomical evaluation of the dorsal and ventral nasal conchal bullae in horses of different ages. The dorsal and ventral conchal bullae are poorly described anatomical structures located in the nasal conchae. Recently, infection of these bullae has been described as a cause of unilateral nasal discharge in horses. Empyema of the dorsal or ventral conchal bulla can occur concurrently with paranasal sinusitis, exacerbating the clinical signs. Less commonly, it can occur as an isolated disorder unrelated to sinusitis (Dixon et al 2015).

The aims of this study were to provide a description of the relationship between the maxillary cheek teeth and the ventral and dorsal conchal bullae and to give a detailed CT anatomical description of both bullae. The new information generated will help to differentiate paranasal sinusitis from primary conchal disease on CT imaging. It should also allow improved surgical approaches for the fenestration and drainage of these bullae.

Conception and design of the study was by Tiziana Liuti and Prof. P.M Dixon

Data acquisition was by Tiziana Liuti

Analysis and data interpretation was by Tiziana Liuti and Richard Reardon Drafting of the article was performed by Tiziana Liuti

Revision of the article for intellectual content was by Prof. P.M Dixon, Sionagh Smith, Richard Reardon and Tiziana Liuti

Final approval of the completed article was by Prof. P.M Dixon and Tiziana Liuti

Equine Veterinary Journal

Equine Veterinary Journal ISSN 0425-1644
DOI: 10.1111/evj.12516

An anatomical study of the dorsal and ventral nasal conchal bullae in normal horses: Computed tomographic anatomical and morphometric findings

T. LIUTI*, R. REARDON†, S. SMITH‡ and P. M. DIXON†

Hospital for Small Animals, Diagnostic Imaging, Royal (Dick) School of Veterinary Sciences, University of Edinburgh, Roslin, Midlothian, UK
†Hospital for Large Animals, Surgery Department, Royal (Dick) School of Veterinary Sciences, University of Edinburgh, Roslin, Midlothian, UK
‡Pathology, Royal (Dick) School of Veterinary Sciences, University of Edinburgh, Roslin, Midlothian, UK.

*Correspondence email: tiziana.liuti@ed.ac.uk; Received: 06.03.15; Accepted: 19.09.15

Summary

Reasons for performing study: Infection of the dorsal nasal conchal bulla and ventral nasal conchal bulla has recently been shown to cause clinical disease in horses, but the anatomy of these 2 structures is poorly documented.
Objectives: To describe the anatomical features, dimensions and relationships to adjacent structures of the dorsal conchal bulla and ventra conchal bulla in normal horses using computed tomography (CT).
Study design: Descriptive imaging study using cadavers.
Methods: Computed tomographic images acquired from 60 equine cadaver heads that were shown to be free of sinonasal disease were categorised into 3 age groups (0–5; 6–15; >16 years old). Linear and volumetric measurements and descriptive anatomical assessments of the dorsal conchal bulla and ventral conchal bulla were produced from these CT images and the anatomical relationships between the dorsal conchal bulla and ventral conchal bulla and the adjacent structures, particularly the maxillary cheek teeth, were examined. The associations between bullae dimensions with horse ages and skull dimensions were assessed using linear regression.
Results: Mean (range) dorsal conchal bulla measurements were: length 7.5 cm (4.6–14), width 1.9 cm (1.3–2.5), height 2.8 cm (1.8–4), volume 24 cm^3 (5.9–50.5). Mean ventral conchal bulla measurements were: length 5.7 cm (2.5–8.5), width 1.6 cm (0.7–2.9), height 2.4 cm (0.8–3.7), volume 15 cm^3 (0.4–30). In both dorsal conchal bulla and ventral conchal bulla, there were significant differences in sizes between the different age groups (smaller in younger animals). In the ventral conchal bulla, this was probably related to protrusion of the large dental alveoli of younger horses into the lateral nasal cavity. Measures of bullae size and volume were significantly associated with head size. The anatomical positions (rostro-caudal boundaries) of the dorsal conchal bulla and ventral conchal bulla were closely associated with specific maxillary cheek teeth.
Conclusions: Computed tomography was a useful technique to establish the linear and volumetric dimensions of the nasal conchal bullae in normal horses. Both dorsal conchal bulla and ventral conchal bulla sizes increased with animal age. Relatively consistent anatomical relationships were shown between the rostral and caudal limits of the bullae and certain maxillary cheek teeth, which would be of diagnostic value with conventional radiography and act as landmarks in the surgical treatment of nasal bulla disease.

Keywords: horse; nasal conchal bulla; ventral conchal bulla; dorsal conchal bulla; anatomy; computed tomography

Introduction

The standard nasal conchal (turbinate) pattern in domestic animals is of large dorsal and ventral conchae attached to the lateral aspect of the nasal cavity, with a smaller middle conchus lying between them [1]. The equine dorsal and ventral nasal conchae are relatively simple in shape compared with many other species. Both comprise a single scroll of mucosa-covered, thin bone, with the dorsal concha scrolled ventrally and the ventral concha scrolled dorsally, without any of the complex, secondary conchal scrolls that are present in many other domestic species [1–4].

The dorsal and ventral equine nasal conchae each contain an air-filled bulla, previously termed the 'scrolled portion of the dorsal turbinate' and 'the large bulla of the middle portion of the ventral turbinate' [5], and more recently and correctly as the *bulla conchalis dorsalis* and *bulla conchalis ventralis* [1,6]. In 1952, Espersen published line diagrams of these nasal bullae [7]. Confusingly, the thin, bulbous, dorsal aspect of the maxillary septum has also frequently been termed the 'ventral conchal bulla' [8]; however, it has recently been recommended that this structure is more appropriately termed the maxillary septal bulla (bulla of the *septum sinuum maxillarium*) [7,9].

Diseases of the paranasal sinuses are the most common cause of unilateral nasal discharge in horses [10,11]. Empyema of the dorsal conchal bulla or the ventral conchal bulla can occur concurrently with paranasal sinusitis, exacerbating the clinical signs, or less commonly as a sole disorder [9]. Despite the clinical importance of the nasal conchal bullae, their anatomy remains poorly described.

Computed tomography (CT) permits much more accurate imaging of the complex equine sinonasal region [3,4,9,12,13]. In a companion study we examined the gross anatomical and histological features of these nasal bullae in normal horses. The aim of the current study was to describe the anatomy of the dorsal conchal bulla and ventral conchal bulla using CT, focusing on their linear and volumetric dimensions, and age-related changes in these parameters, and the anatomical relationships of the bullae to adjacent maxillary cheek teeth.

Material and methods

Specimens

Heads were available from 2 sources:

Group A. The heads of 54 horses with unknown histories and similar in size to Thoroughbreds were collected from an abattoir.

Group B. Anatomical and CT images of a further 36 equine heads that had also been obtained from an abattoir were obtained from Justin Perkins of the Royal Veterinary College.

The age of animals in both groups was estimated by clinical and/or imaging dental examinations and categorised into one of 3 age groups: 0–5 years old (n = 13); 6–15 years old (n = 21); >16 years old (n = 26).

Imaging protocols

CT images of the *Group A* heads were acquired with a multislice scanner (Siemens Volume Zoom)[a] using a 512 × 512 matrix, 120 kV, 300 mA, at a slice thickness of 1.5 mm, with the skulls positioned on their mandibles. Transverse CT images of the head were acquired in a helical scan mode. The CT images of the *Group B* heads were acquired using a 4th generation, Universal Medical Systems CT scanner, GE Lightspeed Ultra[b], at 1.25 mm slice thickness, 120 kV, 300 mA.

The CT images were examined by imaging and surgical diplomates (*Group A*) and by a surgical diplomate (*Group B*) for the presence of sinonasal disease or significant dental abnormalities including: apical changes, presence of gas within dental pulps and apices, dental dysplasia, supernumerary teeth, apical fractures, sinus mucosal thickening, abnormal sinus content, and frontal, nasal or maxillary bone changes. Suspect lesions were subsequently directly examined following transverse or longitudinal sectioning of the skulls using a band saw.

Twenty-six of 54 heads in *Group A* had clinical and/or imaging evidence of dental or sinonasal disease and were excluded from the study leaving 28 heads in this group. Four of the 36 heads in *Group B* had clinical and/or imaging evidence of dental or sinonasal disease and were also excluded leaving 32 heads in this group. (Total of 60 heads.)

Image manipulation

Bone window CT data were collected for review and the CT data were transferred as DICOM images to imaging software (OsiriX, Apple®) [14] which was used to perform multiplanar reconstructions of images to allow identification and descriptions of the dorsal conchal bulla and ventral conchal bulla and to perform all measurements.

Measurements

Bullae linear dimensions: Using OsiriX® software, linear measurements (maximum length, height and width) were made for each dorsal conchal bulla and ventral conchal bulla. Dorsal reconstructions of images (Fig 1a,b) were used for measurements of bullae lengths and widths, while sagittal reconstructions (Fig 2a,b) were used to measure bullae heights. Means and ranges were produced for each linear measurement.

Bullae volumes: The volume of each bulla was calculated using 3-dimensional regions of interest (3D ROIs)/Volume (Osirix® software) in 2 ways:

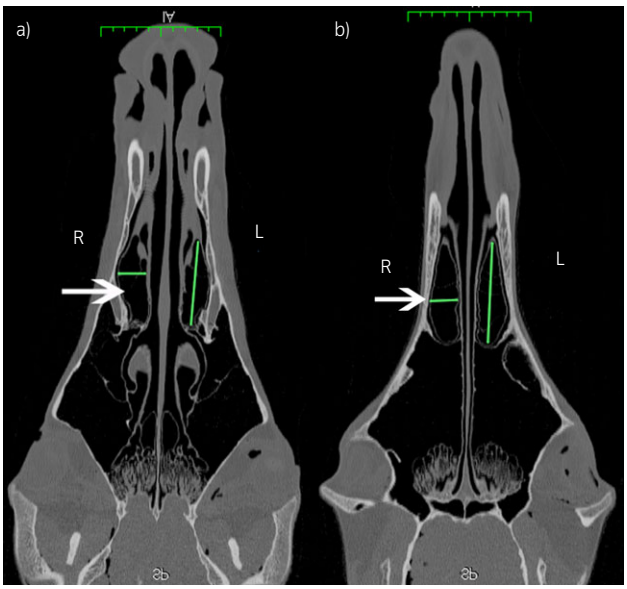

Fig 1: Dorsal multiplanar reconstruction of a cadaver equine head. L, left; R, right. White arrows show sites of measurement of the length and width of the ventral conchal bulla (a) and dorsal conchal bulla (b).

1 Total slice protocol. The internal boundary of each bulla was outlined on *transverse* images using every image slice (with a 1.5 mm slice thickness n = 28 horses; with a 1.25 mm slice thickness n = 32 horses) resulting in a mean of 60 slices per bulla.
2 Limited slice protocol. To reduce the time taken, the internal boundary of each bulla was outlined on *transverse* images using just 4 or 5 slices per bulla.

Head linear dimensions and volumes: 'Head length' was measured from CT sagittal reconstruction from the caudal aspect of the orbit to the naso-incisive notch. 'Head width'was measured from CT dorsal reconstruction across the width of the hard palate at Triadan 06 level and 'head height' was measured using CT sagittal reconstruction from the hard palate to the dorsal aspect of the maxillary bone, also at Triadan 06 level. These 3 measurements were multiplied together to produce a measurement of 'head volume' for each horse.

Assessment of rostral and caudal anatomical limits of bullae in relation to adjacent cheek teeth

In order to describe the anatomical relationships of the bullae to the adjacent maxillary cheek teeth, the rostral and caudal bony limits of each bulla were identified in multiplanar dorsal image reconstructions. The maxillary cheek teeth were subdivided into 5 equal sections rostro-caudally and labelled with odd numbers to facilitate graphing, as shown in Figure 3. Transverse lines (*z*-axis) were drawn from the most rostral and caudal bullae margins and the maxillary tooth and section transected were recorded. A summary of the most rostral and caudal measures from each horse were then plotted, subdivided by age group (Fig 3).

Comparison of head dimensions with those of 12 horses of known breed

To allow comparison of the head sizes in the study population with the head sizes of known breed, computed tomographic studies of 12 Thoroughbreds of known age (4, 0–5 years old; 4, 6–15 years old; 4, >16 years old) that had undergone CT head imaging for clinical reasons other than sinonasal disorders were collected. 'Head' length, width and height were measured and 'head' volume was calculated.

Data analysis

Paired *t* tests were used to examine for statistically significant differences in length, height, width and volume between left and right dorsal conchal bulla and ventral conchal bulla, and between the 2 methods used to calculate conchal bullae volumes. Correlation matrices were calculated and linear regression was used to examine the relationships between bullae sizes and 'head' sizes for each of: length, height, width and volume. Linear regression was used to evaluate the relationship between bullae volumes and age groups.

To examine how the head sizes (length, width, height, volume) of the study population compared with the head sizes of 12 known Thoroughbred breeds, box and whisker plots of head sizes, subdivided by age were produced. Linear regression was used to evaluate whether measures of head size differed significantly between the study population and the known Thoroughbred population. To account for the effect of age, 'age group' was included as an explanatory variable in the linear regression models.

Results

Descriptive morphology

In all cases, the dorsal conchal bulla and ventral conchal bulla were completely enclosed by a thin bony wall, surrounded by *circa* 300° of nasal conchae scrolled ventrally for the dorsal conchal bulla and dorsally for the ventral conchal bulla. The dorsal aspect of the dorsal conchal bulla and the ventral aspect of the ventral conchal bulla had bony and soft tissue attachments to the inner aspects of the nasal conchae that in turn were supported by the bony conchal attachments to the lateral nasal walls. In all

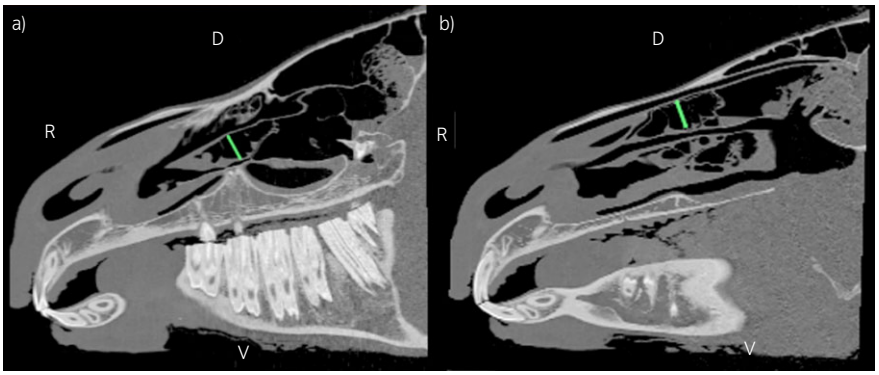

Fig 2: Sagittal multiplanar reconstruction of a cadaver equine head showing sites of measurement of the height of the left ventral conchal bulla (a) and left dorsal conchal bulla (b). D, dorsal; R, rostral; V, ventral.

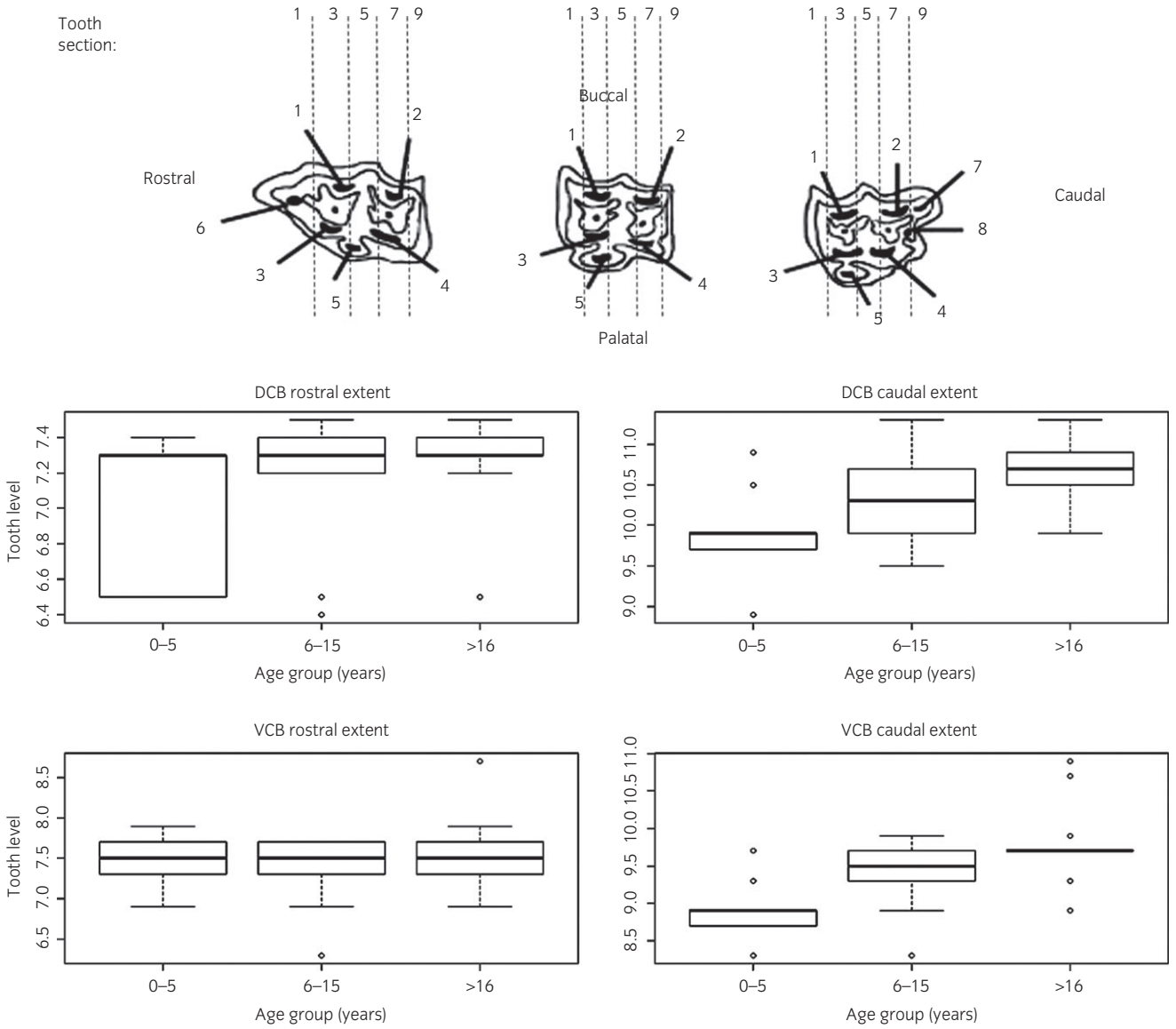

Fig 3: Diagram showing maxillary cheek teeth sections and box plots showing most rostral and caudal extents of the dorsal and ventral conchal bullae, subdivided by age groups. DCB, dorsal conchal bulla; VCB, ventral conchal bulla. Tooth level refers to the level transected: whole number refers to the Triadan number while decimal place refers to the section as depicted at the top of the figure.

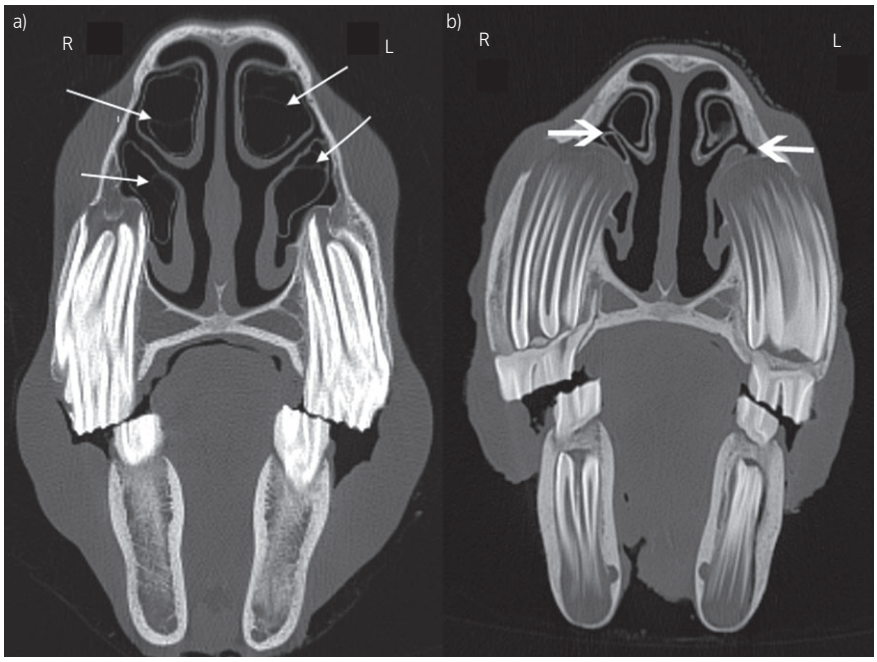

Fig 4: a) Ventral multiplanar reconstruction of a cadaver equine head at the level of 08 maxillary cheek tooth (L, left; R, right). Note white arrows indicating septae formation within the dorsal conchal bulla and ventral conchal bulla. b) Transverse image of a cadaver equine head <4 years old (L, left; R, right). Note the small size of the left and right ventral conchal bullae (arrows) due to protrusion of the tall reserve crowns of the erupting 07 maxillary cheek teeth.

heads a scroll of bone-free nasal conchae overlapped the medial aspect of the conchal bullae, but never fully overlapped their lateral aspects. In particular, the ventromedial aspect of the dorsal conchal bulla and the dorsomedial aspect of the ventral conchal bulla (both in the middle meatus) were not covered by nasal concha. The dorsal conchal bulla lumen was characterised by the presence of multiple, vertical, thin, soft-tissue septae, which transversely divided it into several cellulae, with the ventral conchal bulla containing fewer such septae (Fig 4a). The nasal drainage of bullae could not be detected on CT images due to the small size of the drainage apertures and because of the surrounding soft tissue structures. Many of the horses in the youngest age group had lateral compression of their ventral conchal bullas (Fig 4b). The left ventral conchal bulla in one case had an abnormally shrunken appearance when compared with the contralateral side and other heads, and therefore this case was excluded from further analyses.

Bullae linear dimensions

Mean and ranges of linear dimensions for each dorsal conchal bulla and ventral conchal bulla are presented in Table 1. The dorsal conchal bulla had larger dimensions than the ventral conchal bulla.

There were no significant differences between the left- and right-sided bullae measurements in individual horses. Consequently all further analyses were performed using the mean of the left and right side measurements.

Bullae volumes

There were significant differences in dorsal conchal bulla and ventral conchal bulla volume measurements between the 2 measuring protocols ($P<0.001$, $P<0.001$, respectively), with the 'limited slice protocol' underestimating the bullae volumes, compared with the 'total slice

TABLE 1: Mean dorsal conchal bulla and ventral conchal bulla measurements for 59 horses in study, subdivided by 'head' side

	Left	Right	Mean of left and right
Dorsal conchal bulla			
Mean length (range) (cm)	7.48 (4.4–14)	7.5 (4.7–14)	7.49 (4.55–14)
Mean width (range) (cm)	1.86 (1.3–2.4)	1.88 (1.2–2.6)	1.87 (1.25–2.5)
Mean height (range) (cm)	2.8 (1.8–4)	2.74 (1.8–4.1)	2.77 (1.8–4.05)
TSP mean volume (range) (cm^3)	23.83 (5.5–49)	24.12 (6–53)	23.98 (5.85–50.45)
LSP mean volume (range) (cm^3)	22.54 (5.1–46.1)	22.77 (4.3–51)	22.66 (4.9–48.55)
Ventral conchal bulla			
Mean length (range) (cm)	5.68 (2.4–8.4)	5.67 (2.5–8.5)	5.68 (2.45–8.45)
Mean width (range) (cm)	1.62 (0.5–2.9)	1.64 (0.7–2.8)	1.63 (0.7–2.85)
Mean height (range) (cm)	2.39 (0.8–3.6)	2.41 (0.8–3.7)	2.4 (0.8–3.65)
TSP mean volume (range) (cm^3)	15.13 (0.2–31)	15.01 (0.5–29)	15.07 (0.35–30)
LSP mean volume (range) (cm^3)	14.42 (0.2–30)	14.35 (0.5–27.9)	14.39 (0.35–28.95)

TSP, total slice protocol; LSP, limited slice protocol.

protocol' (Table 1). Consequently, all subsequent volume analyses were made using the total image slice protocol.

There was no statistical difference between the volumes of the left and right dorsal conchal bulla or ventral conchal bulla in individual horses (P = 0.6, P = 0.8). Consequently all further analyses were performed using the mean of the left- and right-side volume measurements.

Associations with head size

All parameters of size and volume were significantly associated between bullae and heads. Results of correlation matrices and linear regressions between bullae and head sizes are shown in Table 2.

Associations with age

Results of linear regression between bullae volumes and age groups are shown in Figure 5. The volumes of both the dorsal conchal bulla and the ventral conchal bulla differed significantly between age groups (model P values=0.005 and 0.0005, respectively) with age group 0–5 years having significantly smaller volumes (mean dorsal conchal bulla volume 15.6 cm^3 [5.9–35.1]; mean ventral conchal bulla volume 8.5 cm^3 [0.4–21.5]) than the >16 years age group (mean dorsal conchal bulla volume 24.7 cm^3 [10.1–41.2]; mean ventral conchal bulla volume 17.2 cm^3 [4.6–26.2]). It appeared that the difference in size with age for the ventral conchal bulla was due in part to the intranasal protrusion of the larger alveoli of maxillary cheek teeth in younger horses (Fig 4b).

Comparison with heads of known size

Box plots showing ranges of head sizes in the study group and known Thoroughbred group, subdivided by age groups, are shown in Figure 6. Heads in the study group were significantly smaller than the known Thoroughbred group, with smaller 'head' lengths (mean length 17.3 cm compared with 18.1 cm, P = 0.04), heights (mean height 9.5 cm compared with 11.1 cm, P<0.001) and volumes (mean volume 1123 cm^3 compared with 1358 cm^3, P = 0.005), but there was no significant difference in widths (mean width 6.6 cm compared with 6.8 cm, P = 0.2).

Anatomical relations of bullae to adjacent cheek teeth

Dorsal conchal bulla: The rostral limit of the dorsal conchal bulla was parallel with the maxillary Triadan 07s in 48/59 (81.3%) horses, parallel with the 06s in 10/59 (17%) cases and parallel with the 08s in 1/59 (1.7%) case. The caudal limit of the dorsal conchal bulla was parallel with the maxillary Triadan 10s in 36/59 (61%), the 09s in 18/59 (30.5%), the 11s in 3/59 (5%) and the 08s in 2/59 (3.5%) cases.

Ventral conchal bulla: The rostral limit of the ventral conchal bulla was parallel with the maxillary Triadan 07s in 46/59 (78%) horses, parallel with the 06s in 11/59 (19%) cases and parallel with the 08s in 2/59 (3%) cases. The caudal limit of the ventral conchal bulla was parallel with the maxillary Triadan 09s in 38/59 (64.5%), the 08s in 19/59 (32%), and the 10s in 2/59 (3.5%) cases.

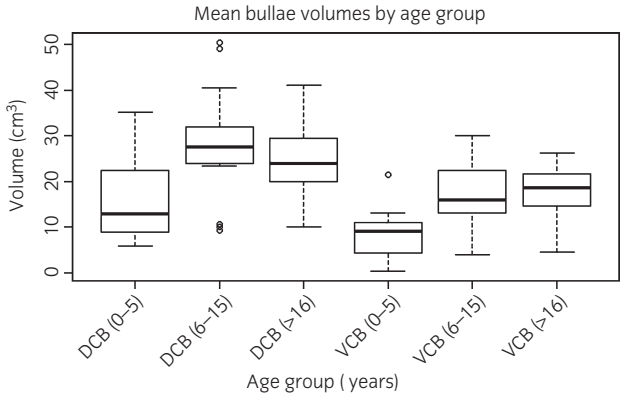

Fig 5: Box plots showing ranges of mean volumes of the dorsal (DCB) and ventral conchal bullae (VCB), subdivided by age groups.

The relations between both dorsal conchal bulla and ventral conchal bulla and sections of the adjacent maxillary teeth are shown in Figure 3.

Discussion

This study describes a computed tomography (CT) investigation of anatomical features and linear and volumetric dimensions of the equine dorsal conchal bulla and ventral conchal bulla, structures that suffer significant clinical disease [9], but whose anatomy remains poorly described. Computed tomography allows evaluation of single image slices in different scanning planes and the use of specialised software additionally allows accurate linear and volumetric measurements to be obtained. Some excellent CT anatomical studies of normal equine head structures, including sinuses and teeth, have recently been described [3,4,15,16]. However, minimal imaging information has been reported on the anatomy of normal or diseased nasal conchal bullae. Morphometric cranial measurements using CT have been described in dogs [17,18], and more recently volumetric measurements of normal equine paranasal sinuses were calculated from 3-dimensional reformatted rendering of CT slices using commercial software (Amira™) [4]. This technique was shown to be of value in demonstrating the complex 3-dimensional anatomical structures of the paranasal sinuses. However, that commercial software is expensive and it takes between 8 and 12 h of work to calculate the sinus volumes for a single head [4], making this technique impractical for routine diagnostic work.

In contrast, calculating nasal conchal bullae volumes using the current software (OsiriX®) [14] was much quicker (1.5 h/head), required minimal

TABLE 2: Results of linear regression and correlation matrix comparisons between individual measures of head sizes and measures of bullae sizes

	Linear regression				
Head/bullae comparison	Coefficient	95% CI	Standard error	P value	Correlation coefficient
Dorsal conchal bulla					
Length (cm)	0.475	0.22–0.73	0.13	<0.001*	0.425
Width (cm)	0.884	0.15–1.6	0.38	0.02*	0.293
Height (cm)	0.708	0.13–1.28	0.29	0.02*	0.299
Volume (cm^3)	16.89	9.02–24.77	4.02	<0.001*	0.480
Ventral conchal bulla					
Length (cm)	0.51	0.15–0.88	0.19	0.006*	0.336
Width (cm)	1.05	0.56–1.54	0.25	<0.001*	0.481
Height (cm)	0.84	0.38–1.29	0.23	<0.001*	0.423
Volume (cm^3)	24.25	13.2–35.3	5.62	<0.001*	0.489

Horse is included as a random effect to account for clustering. Significant associations are indicated by an asterisk against the P value. CI, confidence interval.

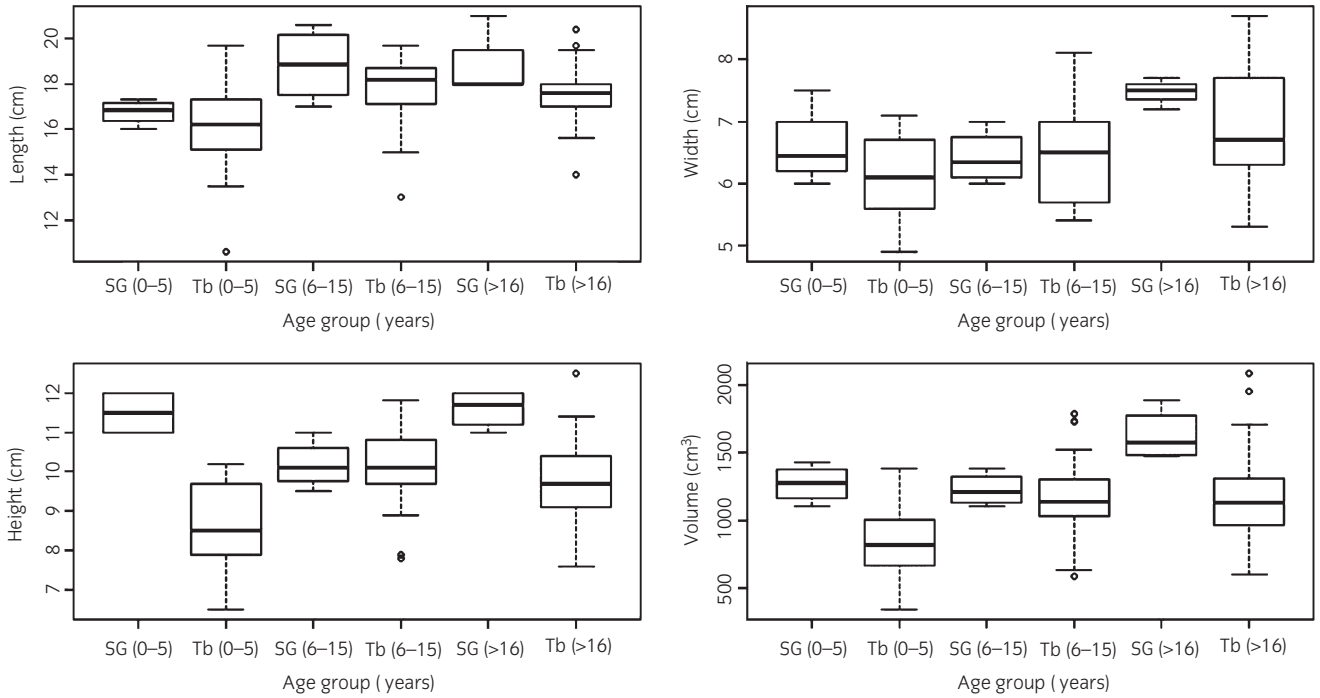

Fig 6: Box plots showing comparison of head sizes in the study group (SG) with known Thoroughbred group (Tb), subdivided by age groups. Lower and upper box lines = 25th and 75th percentiles, respectively; middle box line in bold = median; lower and upper whiskers = lower and upper adjacent values, respectively; open circles represent outliers. Lines in the box plot represent percentiles: 25 percentile, 75 percentile and median (in the middle): 25% of the values fall at or below this value, 75% of the values fall at or below this value; the spacing between the different parts of the box indicated the degree of spread in the data.

training and no software purchase. OsiriX volume calculation necessitates the manual outlining of the inner border of each CT image slice for each bulla, making it prone to human error due to the undulating inner surface of the conchal bulla. This undulating surface might explain the observed significantly lower bullae volumes calculated from the limited slice protocol as compared with the complete slice protocol.

Transverse CT images consistently showed free scrolled nasal conchae overlying most of the surface of the bullae, including the most accessible medial aspects of both bullae that prevent direct trans-nasal surgical access to the conchal bulla, unless the vascular nasal concha is penetrated first. Consequently, surgical drainage of infected bullae generally requires an approach through the middle meatus [9], where both bullae are not covered by the free nasal conchae. The presence of asymmetrical shrinkage of the left ventral conchal bulla in one case was of unknown cause, but considered potentially related to previous disease of this bulla or congenital malformation and, as such, this case was excluded from analysis. The observed lack of significant difference in dorsal conchal bulla and ventral conchal bulla volume and size measurements between left and right sides was expected. While asymmetry in horses that had previous pathology or surgery in the area of the bullae might be expected, an inclusion criteria of this study was that the population were free of sinonasal disease.

'Head' volumes and bullae volumes were found to be significantly associated irrespective of age. Head volume was calculated from the width and height of the maxillary bone at the maxillary Triadan 06, and the distance between the caudal aspect of the orbital bone to the naso-incisive notch, because these parameters were measurable in all specimens. Although measurement from the occipital bone to the incisive bone would have provided a measurement more closely associated with full skull length, the measurements used were thought acceptable for the analyses in this paper, whose aim was to measure bullae sizes.

Considerable ranges in bullae linear and volumetric measurements were observed, and this variation was most marked in the ventral conchal bulla. Horses in the youngest age group had significantly smaller dorsal conchal bullas and ventral conchal bullas than those in the oldest age group. Many of the horses in the youngest age group had significant lateral compression of their ventral conchal bullas due to intrusion of the alveoli of young maxillary cheek teeth apices into the nasal passages. Although previously recognised [19], this feature has not previously been related to ventral conchal bulla compression. The difference in size of the dorsal conchal bulla between youngest and oldest age groups may relate to changes in overall head size as the animal grows. The lack of significance when comparing the middle age group is probably related to reduction in growth rate after the age of 5 years.

A limitation of this study was the absence of breed information for the examined heads. Comparison of head linear and volume parameters with 12 adult Thoroughbred horses indicated the study cases were significantly (*circa* 10%) smaller than those of adult Thoroughbreds and this should be taken into account when considering the normal range of bullae sizes in horses. The difference in frequency of exclusions because of dental or sinonasal abnormalities between the 2 randomly collected groups of cadaver heads (*A* = 48% [26/58]; *B* = 11% [4/36]), is likely to be the result of differences in populations presented to the 2 different abattoirs at time of collection. Although the CT image review for inclusion was performed by different people in the 2 groups, all scans in *Group B* that were included in the study were subsequently examined by an imaging diplomate who reviewed *Group A* images, and they agreed with all inclusions. Another limitation of this study was that it was performed on cadaver heads and thus the normal venous distension of some areas of the nasal mucosa was absent and this venous distension would probably have decreased the volumes of the dorsal conchal bulla and ventral conchal bulla.

The rostral and caudal limits of the dorsal conchal bulla were found to be parallel with the maxillary Triadan 06s and 11s, respectively, in some cases, thus showing that the caudal limit of the dorsal conchal bulla is adjacent to the rostral limit of the dorsal conchal sinuses; however, no overlap between the dorsal conchal bulla and dorsal conchal sinus was found in any head. It is commonly stated that the apices and reserve crowns of the caudal 3–4 cheek teeth (Triadan 08s–11s) lie within the rostral and caudal maxillary sinuses [20,21]. However, there is much variation between horses in these anatomical relationships; with the rostral aspect of the rostral maxillary sinus reported as varying from being level with the Triadan 07–09 cheek teeth, and the maxillary septum varying in

site from being level with the caudal aspect of the Triadan 08 to the caudal aspect of the Triadan 09 [22,23]. In this study population, the rostral and caudal borders of the ventral conchal bulla extended from the level of the Triadan 06s to the 10s, respectively, in some cases, thus showing that the caudal limits of the ventral conchal bulla can overlap with the rostral limits of the ventral conchal and rostral maxillary sinuses. In the presence of concurrent sinusitis and dorsal conchal bulla or ventral conchal bulla empyema, the boundaries between these structures may not be obvious using conventional radiography, but the anatomical relationships between the rostral and caudal limits of these bullae and the adjacent maxillary cheek teeth give useful anatomical guidelines for the diagnosis of bulla empyema using conventional radiography and also landmarks for the trans-nasal surgical treatment of such disorders.

Conclusions

Computed tomography was a suitable technique to establish the linear dimensions and volumes of the nasal conchal bullae in horses of different ages. Both dorsal conchal bulla and ventral conchal bulla sizes increased with animal age, the latter in part due to the eruption of cheek teeth whose reserve crowns were compressing the bulla. Relatively consistent relationships between the rostral and caudal limits of these bullae and the adjacent maxillary cheek teeth were observed that would be of diagnostic value with conventional radiography and also in the surgical treatment of sinonasal disease.

Authors' declaration of interests

No competing interests have been declared.

Ethical animal research

Study protocols were approved by Ethical Committees in both The University of Edinburgh and The Royal Veterinary College. The study was performed on material obtained from abattoirs.

Source of funding

University of Edinburgh.

Acknowledgements

The authors would like to thank Justin Perkins of The Royal Veterinary College for his important contribution to data collection.

Authorship

All authors contributed to the study design. T. Liuti was responsible for data acquisition and study execution and R. Reardon for data analysis and interpretation. P.M. Dixon contributed to study execution. All authors contributed to manuscript preparation.

Manufacturers' addresses

[a]Siemens, Munich, Germany.
[b]General Electric (GE), Highlands Heights, Ohio, USA.

References

1. Dyce, K.M., Sack, O.W. and Wensing, C.J.G. (2010) The head and ventral neck of the horse. In: *Textbook of Veterinary Anatomy*, 4th edn., Eds: Elsevier, Saunders, Edinburgh. pp 501.
2. Waibl, H. (2004) Nase, Luftsack. In: *Lehrbuch der Anatomie der Haustiere*, Band II, Eingeweide 9, Eds. R. Nickel, A. Schummer and E. Seiferle, Verlag Paul Parey, Berlin and Hamburg. pp 275-278.
3. Brinkschulte, M., Bienert-Zeit, A., Lüpke, M., Hellige, M., Ohnesorge, B. and Staszyk, C. (2014) The sinonasal communication in the horse: examinations using computerized three-dimensional reformatted renderings of computed-tomography datasets. *BMC Vet. Res.* **10**, 72.
4. Brinkschulte, M., Bienert-Zeit, A., Lüpke, M., Hellige, M., Staszyk, C. and Ohnesorge, B. (2013) Using semi-automated segmentation of computed tomography datasets for three-dimensional visualization and volume measurements of equine paranasal sinuses. *Vet. Radiol. Ultrasound.* **54**, 582-590.
5. Sisson, S. and Grossman, J.D. (1953) *The Anatomy of the Domestic Animals*, 4th edn., WB Saunders, Philadelphia. 518.
6. International Committee on Veterinary Gross Anatomical Nomenclature. (2012) Nomina Anatomica Veterinaria 5th edn, http://wava-amav.org/Downloads/nav_2012.pdf. Accessed 11 October 2015.
7. Espersen, G. (1952) Cellulae conchales hos hest of aesel. *Nord. Vet. Med.* **5**, 573-608.
8. Perkins, J.D., Windley, Z., Dixon, P.M., Smith, M. and Barakzai, S.Z. (2009) Sinoscopic techniques for examining the rostral maxillary and ventral conchal sinuses of horses: Part 2. 60 Clinical cases. *Vet. Surg.* **38**, 613-619.
9. Dixon, P.M., Froydenlund, T., Liuti, T., Kane-Smyth, J., Horbal, A. and Reardon, R.J. (2015) Empyema of the nasal conchal bulla as a cause of chronic unilateral nasal discharge in the horse: 10 cases (2013–2014). *Equine Vet. J.* **47**, 445-449.
10. O'Leary, J.M. and Dixon, P.M. (2011) A review of equine paranasal sinusitis. Aetiopathogenesis, clinical signs and ancillary diagnostic technique. *Equine Vet. Educ.* **23**, 148-159.
11. Dixon, P.M., Parkin, T.D., Collins, N., Hawkes, C., Townsend, N., Tremaine, W.H., Fisher, G., Ealey, R. and Barakzai, S.Z. (2011) Historical and clinical features of 200 cases of equine sinus disease. *Vet. Rec.* **169**, 439.
12. Probst, A., Henninger, W. and Willmann, M. (2005) Communications of normal nasal and paranasal cavities in computed tomography of horses. *Vet. Radiol. Ultrasound.* **46**, 44-48.
13. Morrow, K.L., Park, R.D., Spurgeon, T.L., Stashak, T.S. and Arceneaux, B. (2000) Computed tomographic imaging of the equine head. *Vet. Radiol. Ultrasound.* **41**, 491-497.
14. OsiriX MD User Manual 2.5.1. (2012). p153.
15. Henninger, W., Frame, M., Willmann, M., Simhofer, H., Malleczek, D., Kneissl, S. and Mayrhofer, E. (2003) CT features of alveolitis and sinusitis in horses. *Vet. Radiol. Ultrasound* **44**, 269-276.
16. Saunders, J., Windley, Z. (2011) Equine sinonasal and dental. In: *Veterinary Computed Tomography*, Eds. T. Schwarz and Saunders, J., John Wiley & Sons Ltd, West Sussex. pp 427-442.
17. Marino, D.J., Loughin, C.A., Dewey, C.W., Marino, L.J., Sackman, J.J., Lessel, M.L. and Akerman, M.B. (2012) Morphometric features of the craniocervical junction region in dogs with suspected Chiari-like malformations determined by combined use of magnetic resonance imaging and computed tomography. *Am. J. Vet. Res.* **73**, 105-111.
18. Garcia-Real, I., Kass, P.H., Sturges, B.K. and Wisner, E.R. (2004) Morphometric analysis of the cranial cavity and caudal cranial fossa in the dog: a computerised tomographic study. *Vet. Radiol. Ultrasound.* **45**, 38-45.
19. Dixon, P.M., Tremaine, W.H., Pickles, K., Kuhns, L., Hawe, C., McCann, J., McGorum, B.C., Railton, D.I. and Brammer, S. (2000) Equine dental disease part 4: a long-term study of 400 cases: apical infection of cheek teeth. *Equine Vet. J.* **32**, 182-194.
20. Ramzan, P.H.L. (2011) Nasal stenosis arising from developing premolar dentition in a horse. *Vet. Rec.* **168**, 217.
21. Dixon, P.M., Parkin, T.D., Collins, N., Hawkes, C., Townsend, N., Tremaine, W.H., Fisher, G., Ealey, R. and Barakzai, S.Z. (2012) Equine paranasal sinus disease: a long-term study of 200 cases (1997–2009): treatments and long-term results of treatments. *Equine Vet. J.* **44**, 272-276.
22. Trotter, G.W. (1993) Paranasal sinuses. *Vet. Clin. N. Am.: Equine Pract.* **9**: 153-169.
23. Dixon, P.M. (2002) The gross, histological, and ultrastructural anatomy of equine teeth and their relationship to disease. *Proc. Am. Ass. Equine Practnrs.* **48**, 421-437.

3.2 Conclusion

Using CT, this study describes anatomical features, as well as linear and volumetric dimensions of the equine dorsal and ventral conchal bullae in different aged horses

CT allowed evaluation of single image slices in different scanning planes and in conjunction with dedicated software, it also facilitated the acquisition of accurate linear and volumetric measurements. The size of both the dorsal and ventral conchal bullae were found to increase with age and horses in the youngest age group had significantly smaller dorsal and ventral conchal bullae than those in the oldest age group.

The use of CT provided a detailed anatomical description of the location and dimensions (linear and volumetric) of both bullae, in relation to horse age and skull dimension. Many horses in the youngest age group had significant lateral compression of their ventral conchal bullae due to intrusion of the alveoli of their tall maxillary cheek teeth apices into the nasal passage that could explain the age-related increase in size of the ventral conchal bulla. The difference in size of the dorsal conchal bulla between the youngest and oldest age groups may relate to changes in overall head size as the animal grows.

Relatively consistent relationships between the rostral and caudal limits of these bullae and the adjacent maxillary cheek teeth were observed that would be of diagnostic value with conventional radiography and also serve as landmarks for the trans-nasal surgical treatment of such disorders.

In the gross morphological description of the dorsal and ventral conchal bullae, the

authors erroneously stated that the ventromedial aspect of the dorsal conchal bulla and the dorsomedial aspect of the ventral conchal bulla (both in the middle meatus) were not covered by nasal conchae. In fact, as shown in the following anatomical images these areas are fully covered by the nasal conchae and it is at the lateral aspects of the conchae that are not fully covered by nasal conchae bullae are partially exposed

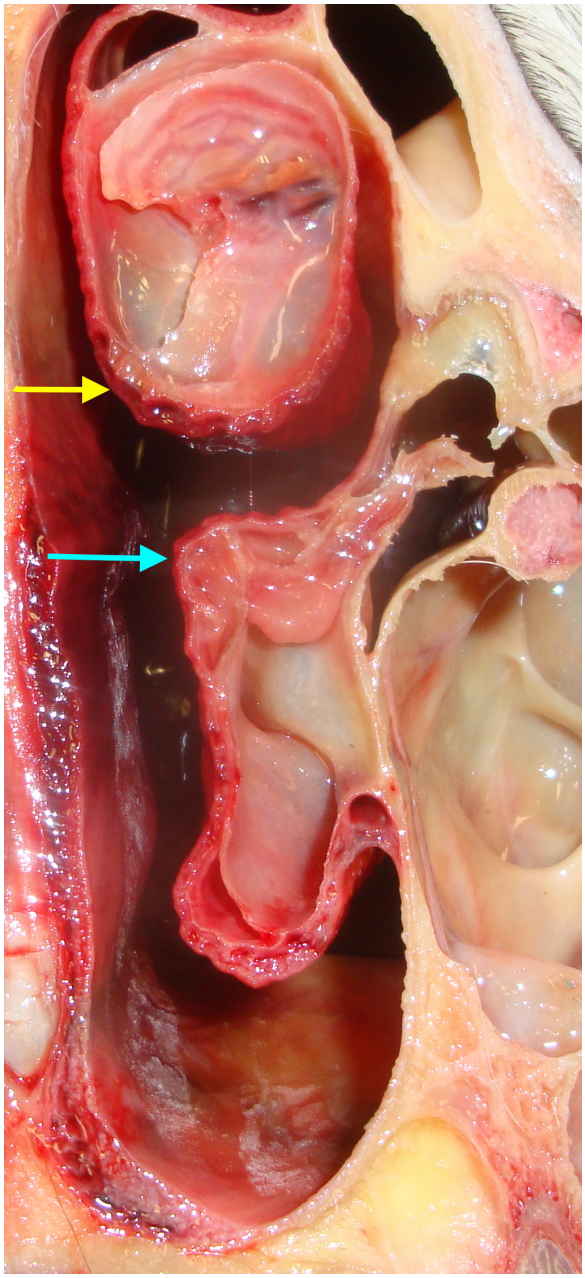

Moreover, in the section "Association with age" the authors erroneously described a box plot as linear regression findings. The linear regression is therefore added below to clarify the comparison between bullae measurements and age groups

Table 3: Results of linear regression comparison between bulla measurements and age groups.

Model	Correlation Coefficient	95% Confidence intervals	Standard error	P-value
Mean DCB Vol / Age (years)				**0.005**
>15	Ref			
6-15	3.02	-2.52 – 8.58	2.77	0.279
0-5	-8.12	-14.53 - -1.71	3.20	**0.014**
Mean VCB Vol / Age (years)				**0.0005**
>15	Ref			
6-15	-0.68	-4.45 – 3.10	1.89	0.722
0-5	-8.68	-13.04 - -4.31	2.18	**<0.001**

Key: DCB=dorsal conchal bulla; VCB=ventral conchal bulla; Vol = volume (cm^3)

Moreover, in the section “Comparison with heads of known size” the text correctly implies that the heads of the study groups were smaller than those of Thoroughbred, however the figure showed the opposite, due to an erroneous labelling on the box plot. The authors have corrected the labelling and a new box plot has been added below, showing the correct results.

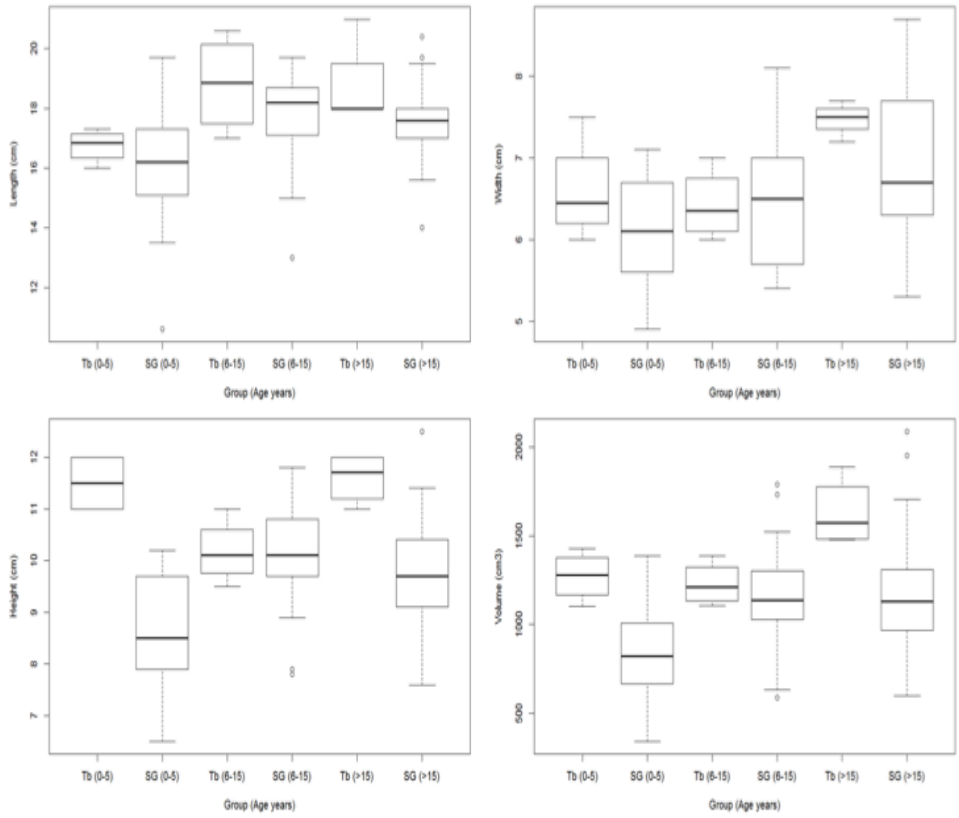

Figure 3 in the text has also been revised

The coding for the DCB rostral extent box plot had been done incorrectly, which changed the recording of where on the tooth the bullae extended to, but not to which tooth they extended to.

Below the correct figure

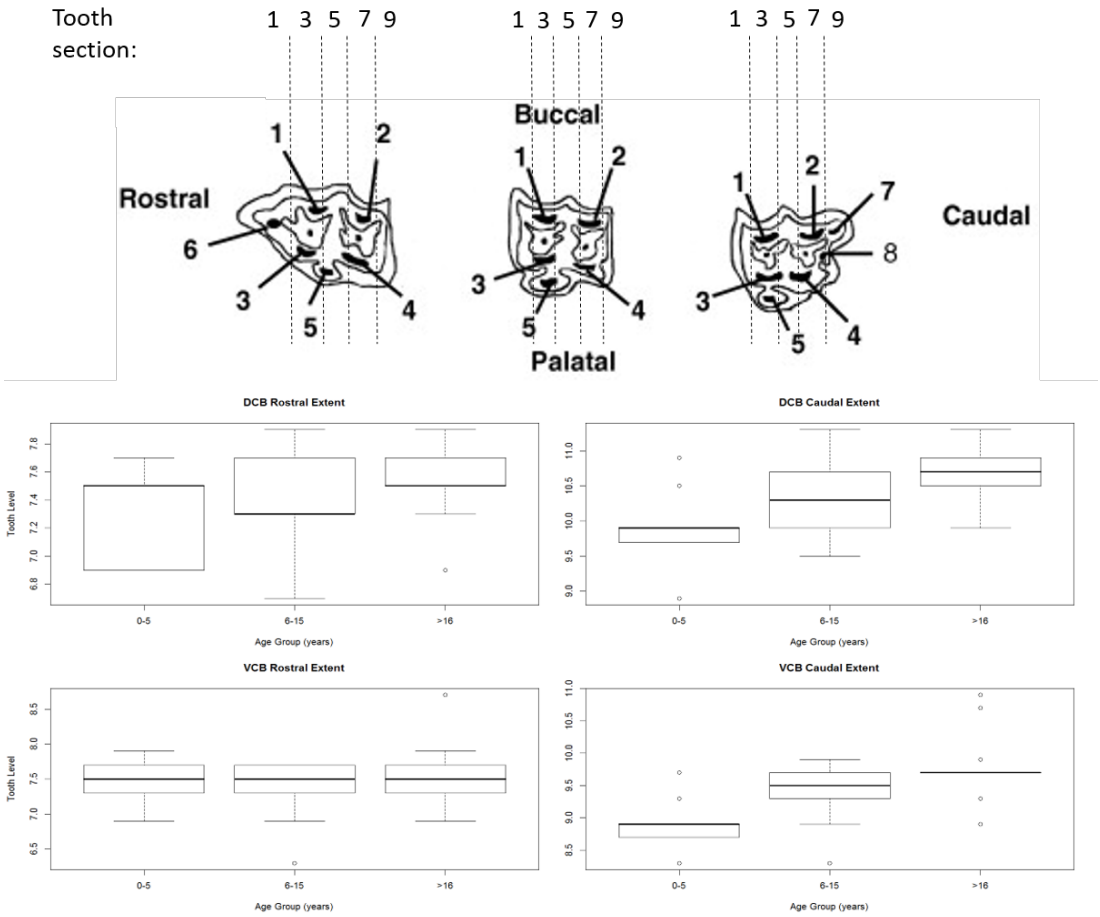

CHAPTER 4: Geometric morphometric shape analysis of the skulls of different aged horses

4.1 Introduction

The study of anatomical shape and its variation is a major topic of medical research. The use of shape analysis is one approach to understanding the causes of variation and the morphological transformation of animals due to evolution, age, disease and selective breeding [1]. Geometric morphometric method (GMM), a technique developed by Bookstein [2,3,4,5], uses landmarks to explore the morphospace of objects to better represent the possible form, shape or structure. GMM makes use of landmarks (two or three-dimensional points placed in specific anatomical areas) based geometric morphometrics (i.e. Cartesian geometric coordinates), rather than linear, areal (of area), or volumetric variables. This allows GMM to more accurately examine the scale and shape relationships of structures.

GMM was developed to address the shortcomings of simple linear, volume or area-based methods that do not preserve the geometric relationships between the measurements, leading to difficulties in the interpretation of spatial relationships [5,6,7]. Moreover, traditional morphometrics apply statistical techniques to a wide range of measurements such as distances and distance ratios, angles, areas and volumes; however the original geometric relationship cannot be reconstructed from a sample of selected distance measurements [8].

One of the main differences between traditional morphometrics and GMM uses Procrustes superimposition to rescale objects to unit size, translate them and rotate

them to minimize the sum of squared differences between points [9]

Another advantage of GMM over traditional morphometric approaches is that it can deconvolute form, separating the effects on shape that are due to, or independent of, size [2,3,4]. GMM is also more amenable to visual representation of shape variation [10].

GMM has been used in numerous veterinary studies including examination of the morphological changes in the skulls of St Bernards dogs: in particular, to evaluate changes of skull shape due to selective breeding [11]. The results suggested that the St Bernards skull has changed considerably over the last 120 years. In particular the upper jaw and palate have tilted, which contributes to their shortened and relatively high muzzle, and the he skull has become wider and the height of the occipital crest has increased. GMM has been of great value in many biological studies in humans and non-domesticated animals and other organisms. It has also been shown to be of value in a limited number of veterinary studies such as the morphological evaluation of the canine skull and its evolutionary changes caused by domestication [12], in the evaluation of the shape and size of Spanish Arabian horses [13] or examining the dental form of equine fossil skulls, to explore differences between horses [14].

However to date, no studies on age-related changes in the shape of equine skulls have been published. However, a similar study can be found in the evaluation of a variety of cattle from South America named the Niata which are extremely brachycephalic [15]. The use of geometric morphometry of the skull and genetic data showed that the Niata was a variety of chondrodysplastic form of cattle and,

according to the authors, the Niata should be considered a true and proper breed.

Bookstein applied GMM to studies on craniofacial growth in both humans and animals [5,6,7] and GMM has since been used in a very wide range of human, animal and plant studies. [16,17,18].

Equine studies have used traditional morphometric studies to determine neck adiposity in relation to body weight, height, length, girth and abdominal circumference [19], and cerebellar abiotrophy in relation to cerebellar size and cerebellar cerebrospinal fluid space [20]. However, to date, GMM does not appear to have been used to study age-related differences in equine skull shape.

The objective of this study was to evaluate the ontogenetic changes that occur in normal equine skulls by using landmarks-based geometric morphometric methods in horses of three different age groups.

4.2 Material and methods

Specimens

Equine heads were obtained from two sources:

Group A

The heads of 54 horses were freshly obtained from an abattoir. Each head had an unknown history and was grossly similar in size to an adult Thoroughbred horse head. Heads were positioned on their mandibles and imaged using a multislice CT scanner (Multislice CT scanner Siemens Volume Zoom, Munich Germany) in a helical scan mode using a 512 x 512 Matrix, 120 Kv, 300 mA, at a slice thickness of

1.5 mm.

Bone windows (H70) were used to review the images at a WW of 4000 Hounsfield Unit (HU) and WL of 1000 (HU). After image acquisition, the heads were frozen (-200 C) and then sectioned transversely at 5 cm intervals with a band saw. After thawing, both sides of each section were examined grossly for sinonasal or significant dental abnormalities.

Group B

Anatomical and CT images were similarly obtained from 36 equine heads with unknown histories that had been freshly obtained from an abattoir by Justin Perkins (Royal Veterinary College, London). CT images were acquired using a 4th generation, Universal Medical System CT scanner, GE light speed ultras, Highland Heights, Ohio, USA, at 1.25 mm slice thickness, 120 kV, 300 mA. The heads and CT images were examined for the presence of sinonasal disease or significant dental abnormalities.

Twenty-six of 54 heads in Group A had clinical and/or imaging evidence of dental or sinonasal disease and were thus excluded from the study, leaving 28 heads available in this group. Four of the 36 heads in Group B also had clinical and/or imaging evidence of dental or sinonasal disease and were also excluded, leaving 32 heads in this group (a total of 60 normal heads available).

Comparison of head dimensions with those of horses of known breed

In order to compare the head sizes in the current study population with head sizes of known breeds, the CT images of 12 Thoroughbreds of known age (0–5 years old [N=4]; 6–15 years old [N=4]; >16 years old [N=4]) that had undergone CT head imaging for clinical reasons other than sinonasal disorders were measured to obtain their head dimensions.

Head linear dimensions and volumes

Head "length" (i.e. distance from the caudal aspect of the orbit to the nasoincisive notch) was measured from CT sagittal reconstructions; head "width" (width of the hard palate at the level of Triadan 06) was measured from CT dorsal reconstructions and head "height" (distance from the hard palate to the dorsal aspect of the maxillary bone at the level of the orbit) was measured using CT sagittal reconstructions. These three measurements were multiplied together to produce a measurement of head "volume" [21].

Statistical analyses of head sizes

A student's T-test was used to assess any differences in dimensions between the cadaver heads used in this study and the 12 control Thoroughbred horses. No significant difference was found between head length ($p=0.196$), width ($p=0.942$), height ($p= 0.086$) or volumes ($p=0.829$) between the two groups.

The 60 heads were aged by clinical incisor examination using standard guidelines along with CT measurements of cheek teeth reserve crown and root length. Heads were placed into three age groups: <5 years old (Group 1: N=15), 6-15 years old

(Group 2: N=21) and >16 years old (Group 3: N=24).

Image-based morphometrics

Bone window CT data of the 60 heads were transferred as DICOM images to Osirix® (www.osirix-viewer.com) imaging software which was used to perform multiplanar image reconstructions and to evaluate the image quality. Isosurfaces of each skull were generated from their constituent DICOM images using Stratovan CheckPoint® (3 WIN x64), which allows collection of x, y and z coordinates from landmarks placed on skull images. Twenty-nine heads were selected for this study: 0-5 years old (Group 1: N=9), 6-15 years old (Group 2: N=10) and >16 years old (Group 3: N=10) based on the accurate identification of all anatomical landmarks (see below) after the isosurface was generated from the DICOM images.

Twenty-nine homologous landmarks (this number coincidental to the number of skulls) were used in each skull (Fig. 1 A-D). Each landmark was uniquely identified using anatomical nomenclatures to denote those on the external and internal skull surfaces (the latter included: the ventral and dorsal conchal bullae, individual tooth pulps, nasolacrimal duct ostium, and caudal aspect of the hard palate), to establish if the morphology of certain skull sites showed age-related variability.

Placement of landmarks was performed on sagittal, dorsal or transverse slice windows or on the isosurface.

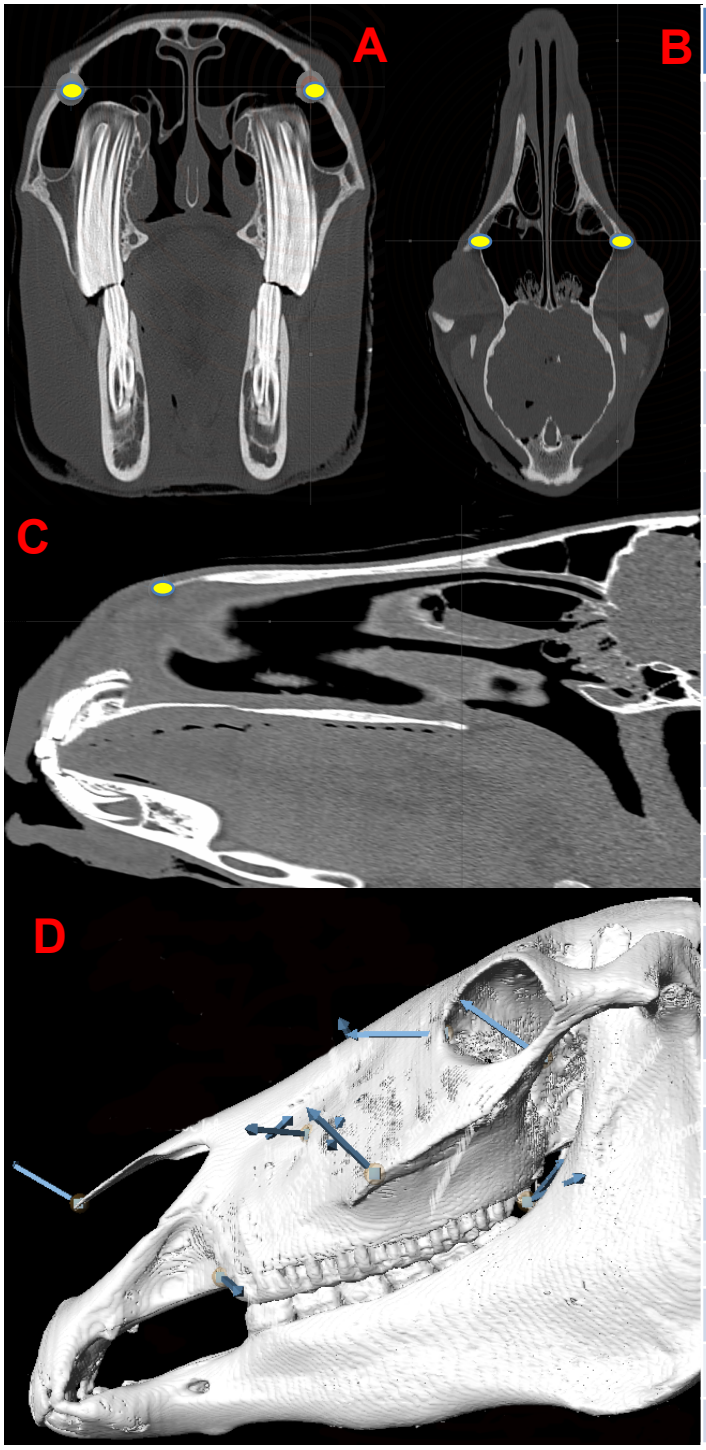

Stratovan check point	Anatomical landmarks
1	Caudal aspect of hard palate
2	207 3rd pulp
3	107 3rd pulp
4	Maxillary bone margin left
5	Maxillary bone margin right
6	Cranial nasolacrimal duct left
7	Cranial nasolacrimal duct right
8	Tip of nasal bone
9	Pterygoid process left
10	Pterygoid process right
11	Basisphenoid bone rostral
12	Rostral 206
13	rostral 106
14	Ventral orbital bone left
15	Ventral orbital bone right
16	Ethmoid sinus caudal to 211
17	Ethmoid sinus caudal to 111
18	Vomer rostral 06 ventrally
19	Rostral VCB left
20	Rostral VCB right
21	Caudal VCB left
22	Caudal VCB right
23	Rostral DCB left
24	Rostral DCB right
25	Caudal DCB left
26	Caudal DCB right
27	Caudal nasolacrimal duct left
28	Caudal nasolacrimal duct right
29	Caudal vomer

Fig 1 Anatomical landmarks

A) Transverse slice reconstruction: note landmarks (yellow dots) at the level of the nasolacrimal duct ostia, left and right

B) Dorsal slice reconstruction: note landmarks (yellow dots) at the level of the maxillary bone lateral margins, left and right

C) Sagittal slice reconstruction (note landmark (yellow dot) at the level of the tip of nasal bone

D) Lateral isosurface showing external landmarks

VCB: Ventral Conchal Bulla, DCB: Dorsal Conchal Bulla

Geometric Morphometrics

Cartesian landmark coordinates were reformatted using custom R scripts and loaded into MorphoJ [22] for data processing. Briefly, a Procrustes fit was used to superimpose, translate, rotate, and uniformly rescale coordinates. The degree of rescaling required to minimise the sum of the squared distances between landmarks (termed centroid size) was used as a proxy for animal scale in this study. A covariance matrix was generated either from coordinates or regression residuals (see the next section). From these matrices, PC analysis was used to describe correlated landmark covariances into orthogonal, uncorrelated systems ("PCs", also termed eigenvectors). In effect, PCs summarise the total variation described across the dataset, with each successive component describing smaller tranches of uncorrelated variance than the preceding PC (i.e. PC1 > PC2, PC2 > PC3,Ä¶). To remove allometric effects, a multivariate regression of Procrustes coordinates against the log-transformed centroid size was used. The resulting residuals produced by the regression were used to generate a covariance matrix, which was analyzed by PC as described above. The multivariate regression was tested with permutation tests against the null hypothesis.

Due to the relatively small contributions of PCs greater than PC2, only the first and second PCs (PC1 and PC2, respectively) analyses were considered in this study.

A Discriminant Function Analysis (DFA) was also considered in the data evaluation to determine any variable present between the three different groups: Group 1 vs Group 2, Group 1 vs Group 3 and Group 2 vs Group 3.

4.3 Results

Principal Components Analysis (PCA)

a) PCA with allometry

PC1 and PC2 findings showed clustering of individuals based on group membership (i.e. age), demonstrating minimal overlap between Groups 1 and 2 and no overlap between Groups 1 and 3. However, the overlap between Groups 2 and 3 was substantial. These results could be interpreted as showing a high variability in skull shape in young horses (Group 1; <5 y.o.), while the skull form of adult (Group 2; 6-15 y.o.) and old horses (Group 3; >15 y.o.) is comparatively fixed. A further explanation for the difference between age groups is provided by the large morphospace the young group (Group 1) occupies in PC1, in relation to Groups 2 and 3 (Fig. 2). A further PC1 vs PC2 run within Group 1 by their age in months to assess for any trend in morphospace (Fig. 3) showed two horses (36 and 48 months old) located further away from the other 7, most likely due to different skull morphology.

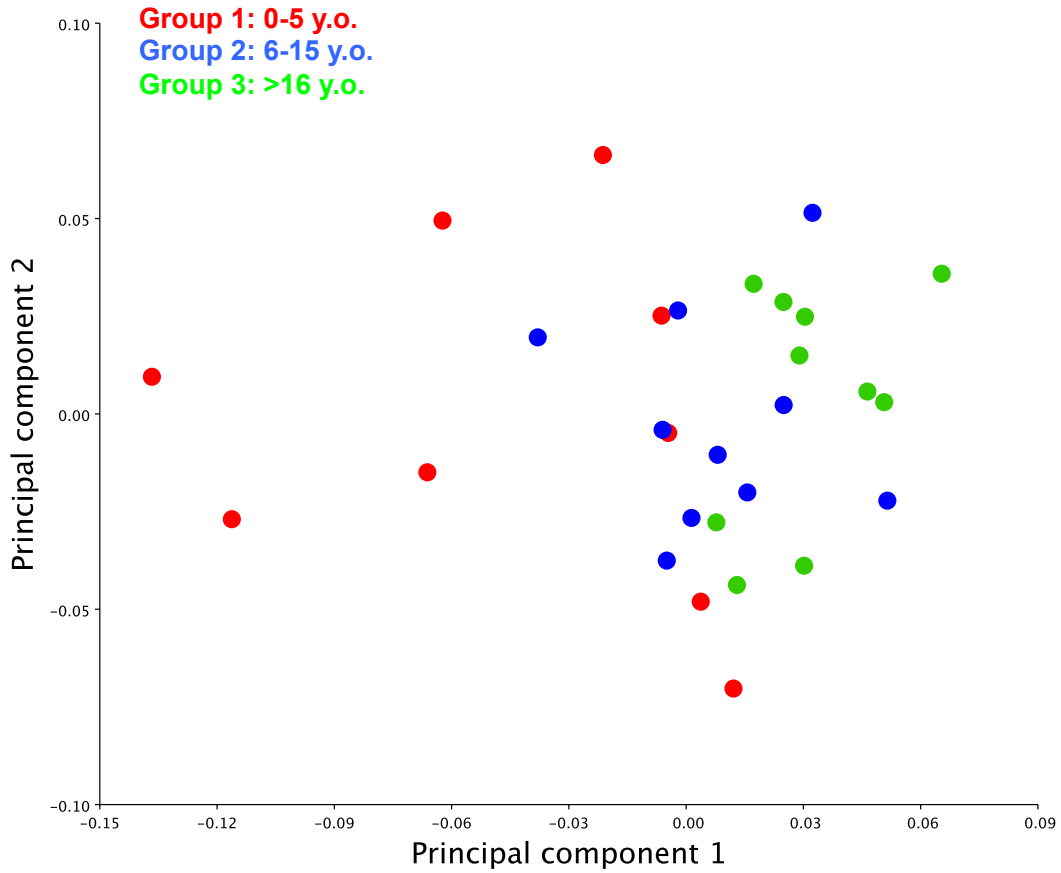

Fig 2. PCA 1 vs PCA 2 with allometry.

There is obvious overlap between Groups 2 (green) and 3 (blue) but much distinction between Groups 1 (red) and 3 (blue).

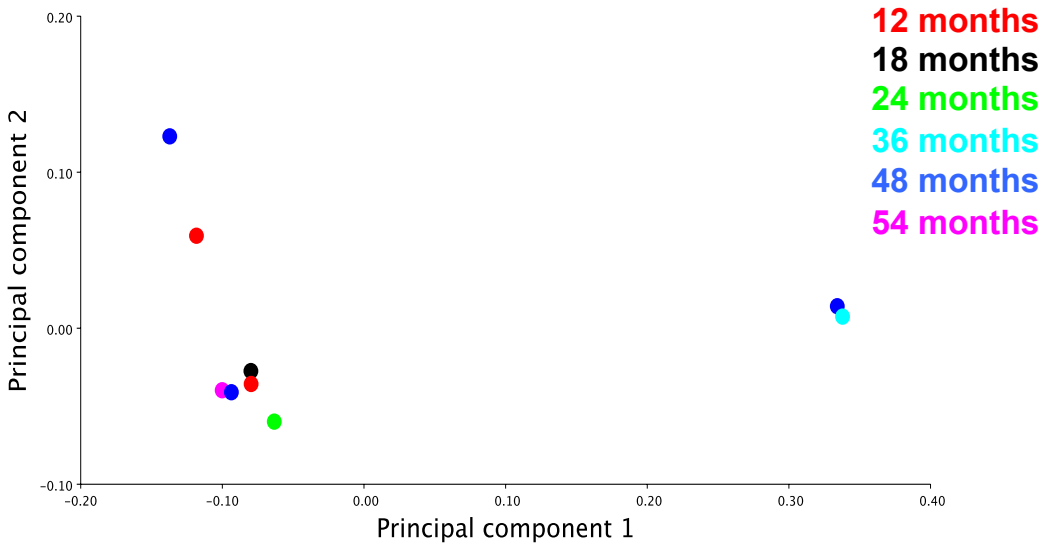

Fig 3. PC1 vs PC2 within Group 1 divided by age in month (colour coded). Two individuals (on right of figure) are located distant from the rest of the group, most likely due to their different skull morphology. This figure shows the relatively large morphospace occupied by these young horses.

In the eigenvalues graph, PC1 allometry explained 27% of the shape variation between all 29 skulls (Fig. 4) but a further eigenvalue graph created within Group 1, showed that 85% of their skull shape variation could be explained by PC1 allometry (Fig. 5).

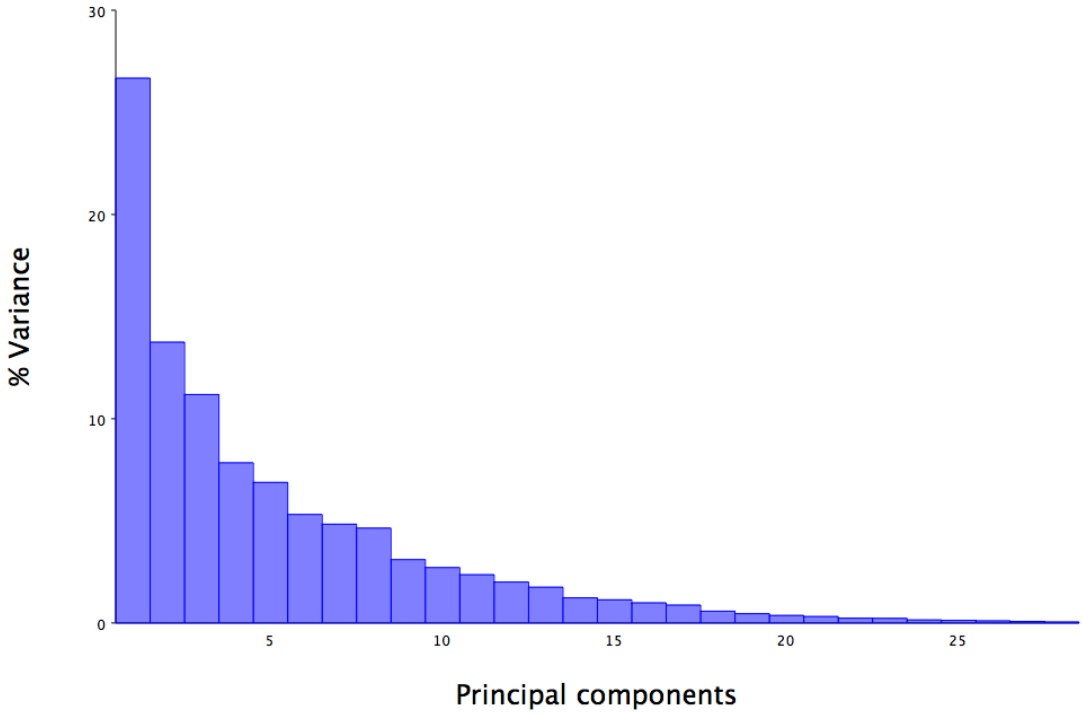

Fig.4 Eigenvalue graph of PCA1 with allometry; note the 27% variance in PC1, with much lower variance in the other Principal Components.

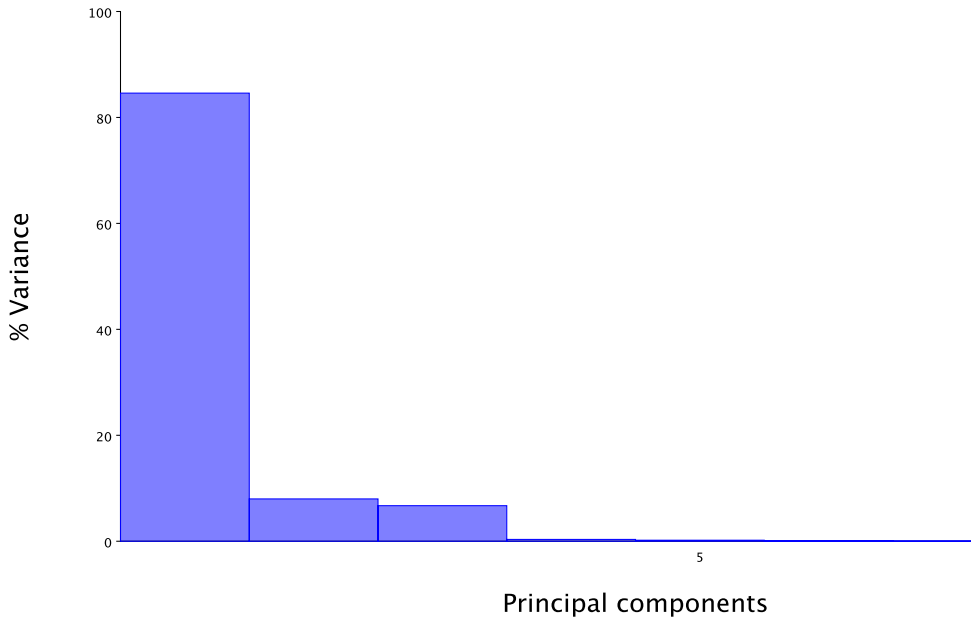

Fig.5

Eigenvalue graph of PCA1 with allometry within Group 1: note the 85% variance in PC1 with minimal (<8%) variance in PC2, PC3 and PC4.

A graphical representation of PCA shows the variability of the chosen landmarks in different planes (dorsal, sagittal and transverse, respectively) (Fig. 6 (A, B, C). In particular, the following landmarks: caudal aspect of hard palate, pterygoid process (left and right), basisphenoid bone, and rostral and caudal aspects of vomer showed minimal changes in direction or size.

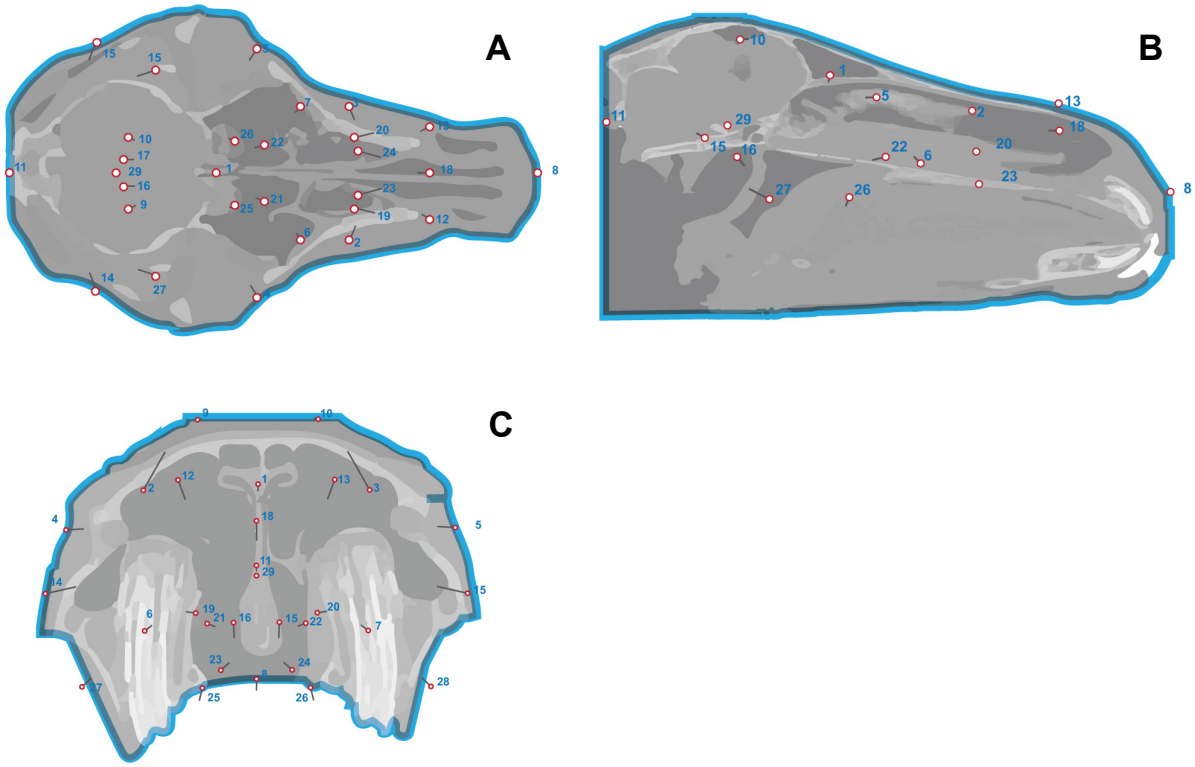

Fig. 6 (A, B, C)

Graphical representation of PCA 1 with allometry in all 29 horses in dorsal, sagittal and transverse reconstructions. Landmarks are represented by “lollipops” with their length and direction indicative of the degree and direction of anatomical variation. In this figure the location of the landmark represents the average of the landmarks in all 29 horses and therefore do not exactly match the landmark shown in Figure 1.

b) PCA without allometry

In order to correct for the effect of size on shape, a regression analysis on log-transformed centroid size with a permutation test was performed. This analysis uses the null hypothesis of complete independence between the dependent and independent variables [23]; which in this study was between the landmarks for each age group and the log-centroid size. A total of 10,000 random permutations were conducted and the multivariate regression result was highly significant (p-value: <0.0001).

PCA without allometry showed no obvious clustering of individuals based on group membership, but showed clustering between Groups 1 and 2, Groups 2 and 3, and Groups 1 and 3, indicating poor separation between the different age groups (Fig. 7).

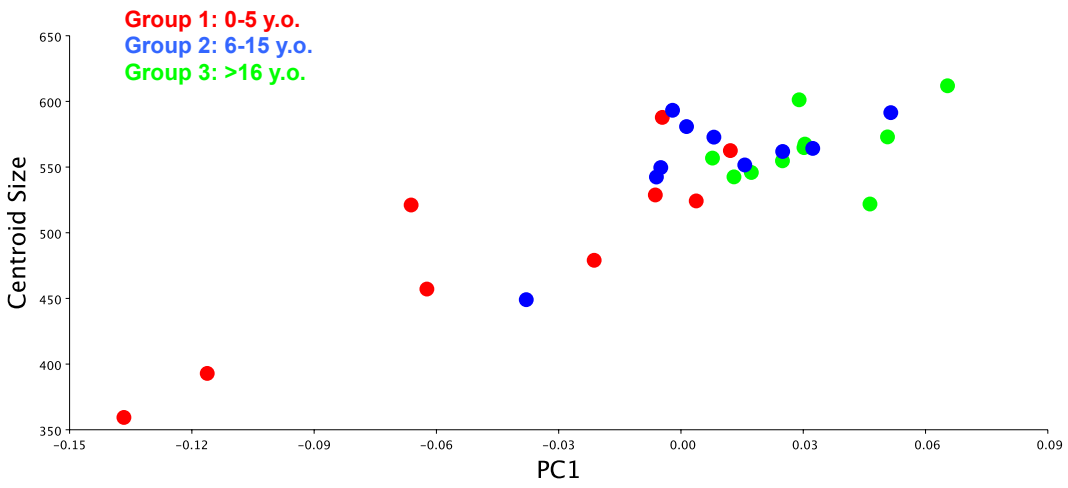

Fig 7

Graphical representation of PC1 without allometry in all 29 horses. The morphospace occupied by each age group overlaps.

Discriminant Functional Analysis

Discriminant Functional Analysis shows direction and associated point variability between age groups (Group 1 vs 2; Group 1 vs Group 3; Group 2 vs 3) in different anatomical orientations (dorsoventral, sagittal and transverse planes).

Two landmarks (pterygoid process; left and right) showed no variability between Groups 1 and 3, whilst three landmarks (caudal aspect of hard palate; pterygoid process, left and right) showed no variability between Groups 1 and 2. Eight landmarks (tip of nasal bone; pterygoid process (left and right) ethmoidal sinus

caudal to 211 and 111; caudal aspect of VCB (left and right) and caudal aspect of vomer bone showed no variability between Groups 2 and 3. These results highlight the variability of the landmarks between age groups, with horses in Group 1 showing most variability in landmarks and only 2/29 landmarks not showing any variability.

4.4 Discussion

This appears to be the first publication that utilises GMM to investigate ontogenic shape differences in normal equine skulls. Previous GMM studies have examined the diversity of populations of late glacial horses in Western Europe by detailed morphological analysis of their metacarpal and metatarsal bones. [24]. Broader GMM studies using multiple body measurements of the size and shape of morpho-functional traits in Spanish Arab horses showed no shape differences in horses bred for different purposes, but a significant difference in size between morphological and endurance aptitude [25]. A further equine GMM study showed significant interbreed, but no age-related differences on occlusal enamel folding of equine Triadan 06 and

11 teeth [26].

In the current study, PCA graphic representation showed a larger morphospace occupied by young horses (Group 1) in comparison to the older horses in Groups 2 and 3 (Fig. 2), whilst a PCA within Group 1 showed seven individuals with similar and two individuals with very different morphological characteristics (Fig.3).

Unfortunately, no histories or signalment information was available for any of these horses, whose skulls were similar in size to Thoroughbred skulls. Gross pathological and CT examinations did not show any evidence of bony malformation secondary to localized or generalized disease, such as nutritional secondary hyperparathyroidism [27]. A possible explanation for the major morphological differences of those two young horses could be related to their breeds, because some ("cold-blooded") ponies have heads similar in size to Thoroughbreds. Further studies on groups of young horses of known breeds would better define interbreed differences in head morphometrics.

On PCA graphic representation, Groups 2 and 3 occupied a smaller morphospace than Group 1, most likely due to lesser skull shape variability between these two older groups of horses.

The second part of the study investigated possible association between size and shape of the skulls. A PCA graphical representation without allometry was performed using multivariate regression analysis with an associated permutation test. This showed poor differentiation between different age groups, in particular between Groups 1 and 3 where minimal overlap was visible. In this graph, a large morphospace is occupied by Group 1 in relation to Groups 2 and 3. In order to test

the statistical significance of the association between size and shape, a permutation test was carried out. This permutation test implemented the null hypothesis of independence between size and shape [23] without making assumptions about the data distribution and showed a statistically significant positive correlation between size and shape, thus making allometry essential in differentiating individuals from the different age group

In the third part of the analysis, a DFA was calculated to examine differences and relationships between age groups. DFA has been used in multiple human and animal studies, including an investigation of the relationship between cranial morphology and body build in horses [16].

Much variability was found in landmark orientation in Group 1 (<5y.o.) vs Groups 2 and 3 (>5 y.o.) horses, with lesser variability found between Groups 1 and 2, and Groups 2 and 3. In particular, the results revealed that PC loadings between Groups 1 and 3 were located at the pterygoid process bilaterally, while PC loadings between Groups 1 and 2 were located at the pterygoid process bilaterally and also at the caudal aspect of the hard palate. PC loadings between Groups 2 and 3 were located at multiple locations (tip of nasal bone, pterygoid process, bilaterally; ethmoid sinus, bilaterally; caudal ventral conchal bulla, bilaterally; and the caudal aspect of the vomer).

These findings showed that the variation in equine skull shape between age groups is not uniform, but more pronounced in specific anatomical areas. However, the pterygoid bone showed minimal variation and appeared to be at a constant location within the three groups. Vidic (1968) examined the pterygoid process in human and

animal skulls (including dogs, sheep, pigs, cattle and horses) and described the length of the pterygoid process as a function of the variation of the sphenoid angles and also showed slight age-related variation in the human pterygoid process length [28].

Future GMM studies could investigate changes in equine skulls of defined known age, breed and gender in relation to their genotype to characterize breed-related disorders affecting teeth and sinonasal compartments. For example, miniature horses are predisposed to dental overcrowding due to their small skull and large teeth conformation, predisposing them to severe dental and sino-nasal problems.

Overjet/overbite ("Parrot mouth"), a rostral malocclusion of the upper incisors in relation to the lower incisors is the most common equine congenital craniofacial abnormality [29,30]. This appears to be an inherited disorder and Thoroughbred horses are more predisposed than other breeds [31]. However it remains unclear if this condition is due to mandibular brachygnathism or maxillary prognathism. DNA and associated GMM analysis of an affected population could also identify the relationship between the genotype and phenotype responsible for this condition.

Cheek teeth diastemata, the most common, painful equine dental disease affecting 50% of UK horses [32], is believed to be due to an imbalance between jaw size and cheek tooth size and orientation. This disorder could also be effectively examined by GMM in order to better determine the morphological characteristics of this disease.

The small sample size and the lack of knowledge of age and breed of each group of horses are the main limitation in this study. The age of specimens was estimated, based on their dentition and potential error should have been taken into account.

However, this pilot study proved that morphological differences exist between young and old horses. This study should be considered the foundation for future research which will aim to compare the morphological changes in equine skull with the genotype, in order to create a genotype mapping

4.5 Conclusion

This GMM study showed age-related shape changes in equine skulls. These changes in the growing equine skull are not uniform, with the allometric shape of skulls of horses under 5 years old differing substantially from those of older age groups.

Acknowledgement

The authors would like to thank Justin Perkins from the Royal Veterinary College in London for his contribution of CT data from 36 horses.

4.6 References

1. Zelditch M.L (2004). Introduction: In Geometric morphometric for Biologist, Elsevier Ltd, 1-8
2. Bookstein F.L (1984). A statistical method for biological shape comparisons. *Journal of Theoretical Biology* 107; 475-520
3. Bookstein F.L (1986). Size and shape spaces for landmark data in two dimensions. *Statistical Science* 1; 181-222
4. Bookstein F.L (1991). Introduction; In Morphometric tools for landmark data. Geometry and Biology. Cambridge University Press; 1-4
5. Bookstein F.L (1987). Describing a craniofacial anomaly: finite elements and the biometrics of landmark locations. *American Journal of Physical Anthropology* 74; 495-509
6. Glat P.M, Freund R.M, Spencer J.A, Levine J, Noz M, Bookstein F.L, McCarthy J.G, Cutting C.B (1996). A classification of plagiocephaly utilizing a three-dimensional computer analysis of cranial base landmarks. *Annal of Plastic Surgery* 36; 469-74
7. Mitteroecker P, Guz P, Bernhard M, Schaefer K, Bookstein F.L (2004). Comparison of cranial ontogenic trajectories among great apes and humans. *Journal of Human Evolution* 46; 679-97
8. Mitteroecker P, Gunz P (2009). Advances in Geometric Morphometrics. *Evolutionary Biology* 36: 235-247
9. Polly P.D, Stayton C.T, Dumont E.R, Pierce S.E, Rayfield E.P, Angielczyk R &K (2016). Combining geometric morphometric and finite element analysis with evolutionary modeling: towards a synthesis. *Journal of Vertebrate*

Paleontology

10. Webster M, Sheet H.D (2010). A practical introduction to landmark-based geometric morphometrics. *The paleontological Society Papers* 16; 163-188
11. Drake A.B, Klingenberg C.P, (2008). The pace of morphological change: historical transformation of skull shape in St.Bernard dogs. *Proceeding of the Royal Society* 275: 71-76
12. Drake A.B, Coquerelle M, Kosintev P.A, Bachura O.P, Sablin M, Gusev A.V, Fleming L.S, Losey R.J (2017). Three-Dimensional Geometric Morphometric Analysis of fossil canid mandibles and skulls. *Scientific Reports* 7, Article number 9508
13. Cervantesa I, Baumung R, Molina A, Druml T, Gutierrez J.P, Solkner J, Valera M (2009). Size and shape analysis of morphofunctional traits in the Spanish arab horse. *Livestock Science* 125; 43-49
14. Seetah K, Cucchi T, Dobney K, Barker G, (2014). A geometric morphometric re-evaluation of the use of dental form to explore differences in horse (Equus caballus) population and its potential zooarchaeological application. *Journal of Archaeological Science* 41; 904-910
15. Veitschegger K, Wilson L.A.B, Nussberger B, Camenisch G, Keller L.F, Wroe S, Sanchez-Villagra M.R (2018). Resurrecting Darwin's Niata-anatomical, biomechanical, genetic, and morphometric studies of morphological novelty in cattle. *Scientific Reports* 8: 9-129
16. Komosa M, Molinski K, Godynicki S (2006). The variability of cranial morphology in modern horses. *Zoological Science* 23; 289-98

17. Okumura M, Araujo A.G.M (2014). Long-term cultural stability in hunter–gatherers: a case study using traditional and geometric morphometric analysis of lithic stemmed bifacial points from Southern Brazil. *Journal of Archeological Science* 45; 59-71
18. Muylle, S, Simoens P, Lauwers H (1999). Age-related morphometry of equine incisors. *Zentralblatt Fur Veterinarmedizin. Reihe A* 46; 633-43
19. Carter R.A, Raymond J.G, Burton Staniar W, Cubitt T.A, Harris P.A (2009). Apparent adiposity assessed by standardised scoring system and morphometric measurements in horses and ponies. *Veterinary Journal* 179; 204-210
20. Cavalleri J.M, Metzger J, Hellige M, Lampe V, Stuckenschneider K, Tipold A, Beineke A, Becker K, Disti O, Feige K (2013). Morphometric magnetic resonance imaging and genetic testing in cerebellar abiotrophy in Arabian horses. *BMC Veterinary Research* 23; 105
21. Liuti T, Reardon R, Smith S, Dixon P.M (2016). An anatomical study of the dorsal and ventral nasal conchal bullae in normal horses: Computed Tomographic anatomical and morphometric findings. *Equine Veterinary Journal* 48; 749-755
22. Klingenberg C.P (2011). MorphoJ: an integrated software package for geometric morphometrics. *Molecular ecology Resources,* 11; 353-357
23. Good P (2000). Permutation tests: a practical guide to resempling methods for testing hypothesis 2nd edn Springer New York; 1-12
24. Bignon O, Baylac M, Vigne J.D, Eisenmann V (2005). Geometric morphometric and the population diversity of Late Glacial horses in Western

Europe (Equus caballus arcelini): phylogeographic and anthropological implication. *Journal of Archeological Science* 32; 375-391

25. Joyce J.R, Pierce K.R, Romane W.M, Baker J.M. (1971). Clinical study of nutritional secondary hyperparathyroidism in horses. *Journal of American Veterinary Medicine Association* 158; 2033-42
26. Vidic B (1968). The variation in length of the pterygoid process as a function of the variations of the sphenoid angle. *The anatomical record* 160; 527-530
27. Easley J, Dixon P.M, Reardon R.J.M. (2016). Orthodontic correction of overjet/overbite ('parrot mouth') in 73 foals (1999-2013). *Equine Veterinary Journal* 48; 565-572
28. De Bowes, R.M. and Gaughan, E.M. (1998). Congenital dental disease of horses. *Veterinary Clinic North America Equine Practice* 14; 273-289.
29. Dixon P.M, Ceen, S, Barnett T, O'Leary J.M, Parkin T.D, Barakzai S. (2014). A long-term study on the clinical effects of mechanical widening of cheek teeth diastemata for treatment of periodontitis in 202 horses (2008–2011). *Equine Veterinary Journal*, 46; 76-80
30. Walker H, Chinn E, Holmes S, Barwise-Munroe L, Robertson V, Mould R, Bradley S, Shaw D.J. and Dixon P.M.(2012). Study of the prevalence and some clinical characteristics of equine cheek teeth diastemata in 471 horses examined in a UK first opinion equine practice (2008–2009). *Veterinary Record* 171; 44.

CHAPTER 5: Radiographic, computed tomographic, gross, pathological and histological findings with apical infection of 32 maxillary cheek teeth

Paper published on Equine Veterinary Journal: doi: 10.1111/evj.12729

5.1 Introduction

Equine maxillary cheek teeth apical infection is a serious disorder, which can extend to the supporting bony structures and overlying sinuses. Unilateral or bilateral nasal discharge caused by sinus or nasal infections and facial swelling are the most common clinical findings in horses affected by maxillary cheek teeth apical infection.

CT has been described as the imaging modality of choice to best outline the anatomy and the relationship between different skull structures in healthy horses and horses with infected cheek teeth. With the advent of standing equine CT, this imaging modality has become more readily available not only within University Institutions but also within large referral practices. To date, assessment of the value of CT in diagnosing equine cheek teeth apical infection has largely been anecdotal and no objective study has yet assessed the value of CT in this regard.

The aims of this study were (i): to compare conventional radiographic and CT dental imaging findings in clinical cases presented with nasal discharge and facial swelling believed to be caused by maxillary cheek teeth apical infections, with the gross pathological and histological findings in extracted cheek teeth and (ii): to assess the accuracy of these imaging modalities in detecting dental infections.

Conception and design of the study was by Tiziana Liuti and Prof. P.M Dixon

Data acquisition was by Tiziana Liuti

Analysis and data interpretation was by Tiziana Liuti with assistance from Dr. Sionagh Smith and Prof. P.M Dixon

Drafting of the article was by Tiziana Liuti

The revision of the article for intellectual content was by Tiziana Liuti, Prof. P.M Dixon and Dr Sionagh Smith

Final approval of the completed article was by Prof. P.M Dixon and Tiziana Liuti

Equine Veterinary Journal

Equine Veterinary Journal ISSN 0425-1644
DOI: 10.1111/evj.12729

Descriptive Clinical Reports

Radiographic, computed tomographic, gross pathological and histological findings with suspected apical infection in 32 equine maxillary cheek teeth (2012–2015)

T. LIUTI*, S. SMITH and P. M. DIXON

Royal (Dick) School of Veterinary Studies and The Roslin Institute, The University of Edinburgh, Roslin, UK.

*Correspondence email: tiziana.liuti@ed.ac.uk; Received: 28.03.17; Accepted: 28.07.17

Summary

Background: Equine maxillary cheek teeth apical infections are a significant disorder because of frequent spread of infection to the supporting bones. The accuracy of computed tomographic imaging (CT) of this disorder has not been fully assessed.
Objectives: To compare the radiographic and CT findings in horses diagnosed with maxillary cheek teeth apical infections with pathological findings in the extracted teeth to assess the accuracy of these imaging techniques.
Study design: Observational clinical study.
Methods: Thirty-two maxillary cheek teeth (in 29 horses) diagnosed with apical infections by clinical, radiographic and principally by CT examinations, were extracted orally. The extracted teeth were subjected to further CT, gross pathological and histological examinations. Four normal teeth extracted from a cadaver served as controls.
Results: Pulpar and apical changes highly indicative of maxillary cheek teeth apical infection were present in all 32 teeth on CT, but in just 17/32 teeth (53%) radiographically. Gross pulpar/apical abnormalities and histological pulpar/periapical changes were present in 31/32 (97%) extracted teeth. On CT, one tooth contained small gas pockets in the apical aspect of one pulp and adjacent periodontal space, however no pathological changes were found following its extraction.
Main limitations: The study is descriptive and is confined to a small number of cases.
Conclusion: This study showed a 97% agreement between CT diagnosis of maxillary cheek teeth apical infection and the presence of pathological changes in the extracted teeth, confirming the diagnostic accuracy of CT compared with radiography for this disorder.

Keywords: horse; maxillary cheek teeth; apical infection; radiography; computed tomography; dental pathology

Introduction

Dental apical (periapical) infections are caused by multispecies bacterial infection of one or more pulp horns that spreads to the adjacent periapical periodontal membranes as well as, to a varying degree, to adjacent alveolar bone and calcified dental tissues [1–7]. Equine apical infections can be caused by dental fractures, infundibular caries, anachoresis (blood borne infection) and descending periodontal disease [2,8]. Regardless of aetiology, apically infected teeth usually have pathological changes to one or more pulp horns and the adjacent periapical periodontal membranes. An exception is periapical infection caused by patent maxillary cheek teeth infundibulae that usually do not have pulpar involvement [2,9].

Because of the great length of equine maxillary cheek teeth, apical infections are a very significant disease and commonly extend to the supporting maxillary bones, especially in younger horses, causing chronic, unilateral malodorous nasal discharge or bony facial swellings and/or sinus tracts [6]. Such cases require extraction (or endodontic therapy) of affected teeth for permanent resolution of signs. However, extraction of equine cheek teeth is a major undertaking with numerous possible short and long-term complications [6,9], hence the great reliance on imaging for the accurate diagnosis of apical infections.

Radiography is the most commonly used imaging technique for such cases, but conventional radiography has a reported sensitivity of only 50–69% [10–12], and digital radiography of 76–80% [13]. Scintigraphy also has a poor sensitivity (56%) in diagnosing apical infections [11], but a better sensitivity (79%) in diagnosing dental-related sinusitis [12].

Because of the above-noted limitations of radiography, computed tomography (CT) is increasingly used to diagnose equine sinonasal and dental disorders [14–16] and for anatomical dental studies [17–19]. Henninger *et al.* [14] and Buhler *et al.* [16] noted the diagnostic advantage of CT for equine cheek teeth apical infection, with the former noting the diagnostic significance of intrapulpar gas or root fragmentation, whilst the latter noted the significance of increased volume and irregular margins of pulp horns, and heterogeneous pulp density.

The aim of this study was to compare the radiographic and CT findings in horses diagnosed with maxillary cheek teeth apical infections with the gross pathological and histological findings in the extracted teeth, to assess the accuracy of these imaging techniques for this disorder.

Materials and methods

Twenty-nine horses presented to the Hospital for Large Animal, Royal (Dick) School of Veterinary Studies (2012–2015) with chronic unilateral nasal discharge (n = 24) or maxillary swelling (n = 5) of 1–20 weeks' duration, including Thoroughbred (n = 16); Warmblood (N = 5); Irish Draught (N = 4); Cob (N = 3) and Arabian (n = 1) with a mean age of 9 years (range 3–15 years). Clinical examination, including oral endoscopy, was performed in each case, followed by radiographic and standing CT. Teeth diagnosed with apical infection on the basis of these clinical and imaging findings were orally extracted. The extracted teeth underwent further CT, gross pathological and histological examinations. Four normal maxillary cheek teeth (Triadan 07–10) extracted from a cadaver were used as controls.

Diagnostic imaging

Four computed radiographic projections were acquired from each case (Agfa CR 25 digitiser[a]): lateral, dorsoventral, two latero 30° dorsal-lateroventral oblique projections of the affected and of the contralateral maxillary arcade (for comparison) and assessed for features of apical infection using standard criteria [13,20].

CT images were acquired using a multislice scanner (Siemens Volume Zoom[b]) at Kv 120, mAs 100 and H70 algorithm, at 3 mm intervals, with

images saved in a DICOM format. The extracted teeth were re-imaged by CT within 24 h of extraction, at 0.5 mm intervals in a vertical position. The main emphasis on CT was assessment of the pulp horns including for the presence of gas or heterogeneity of pulp; pulpar volume and regularity of pulp horns margins; changes in periapical periodontium including presence of gas and widening; root clubbing and fragmentation and periapical alveolar bone lysis [16,18,19,21]. All radiographic and CT images were independently assessed by two observers.

Gross anatomical examination: Extracted and control teeth were grossly examined and photographed before being fixed in neutral buffered formalin within 24 h of extraction. They were later transversely sectioned with a lapidary blade into 4 equal parts, i.e. occlusal; two mid-crown and apical aspects. These four sections were examined and photographed on both sides before a 5 mm thick section was cut from each for histology.

Histological examination: The sectioned dental specimens were placed into Decal II^{c} for 4 days and then transferred into Decal I^{c} for 2–4 weeks until decalcified. Specimens were then embedded in paraffin wax and 4 μm thick sections were prepared and stained with haematoxylin and eosin.

The four histological slides of each tooth, including controls, were anonymised, and re-labelled before examination, that documented findings in pulp, dentine, periodontal ligament, peripheral cementum and infundibulum in all teeth. All enamel was lost during decalcification. Pulpar features assessed included: the presence of intrapulpar bacteria, neutrophilic or lympho-plasmacytic infiltration, food material, tertiary dentine and pulp stones.

Results

Clinical dental findings

Oral examinations showed that 12 teeth (from 12 horses) had no clinical crown abnormalities; nine teeth (from nine horses) had defective or absent secondary dentine overlying one or more pulp horns and 11 teeth (from eight horses) had fractures (10 idiopathic fractures through pulp horns and one infundibular, caries-related midline sagittal fracture). The 09s were the most commonly affected Triadan position (16/32 teeth); 08s (n = 8); 07s (n = 3); 10s (n = 3); 06s (n = 1); 11s (n = 1).

Pre extraction CT (3 mm intervals) and post extraction CT (0.5 mm intervals)

No apparent difference was found between pre- and post extraction CTs in the detection of pulpar or calcified dental tissue changes (other than extraction forceps marks on the clinical crown). Iatrogenic, extraction-related periodontal changes were present post extraction, mainly characterised by localised loss of reserve crown periodontium. The width of the periodontal space could not be assessed on post extraction CT. The pre extraction CT findings were further used in the study.

Radiography

The main radiographic findings included: periapical sclerosis in 12/32 teeth; apical blunting (n = 10); periapical halo (n = 3) and crown fracture (n = 6). Periapical halo is a well-defined osteolucency surrounding the apex. On the basis of these findings, a consensus was reached that radiographic changes highly indicative of apical infection were present in 17/32 (53%) teeth.

Pre extraction CT findings

The main CT findings included: gas (areas with a density of <1000 Hounsfield units) within pulps in 32/32 teeth, increased pulpar volume (n = 16), irregular pulp horns margins (n = 13); gas within periapical tissues (n = 15), widened periodontal space (n = 8); root clubbing (n = 24), root fragmentation (n = 14); periapical halo (n = 31), periapical alveolar bone lysis (n = 11), dental fracture (n = 11) and infundibular changes (other than cemental hypoplasia) (n = 10) (Figs 1–3). A consensus was reached by both examiners that all 32 teeth had CT evidence of apical disease, in particular the presence of pulpar changes in all teeth. Largely on the basis of these CT findings, all 32 teeth were extracted. No CT changes (post extraction imaging only) were found in the four control cheek teeth.

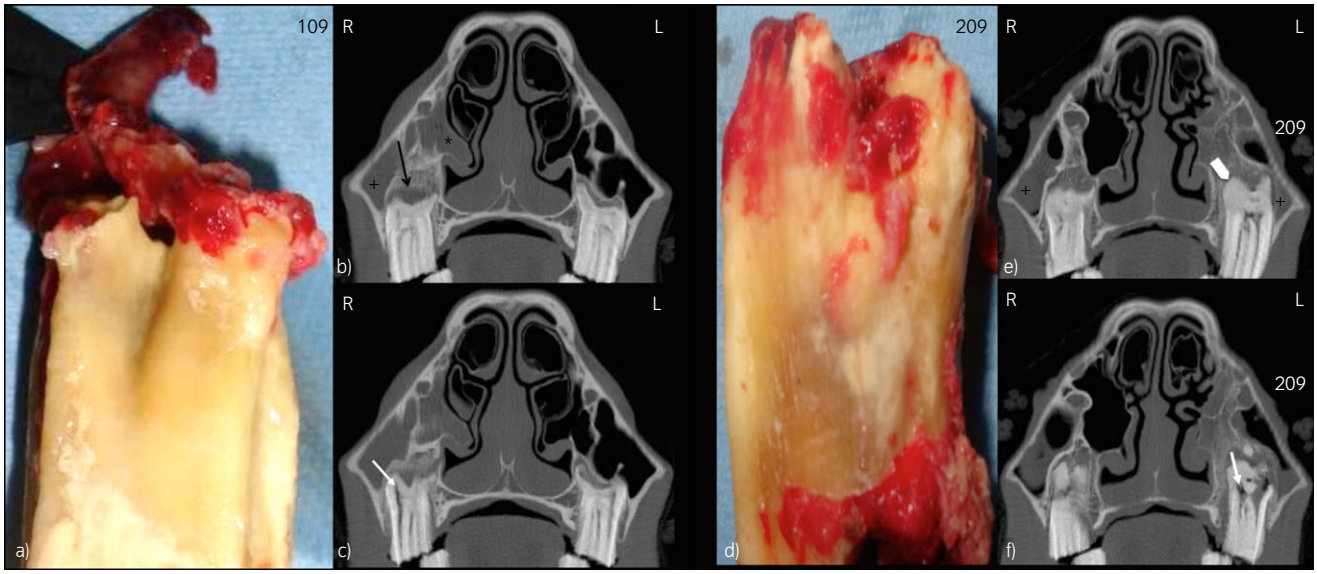

Fig 1: Tooth 2: (a) Apex post extraction, showing abnormal, thickened periodontium attached to one blunt root tip and much periodontal loss. (b) Transverse CT image of its rostral aspect showing; widened perialveolar space (arrow), blunting and shortening of roots and fluid filled right ventral conchal sinus (VCS) (*) and rostral maxillary sinus (RMS) (+). (c) Transverse CT image of its caudal aspect showing intrapulpar gas (arrow). Tooth 4: (d) Apex post extraction, showing shortened roots, generalised hypercementosis and thickened periodontal remnants. (e) Transverse CT image of its rostral aspect showing enlarged perialveolar space, blunting of root with hypercementosis (arrow head), and bilateral fluid filled RMS (+) (horse has intercurrent contralateral sinus disease). (f) Transverse CT image of its caudal aspect showing distorted apex, intrapulpar gas (arrow) and a round cemental structure ('pearl') in periodontium. R: Right, L: Left.

Gross pathological findings in extracted teeth

Pulp: The 11 teeth with pre-existing fractures contained pulpar changes (including discoloured pulps, food material in pulp horns and staining of adjacent dentine in sectioned teeth) in one or more pulp horns in all 11 teeth, but 10/11 teeth had one or more apparently viable pulps remaining. The nine teeth with occlusal pulpar exposure contained pulpar changes (to apical level of the occlusally exposed pulps) in all nine teeth, but one or more apparently viable pulps remained in 7/9 teeth. In the 12 teeth without clinical crown abnormalities, gross pulpar changes were present in 9/12 teeth, with one or more apparently viable pulps remaining in four of these nine teeth. Overall, gross pulpar abnormalities were present in the pulps of 29/32 teeth, with every pulp diseased in eight teeth and apparently viable pulps remaining in the other 24 teeth.

Dentine: Gross dentinal changes, mainly the presence of circumpulpar dentine staining and irregular dentinal-pulpar margins, were present around one or more pulp horns in 26/32 teeth. In five teeth, gross communication was present between a carious infundibulum and infected pulp horn(s).

Periodontal changes: Localised apical periodontal thickening or focal, firm, pink, soft tissue swellings were present, especially over the roots, in 26 teeth (Figs 1–3). Localised loss of periodontal membranes and discolouration of roots were present in three teeth (Fig 3a) and gross abscess formation was identified in one tooth (Fig 2d).

Calcified apical tissue changes: Proliferative calcified apical changes, including thickened, irregular-shaped and/or more generalised apical hypercementosis, were present in 17/32 teeth, with more destructive calcified changes including shortened roots and root destruction present in 8/32 teeth (Figs 1–3).

Infundibulae: Gross caries was identified in the infundibulae of 16 teeth, with the Triadan 09 position affected in seven of these 16 teeth.

In summary, gross examination showed pulpar changes in 29 teeth and apical changes in 31 teeth. No grossly detectable changes were present in one tooth, or in the four control teeth.

Histological findings

Pulp: Histologically pulpar changes were present in 31/32 teeth, involving 112/162 pulps (mean 3.5, range 1–5 affected pulps/tooth) with every pulp diseased in eight teeth. Histologically, 24/32 teeth were found to contain normal appearing pulp in a total of 50 pulp horns (mean 1.6, range 1–4, normal pulps/tooth). All five pulps in each control tooth were normal.

Histological pulpar abnormalities included what was termed 'faded pulp' in 29/32 teeth. This feature was characterised by a pulp stroma that was much paler than that of normal viable pulps and which there was loss of nuclear detail in stromal fibroblasts, loss of normal vasculature and often superimposed dentinal debris at the periphery; intrapulpar bacteria and neutrophils (n = 16); intrapulpar bacteria (n = 2); food material (n = 15) and pulp necrosis (n = 2) (Fig 4). Pulp stones (1–8/section) were present within pulp and secondary dentine in 20/32 infected and in 2/4 control teeth.

Of particular interest were the three teeth without gross pulpar changes; one histologically contained intrapulpar bacteria and neutrophils; one contained 'faded pulps'; and one had no detectable pulpar abnormalities. Five further histological sections of the apical region of the latter (anatomically normal) tooth were obtained but no histological changes were identified.

Periodontal membranes: Histological periodontal abnormalities were present in 25/32 (78%) teeth, including the presence of: haemorrhage/fibrin (n = 19), bacteria/neutrophils (n = 7), plasma cells (n = 6), lymphocytes (n = 6) and, less commonly, chondroid metaplasia, micro-abscesses, periodontal thickening and granulation tissue (Fig 4).

Dentine: Histological dentinal changes were found in 22/32 (69%) teeth, including: irregular pulpar-dentinal margins (n = 15), dentinal lysis at the pulp canal periphery (n = 7) and tertiary dentine formation (n = 4) (Fig 5).

Cementum: Some roots/apices were lost during sectioning, decalcification and histological processing. In addition to the proliferative apical remodelling grossly recognised in 17 teeth (53%), histological abnormalities of apical and adjacent reserve crown peripheral cementum were found in 21/32 teeth (65.6%) and

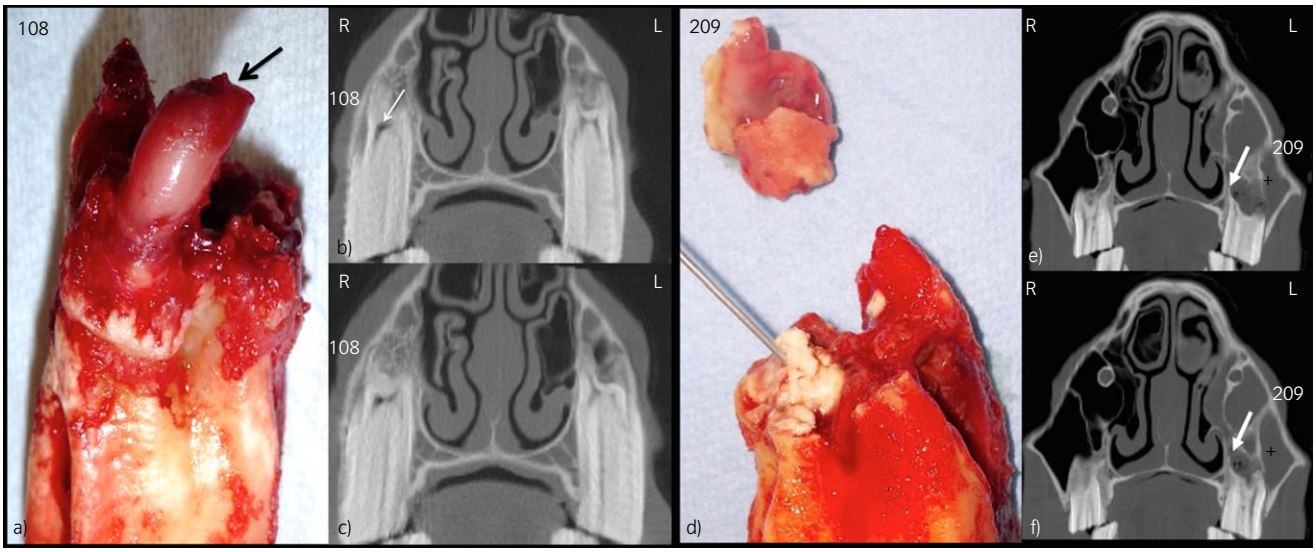

Fig 2: Tooth 15: (a) Apex post extraction, showing a swollen pulp (arrow) protruding through a thickened, short, caudo-buccal root with thickened remnants of apical periodontal membranes. (b) Transverse CT image of its rostral aspect showing an enlarged perialveolar space, blunting of root and intrapulpar gas (arrow). (c) Transverse CT image of its caudal aspect with intrapulpar gas. Tooth 27: (d) Apex post extraction, showing inspissated exudate lying in a lytic palatal root that fractured during extraction. (e) Transverse CT image of its rostral aspect showing; enlarged perialveolar space, blunting of buccal root, perialveolar gas (arrow) and a fluid filled RMS (+). (f) Transverse CT image of its caudal aspect showing much perialveolar gas (arrow) and a fluid filled RMS (+). R: Right, L: Left.

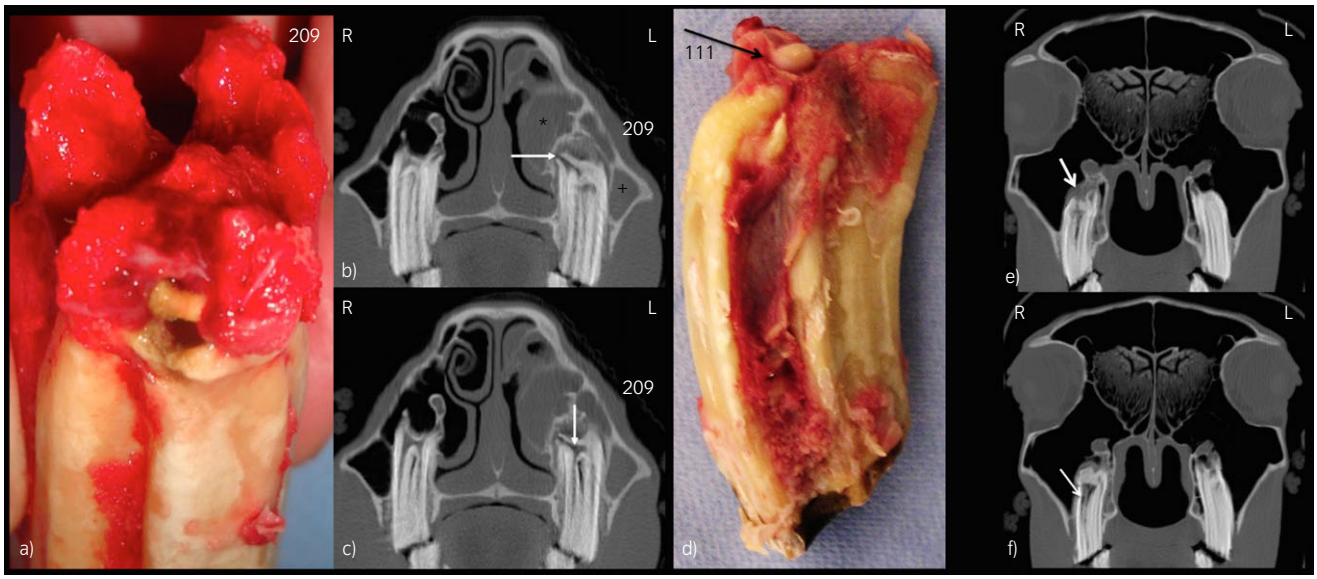

Fig 3: Tooth 6: (a) Apex post extraction, showing chronically infected apex with focal, brown discolouration of roots. Periodontium is lost on crown and thickened over apex. (b) Transverse CT image of its rostral aspect showing widened perialveolar space, blunting of the gas-filled buccal root (arrow), and fluid filled VCS (*) and RMS (+). (c) Transverse CT image of its caudal aspect showing intrapulpar gas (arrow). Tooth 5: (d) Apex post extraction showing widened apex, apical granuloma (arrow) and thickened apical periodontal membranes. (e) Transverse CT image of its rostral aspect showing an enlarged perialveolar space (arrow), blunt roots and abnormal apical architecture. (f) Transverse CT image of its caudal aspect showing intrapulpar gas (arrow). R: Right, L: Left.

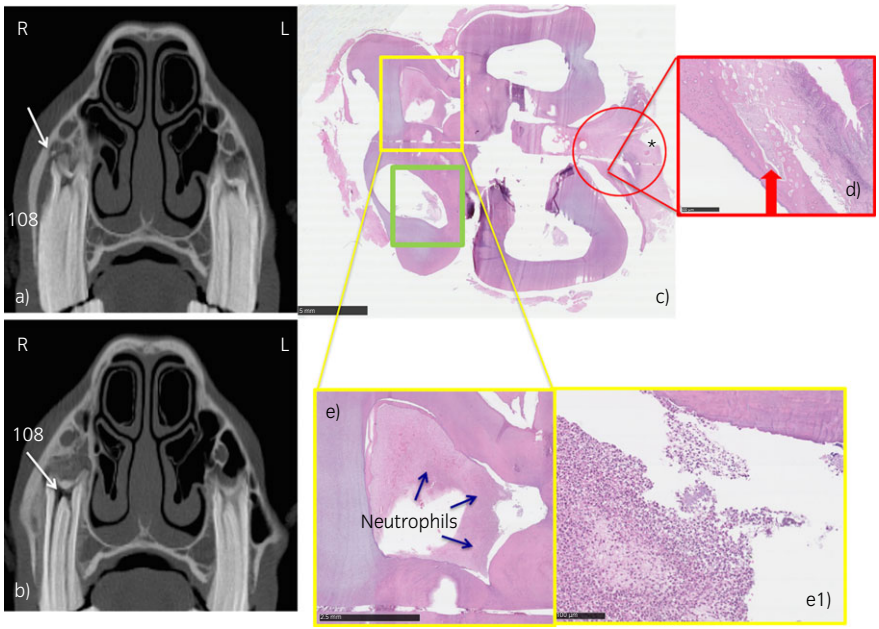

Fig 4: Tooth 8: (a) Transverse CT image of its rostral aspect showing an enlarged perialveolar space, fragmented root (arrow) and maxillary bone thickening. (b) Transverse CT image of its caudal aspect showing intrapulpar gas (arrow). (c) Histological image of apex. Yellow box: Chronic suppurative focus indicative of chronic abscessation with granulation tissue; cemental erosion and loss of viable pulp (e). e1 (higher power) shows many neutrophils and a few bacteria. Green box: Pulp cavity containing small area of suppurative inflammation and no viable pulp. Red circle: Granulation tissue and fibrosis with fragment of embedded cementum (*). Within the granulation tissue, there is an infolding of periodontium surrounded by lymphocytes and plasma cells and peripheral cemental erosion where the granulation tissue extends into cementum (arrow) (d). R: Right, L: Left.

included: cemental erosion/lysis (n = 12) (Fig 6), overlying plaque/biofilm (n = 8) and cemental necrosis (n = 1).

Infundibulae: Sixteen (50%) teeth had histological infundibular changes (other than central cemental hypoplasia/occlusal caries) including the presence of plant material, bacteria, carious infundibular cementum, fibrin, haemorrhage and granulation tissue in infundibulae. The latter three findings indicated involvement of adjacent pulp.

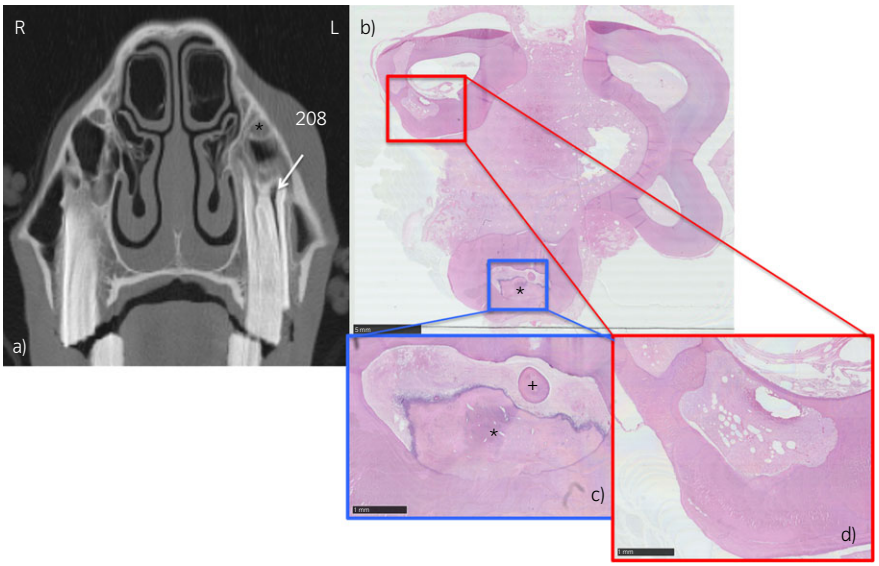

Fig 5: Tooth 18: (a) Transverse CT image showing enlarged perialveolar space; intrapulpar gas (arrow) and an extensive soft tissue facial swelling (*). (b) Histological image of apex. Red box: Well demarcated area of severe dentinal lysis. The resultant cavity is filled with granulation tissue, blood and small numbers of lymphocytes and macrophages. Blue box: Pulp necrosis with granular material and some necrotic cell debris. Tertiary dentine (*), which is partly degenerate and pulp stones are also visible (+). R: Right, L: Left.

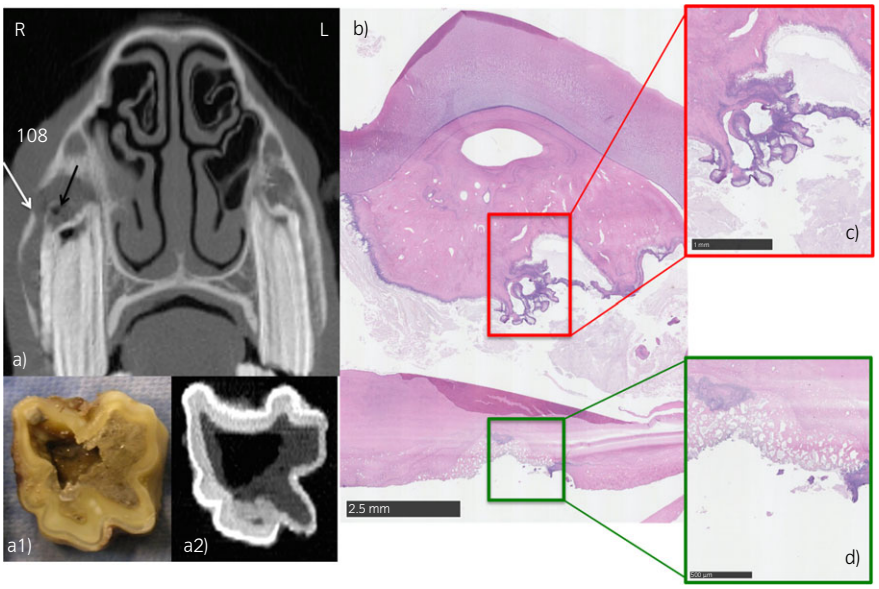

Fig 6: Tooth 10: (a) Transverse CT image showing an enlarged perialveolar space, gas within the common pulp, widened periapical region (black arrows); maxillary bone lysis (white arrow), and a blunt, shortened palatal root. (a1) Gross transverse section just above the apex showing an enlarged, discoloured common pulp. (a2) Transverse CT section of tooth corresponding to the gross section a1. (b) Histological image just above the apex showing reactive peripheral cementum deposition and subsequent lysis (c, d) at the level of the common pulp cavity. R: Right, L: Left.

Discussion

Indications for CT

Twenty teeth examined in this study had fractured crowns or occlusal pulpar exposure and it could be questioned whether advanced imaging was required to diagnose apical infection in these teeth. The presence of clinical crown ('idiopathic') fractures indicates oral cavity exposure of one or more pulp horns [1,2], however, 72% of such fractured teeth may not develop clinical apical infection, likely due to sealing of the exposed pulp horn with tertiary dentine [22–25]. The presence of occlusal pulpar exposure is usually indicative of pulpar and thus apical disease [23,24], but some clinically normal horses have cheek teeth occlusal pulpar exposure, with dentinal bridges beneath the exposed pulp but overlying the deeper healthy pulp [24–26]. Consequently, the presence of occlusal pulpar exposure is not definitive evidence of pulpar death and apical infection.

Usefulness of radiography

As noted earlier and as recently reviewed [20,27], radiographic diagnosis of equine cheek teeth infection has a low sensitivity, particularly in early cases, where radiographic identification of diseased teeth is frequently

impossible. Interpretation of some of the radiographic changes of apical infections is subjective and differences in the interpretation of specific radiographic features can occur between examiners [1,2,13]. In the current study, a consensus was reached that imaging changes, sufficient to advise extraction, were present in only 53% (17/32) of infected teeth, albeit many were believed to be of short duration. Consequently, on the basis of a radiographic diagnosis, 15 teeth (47%) in this study would not have been extracted, including 14 (44%) that were later shown to have apical infection. These horses would very likely have had recurrence of clinical signs following conservative therapy such as antibiotic administration and/or sinus lavage. Later radiographic examination would likely have shown a higher proportion with definitive radiographic changes.

Usefulness of CT

Periapical infection was diagnosed by both examiners in all 32 cheek teeth by CT. In particular, the presence of pulpar changes, including intrapulpar gas and other changes in pulp density, such as those caused by the presence of food or necrotic pulp, enlarged pulp horns and irregular pulp margins were important diagnostically, along with changes to the periapical region. Many of these CT changes are not, or are only poorly, detectable radiographically. These CT findings were a significant basis for extraction of the 15 infected cheek teeth that did not have definitive radiographic evidence of apical infection and also the sole reason for extracting the apparently healthy tooth.

The pathology of equine apical infections

Apically infected cheek teeth can grossly present with the presence of: thickening, granuloma formation or even loss of the apical periodontal membranes; proliferative (hypercementosis) to destructive (shortening of roots –'clubbing') remodelling of the dental apex or even necrotic apical changes. Affected pulp horn(s) can contain discoloured, necrotic or absent pulp or food debris, with possible staining of the adjacent dentine [1–3,6,9,25,26]. Histologically, affected pulp may be oedematous, with inflammatory cell and bacterial infiltration with necrosis and/or destruction of dentine surrounding infected pulps [1–4,26].

Apical pathological findings in the current study

Gross, but often localised, apical changes were present in 30/32 (94%) extracted teeth, including thickened periapical periodontal membranes or focal, granulation tissue swellings, especially over the roots, in 81% of teeth; and proliferative and destructive cemental remodelling of the roots and adjacent apex in 78% (Figs 1–3). Histological periodontal or calcified apical changes were identified in 91% of teeth, although some periodontal changes, such as the presence of haemorrhage and fibrin, were likely related to the extraction procedure. Variation between gross and histological apical findings could be explained by the loss and disintegration of some more lytic roots/apices during tooth sectioning, decalcification and histological processing.

Pulpar pathological findings

Gross pulpar changes were present in 91% of teeth, including: intrapulpar food, discoloured or necrotic pulp horns and stained adjacent dentine. There was histological evidence of pulpar disease in 97% of teeth (all teeth had shown pulpar changes on CT). Histological, pulpar changes included the presence of avascular pulp with pallor of the stroma; bacterial and neutrophil infiltration; and/or the presence of food in pulp horns. Pulp stones were histologically found in 66% of diseased and 50% of control teeth and were considered a normal finding [28].

Dentinal changes

In the current study, dentine was grossly abnormal in 81% of teeth but histologically abnormal in just 64% of teeth. Changes included the presence of irregular margins, dentinal lysis, dentinal degeneration, tertiary dentine and intradentinal abscess formation (Fig 5). This difference is speculated to be due to localised areas of dentinal damage recognised on gross examination not being captured in the histological sections and/or disintegrating during processing. Significant dentinal disease can make affected pulp horns appear larger, with or without irregular margins, as noted on CT in 17/32 teeth (12 with both of these changes).

Although sometimes termed as apical abscesses (which indicates the accumulation of pus) only 4/32 teeth (13%) could be grossly classified as such (one apex contained pus and three apices had localised, necrotic changes). However, with spread of infection to the adjacent maxillary bone or sinuses, as occurred in these cases, a marked purulent infection of these other structures then ensued. Surprisingly, 24/32 teeth (75%) still had one or more histologically normal pulps remaining, further demonstrating the localisation of infection in affected teeth. Overall, the changes in most extracted teeth were indicative of a chronic, low-grade infection. It is likely that the current early recognition and referral of these cases for advanced imaging could explain the lower grade changes found in these teeth than previously reported [1,28].

One tooth (207) that lay in an adjacent alveolus to a tooth (208) with gross and histological changes of apical infection, showed gas in the apical aspect of its pulp and in the adjacent periodontal space on CT. However, gross and histological examinations did not detect any abnormalities of this tooth, or of the attached periodontal membranes. The reason for this discrepancy between CT and pathological findings is unclear. It is unlikely that free gas, usually indicative of gas-producing bacteria, could be present in a healthy pulp. The possibilities include that the apparent presence of pulpar and periapical gas in this tooth on CT was artefactual, and possibly related to an immediately adjacent apically infected tooth that also contained pulpar gas. It is also possible that localised pathological pulpar changes were present, that were not detected using the current sampling technique, or that pathological changes were confined to the apical periodontium that remained attached to the alveolus during extraction or was lost during processing. Following extraction of these two teeth, the clinical signs permanently resolved in this horse.

Infundibular lesions

Interpreting the significance of infundibular changes in equine cheek teeth on clinical, imaging or pathological examinations is very problematic. Imaging [20,21] and pathological [29,30] studies have shown that up to 90% of infundibulae are incompletely filled with normal cementum. Extension of infundibular caries has been reported to cause 16% [2] and 27% [9] of maxillary cheek teeth apical infections although another CT study found no relationship between infundibular and apical abnormalities [23]. Hypoplastic or carious infundibular lesions can look dramatic on imaging, gross and histological examinations, but if the enamel 'cup' of the infundibulum remains intact, none of these lesions can cause endodontic and thus apical infection. However, in some cases extension of infundibular caries through infundibular enamel defects can cause endodontic and apical infection [1,2,9,20,21] as was found in five of the current 32 teeth.

Limitations and conclusions

The study is limited to a small number of animals and its descriptive nature. Nevertheless, pathological examination of the extracted teeth in this group of animals confirmed the advantage of CT over radiography in the diagnosis of early equine maxillary cheek teeth apical infections.

Authors' declaration of interests

No competing interests have been declared.

Ethical animal research

This study was approved by the Ethical Committee of the University of Edinburgh. Owners of horses with apical infection and one control horse subjected to post mortem examination for unrelated reasons gave permission for use of images and tissues for research.

Source of funding

University of Edinburgh.

Acknowledgement

The authors would like to thank Mr Neil MacIntyre and Craig Pennycook for their technical assistance.

Authorship

All authors contributed and accepted full responsibility for the study design.

Manufacturers' addresses

[a]Agfa Healthcare UK Ltd, Brentford, Middlesex, UK.
[b]Siemens, Germany.
[c]Leica MicroSystems, Knowlhill, Milton Keynes, Buckinghamdshire, UK.

References

1. Dacre, I.T., Kempson, S. and Dixon, P.M. (2008) Pathological studies of cheek teeth apical infections in horse: 5. Aetiopathological findings in 57 apically infected maxillary cheek teeth and histological and ultrastructural findings. *Vet. J.* **178**, 352-363.
2. Siqueira, J.F. and Rôças, I.N. (2013) Microbiology and treatment of acute apical abscesses. *Clin. Microbiol. Rev.* **2**, 255-273.
3. Casey, M.B., Person, G.R., Perkins, J.D. and Tremaine, W.H. (2015) Gross, computed tomographic and histological findings in mandibular cheek teeth extracted from horses with clinical signs of pulpitis due to apical infection. *Equine Vet. J.* **47**, 557-567.
4. Lundström, T. and Wattie, O. (2016) Description of a technique for orthograde endodontic treatment of equine cheek teeth with apical infection. *Equine Vet. Educ.* **28**, 641-652.
5. Nair, P.N.R. (2004) Pathogenesis of apical periodontitis and the causes of endodontic failures. *Crit. Rev. Oral Biol. Med.* **15**, 348-381.
6. Dixon, P.M., Tremaine, W.H., Pickles, K., Kuhns, L., Hawe, C., McCann, J., McGorum, B.C., Railton, D.I. and Brammer, S. (2000) Equine dental disease Part 4: a long-term study of 400 cases: apical infections of cheek teeth. *Equine Vet. J.* **32**, 182-194.
7. Suske, A., Poschke, A., Muller, P., Wober, S. and Staszyk, C. (2016) Infundibula of equine maxillary cheek teeth Part 2: morphological variations and pathological changes. *Vet. J.* **209**, 66-73.
8. Pearce, C.J. (2016) Treatment of maxillary cheek teeth apical infection caused by patent infundibula in six horses (2007–2013). *Equine Vet. Educ.* **11**, 600-608.
9. Tremaine, W.H. and Schumacher, J. (2011) Exodontia. In: *Equine Dentistry*, 3rd edn., Eds: J. Easley, P. Dixon and J. Schumacher, Elsevier, Saunders, Edinburgh. pp 319-344.
10. Gibbs, C. and Lane, J.G. (1987) Radiographic examination of the facial, nasal and paranasal sinus regions of the horse. II. Radiological findings. *Equine Vet. J.* **19**, 474-482.
11. Weller, R., Livesey, L., Maierl, J., Nuss, K., Bowen, I.M., Cauvin, E.R., Weaver, M., Schumacher, J. and May, S.A. (2001) Comparison of radiography and scintigraphy in the diagnosis of dental disorders in the horse. *Equine Vet. J.* **33**, 49-58.
12. Barakzai, S., Tremaine, H. and Dixon, P.M. (2006) Use of scintigraphy for diagnosis of equine paranasal sinus disorders. *Vet. Surg.* **35**, 94-101.
13. Townsend, N.B., Hawkes, C.S., Rex, R., Boden, L.A. and Barakzai, S.Z. (2011) Investigation of the sensitivity and specificity of radiological signs for the diagnosis of periapical infection of equine cheek teeth. *Equine Vet. J.* **43**, 170-178.
14. Henninger, W., Frame, M., Willmann, M., Simhofer, H., Malleczek, D., Kneissl, S. and Mayrhofer, E. (2003) CT features of alveolitis and sinusitis in horses. *Vet. Radiol. Ultrasound* **44**, 269-276.
15. Veraa, S., Voorhout, G. and Klein, W.R. (2009) Computed tomography of the upper cheek-teeth in horses with infundibular changes and apical infection. *Equine Vet. J.* **41**, 872-876.
16. Buhler, M., Furst, A., Lewis, F.I., Kummer, M. and Ohlerth, S. (2014) Computed tomographic features of apical infection of equine maxillary cheek teeth: a retrospective study of 49 horses. *Equine Vet. J.* **46**, 468-473.
17. Windley, Z., Weller, R., Tremaine, W.H. and Perkins, J.D. (2009) Two-dimensional and three-dimensional computer tomographic anatomy of the enamel, infundibulae and pulp of 126 equine cheek-teeth. Part 1: findings in teeth without macroscopic occlusal or computer tomographic lesions. *Equine Vet. J.* **41**, 433-440.
18. Windley, Z., Weller, R., Tremaine, W.H. and Perkins, J.D. (2009) Two-dimensional and three-dimensional computer tomographic anatomy of the enamel, infundibulae and pulp of 126 equine cheek-teeth. Part 2: findings in teeth with macroscopic occlusal or computer tomographic lesions. *Equine Vet. J.* **41**, 441-447.
19. Kopke, S., Angrisani, N. and Staszyk, C. (2012) The dental cavities of equine cheek teeth: three-dimensional reconstructions based on high resolution micro-computed tomography. *BMC Vet. Res.* **8**, 173.
20. Isgren, C.M. and Townsend, N.B. (2015) The use of radiography for diagnosis of apical infection of equine cheek teeth. *Equine Vet. Educ.* **8**, 448-454.
21. Barakzai, S.Z. and Barnett, T.P. (2015) Computed tomography and scintigraphy for evaluation of dental disease in the horse. *Equine Vet. Educ.* **6**, 232-331.
22. Casey, M.B. and Tremaine, W.H. (2010) The prevalence of secondary dentinal lesions in cheek teeth from horses with clinical signs of pulpitis compared to controls. *Equine Vet. J.* **42**, 30-36.
23. Du Toit, N., Burden, F.A., Kempson, S.A. and Dixon, P.M. (2008) Pathological investigation of caries and occlusal pulpar exposure in donkey cheek teeth using computerised axial tomography with histological and ultrastructural examinations. *Vet. J.* **178**, 387-395.
24. Taylor, L. and Dixon, P.M. (2007) Equine idiopathic cheek teeth fractures: Part 2: a practice-based survey of 147 affected horses in Britain and Ireland. *Equine Vet. J.* **4**, 322-326.
25. Dixon, P.M., Barakzai, S.Z., Collins, N.M. and Yates, J. (2007) Equine idiopathic cheek teeth fractures: Part 3: a hospital-based survey of 68 referred horses (1999–2005). *Equine Vet. J.* **4**, 327-332.
26. Dacre, I., Kempson, S. and Dixon, P.M. (2007) Equine idiopathic cheek teeth fractures. Part 1: pathological studies on 35 fractured cheek teeth. *Equine Vet. J.* **4**, 310-318.
27. Du Toit, N. (2016) Does radiography help or hinder in apical infection?. *Equine Vet. Educ.* **28**, 470-471.
28. Dixon, P.M., Du Toit, N. and Dacre, I.T. (2011) Equine dental pathology. In: *Equine Dentistry*, 3rd edn., Eds: J. Easley, P. Dixon and J. Schumacher, Elsevier, Saunders, Edinburgh. pp 129.
29. Fitzgibbon, C.M., Du Toit, N. and Dixon, P.M. (2010) Anatomical studies of maxillary cheek teeth infundibula in clinically normal horses. *Equine Vet. J.* **1**, 37-43.
30. Suske, A., Poschke, A., Schrock, P., Kirschner, S., Brockmann, M. and Staszyk, C. (2016) Infundibula of equine maxillary cheek teeth Part 1: development, blood supply and infundibular cementogenesis. *Vet. J.* **209**, 57-65.

5.2 Conclusion

This study confirmed the high sensitivity of CT (97%) in detecting apical infection in equine maxillary cheek teeth. In particular, the presence of pulpar changes on CT imaging, including changes indicative of intrapulpar gas and other changes in pulp density (e.g. resulting from the presence of food or necrotic pulp, enlarged pulp horns and irregular pulp margins) were important diagnostically, along with changes to the periapical region. Computed tomographic images of pulpar changes rather than presence of gas are included below.

Fig 1 The apical aspect of the 2nd pulp horn of 209 iis enlarged, has irregular margins and is filled with gas. The apex of tooth also has a blunt appearance. (blue arrow). Three scan planes are shown: A: transverse, B: sagittal and C: dorsal.

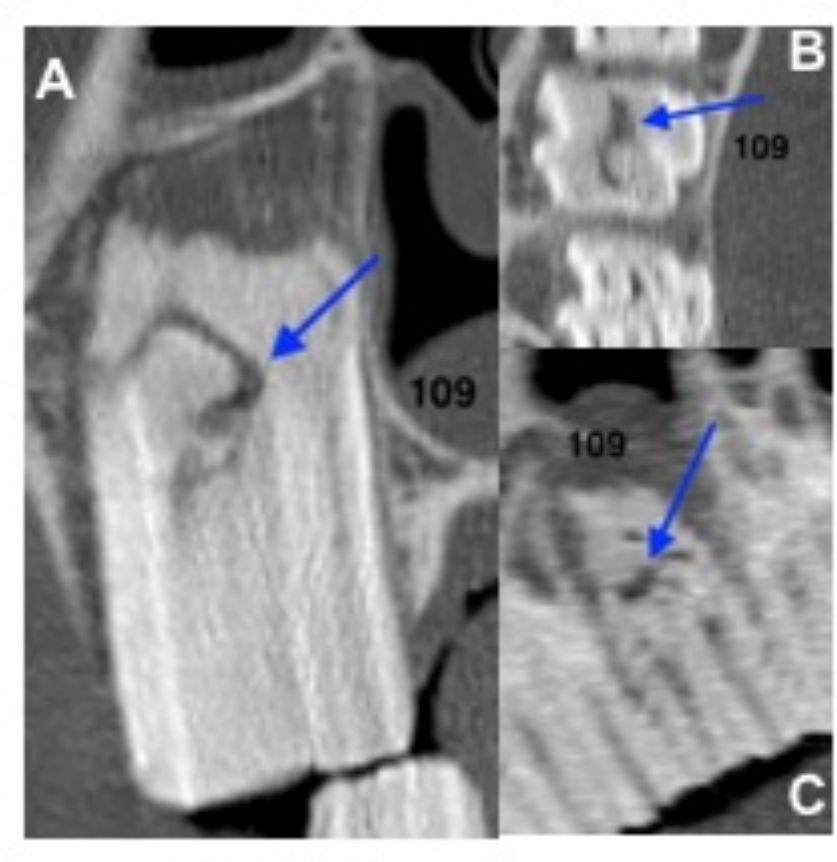

Fig.2. In Figure 2, the common pulp horn of a 109 has an irregular, tortuous appearance and is slightly enlarged and contains gas. The apex of tooth also shows destructive changes, with loss of outline of roots and widened periodontal space.(blue arrow): Three scan planes are shown: A: transverse, B: dorsal and C: sagittal.

CT (97% sensitivity) was demonstrated to be superior to radiography (53% sensitivity) in detecting early apical infection. Interpretation of some of the radiographic changes of apical infections is subjective and differences in the interpretation of specific radiographic features can occur between examiners. Many of the above-noted CT changes in apically infected teeth are either not detectable radiographically or are very subtle. These CT findings were a justifiable basis for the extraction of infected cheek teeth that did not have definitive radiographic evidence of apical infection. They were also the sole reason for extracting one otherwise apparently healthy tooth.

Gross pathological pulpar changes included the presence of: intra-pulpar food, discoloured or necrotic pulp horns and stained adjacent dentine. Histological evidence of pulpar disease was present in 97% of teeth (all teeth had shown pulpar changes on CT). Histological pulpar changes included the presence of avascular pulp with pallor of the stroma; bacterial colonies; neutrophilic infiltration; and/or the presence of food in pulp horns. Pulp stones were visible microscopically in 66% of diseased and 50% of control teeth and were considered a normal, or at least incidental, finding.

In our conclusion, the authors noted that apically teeth without crown abnormalities (primarily those with blood borne (anachorectic) pulpar infecions had less chance of having some remaining viable pulps than those with fractures.t Possible reason for this finding can be found in the proliferation of tertiary dentine in response to pulpar disease which could seal off the affected pulp without dissemination of infection to other pulps. A further explanation could be related to how each tooth was sectioned after extraction.In order to avoid any bias, each tooth was sectioned in 4 parts in the

same regions; therefore it is also possible that additional non-viable pulps were present in teeth with fracture but not visible in the particular acquired section because of loss of occlusal aspects of these teeth.

Although histology should be considered the gold standard in the diagnosis of apical infection, due to the aggressiveness of the decalcification process, pulp histology was occasionally difficult to interpret, due to a change in colour of the pulp; for this reason, the authors used the expression of "normal appearing pulp" if the discolouration of the pulp was deemed to be due to the described process or due to the decalcification

CHAPTER 6: A comparison of Computed Tomographic, radiographic, gross, histological, dental and alveolar findings in 30 abnormal cheek teeth from equine cadavers

Published in Frontiers Veterinary Science; doi:10.3389/fvets.2017.00236

6.1 Introduction

The study performed in this chapter was a comparison of CT and radiographic imaging findings with gross and histological findings in abnormal teeth and attached alveolar bone collected from equine cadavers.

As noted, cheek teeth apical infection can be a serious disorder in horses, especially if the infection spreads to the supporting bone or the adjacent paranasal sinuses. CT is considered an excellent imaging modality for detecting changes within the dental structure and alveolar bone (Buhler et al 2014); however, no gross or histological confirmation of disease has ever been published.

The aim of this study was to validate the accuracy of radiography and CT in detecting dental and alveolar bone disease by comparing imaging findings with gross and histological examinations of the extracted teeth and alveoli.

Conception and design of the study was by Tiziana Liuti and Prof. P.M Dixon Data acquisition was by Tiziana Liuti

Data analysis and interpretation was by Dr. Sionagh Smith, Prof. P.M Dixon and Tiziana Liuti

Drafting of the article was by Tiziana Liuti

Revision of the article for intellectual content was by Prof. P.M Dixon, Dr. Sionagh Smith and Tiziana Liuti

Final approval of the completed article was by Prof. P.M Dixon and Tiziana Liuti

frontiers in Veterinary Science

ORIGINAL RESEARCH
published: 05 January 2018
doi: 10.3389/fvets.2017.00236

A Comparison of Computed Tomographic, Radiographic, Gross and Histological, Dental, and Alveolar Findings in 30 Abnormal Cheek Teeth from Equine Cadavers

*Tiziana Liuti, Sionagh Smith and Padraic M. Dixon**

Royal (Dick) School of Veterinary Studies and The Roslin Institute, The University of Edinburgh, Roslin, United Kingdom

OPEN ACCESS

Edited by:
Carsten Staszyk, Justus Liebig Universität Gießen, Germany

Reviewed by:
Derek Cissell, University of California, Davis, United States
Kevin S. Stepaniuk, Columbia River Veterinary Specialists, United States

***Correspondence:**
Padraic M. Dixon
p.m.dixon@ed.ac.uk

Specialty section:
This article was submitted to Veterinary Dentistry and Oromaxillofacial Surgery, a section of the journal Frontiers in Veterinary Science

Received: *18 October 2017*
Accepted: *15 December 2017*
Published: *05 January 2018*

Citation:
Liuti T, Smith S and Dixon PM (2018) A Comparison of Computed Tomographic, Radiographic, Gross and Histological, Dental, and Alveolar Findings in 30 Abnormal Cheek Teeth from Equine Cadavers. Front. Vet. Sci. 4:236. doi: 10.3389/fvets.2017.00236

Background: Equine cheek teeth disorders, especially pulpar/apical infections, can have very serious consequences due to the frequent extension of infection to the supporting bones and/or adjacent paranasal sinuses. Limited studies have assessed the accuracy of computed tomographic (CT) imaging in the diagnosis of these disorders, and no study has directly compared imaging and pathological findings of the alveoli of diseased equine cheek teeth.

Objective: To validate the accuracy of CT and radiographic imaging of cheek teeth disorders by comparing CT and radiographic imaging, gross and histological findings in abnormal cheek teeth and their alveoli extracted from equine cadaver heads.

Study design: *Ex vivo* original study.

Methods: Fifty-four cadaver heads from horses with unknown histories that had died or been euthanized on humane grounds obtained from a rendering plant had radiography, CT imaging, and gross pathological examinations performed. Based on imaging and gross examination findings, 30 abnormal cheek teeth (26 maxillary and 4 mandibular) identified in 26 heads were extracted along with their dental alveoli where possible, and further CT imaging, gross, and histological examinations were performed. Eight maxillary cheek teeth (including four with attached alveolar bone) from these heads, that were normal on gross and CT examinations, were used as controls.

Results: Gross pathological and histological examinations indicated that 28/30 teeth, including two supernumerary teeth, had pulpar/apical infection, including pulpar and apical changes. A further supernumerary and a dysplastic tooth were also identified. Abnormal calcified tissue architecture was present in all three supernumerary and in the dysplastic tooth. CT imaging strongly indicated the presence of pulpar/apical infection in 27 of the 28 (96.4%) pulpar/apically infected teeth, including the presence of intrapulpar gas (N = 19/28), apical clubbing (N = 20), periapical halo (N = 4), root lysis or fragmentation (N = 7), and periapical gas (N = 2). Also present were alveolar bone sclerosis (N = 20), alveolar bone thickening (N = 3), and lytic/erosive changes (N = 8).

Radiographic abnormalities strongly indicative of pulpar/apical infection including periapical sclerosis (*N* = 8/28) and apical clubbing (*N* = 14/28) were found in 14/28 (50%) of apically infected teeth. Histological changes were present in alveolar bone of all 21 cases of apical infection where alveolus remained attached to the tooth and was marked in 16 cases, all which had CT alveolar changes. Histological changes included disruption of the normal trabecular pattern, increased osteoclastic activity, and the presence of islands of bone with a scalloped profile within the thickened attached periodontal ligament. No gross pathological or histological changes were present in the eight control teeth or their alveoli (*N* = 4).

Main limitations: No history or breed-related information was available on these cases.

Conclusion: There was a 96.4% correlation between a CT diagnosis and confirmative pathological findings in 28 apically infected teeth confirming the accuracy of CT imaging in diagnosing equine pulpar/apical infections. There was also excellent correlation between CT and histological alveolar bone findings.

Keywords: equine dental imaging, equine computed tomography, equine pulpar/apical disease, equine dental pathology

INTRODUCTION

Equine cheek teeth disorders, especially bacterial pulpar infection that lead to apical infections (hereafter termed *apical infection*), can be very problematic due to the frequent spread of infection into the mandibles or the maxillary bones and sinuses (1, 2). These infections involve the subgingival aspect of the teeth, which cannot be directly clinically examined, and therefore, imaging including radiography, scintigraphy, and more recently computed tomography (CT) is necessary to assess these disorders. Since treatment is usually by extraction (a major surgical procedure with many potential complications), a definitive diagnosis of apical infection is important before any surgical intervention and imaging contributes significantly to achieving this goal.

Currently, radiography is the main imaging technique used to diagnose equine dental disease, but it is frequently inaccurate in early cases of cheek teeth apical infections (3–9). Scintigraphy also has poor sensitivity (56%) in diagnosing apical infections (4, 5) and is expensive and time consuming. Magnetic resonance imaging requires general anesthesia and is poor at imaging calcified tissues, and thus it has not proven to be reliable in imaging equine dental disorders (10).

Computed tomography (9, 11–14) is more sensitive than radiography in detecting cheek teeth apical infection and is currently the imaging modality of choice for this purpose (9, 14). In addition to detecting lytic or proliferative changes of the alveolar bone and apices of affected teeth (that can often be detected radiographically if advanced enough), CT can detect subtler changes such as root fragmentation, pulp horn irregularities and, especially, the presence of gas [i.e., attenuating structures of −900 to −1,000 Hounsfield unit (HU)] within the pulp or periapical periodontal tissues (9, 13–16).

Several studies (13, 14, 16) have indirectly evaluated the accuracy of CT imaging, primarily by relating clinical and CT findings. A more recent study (9) directly compared CT and radiographic findings with the gross and histological features of 32 extracted apically infected maxillary cheek teeth and showed a 97% correlation between a CT imaging diagnosis of apical infection and the presence of pathological changes of apical infection in the extracted teeth. As significant imaging changes also occur in the alveolar bone of infected teeth, a limitation of the above study of clinical cases is that no alveolar bone was available for pathological examination. The purpose of this study was to examine the alveolar bone of infected teeth for pathological changes where possible to allow comparison with imaging alveolar bone findings, in addition to pathological examination of the extracted teeth to further assess the accuracy of CT and radiographic imaging in the detection of cheek teeth disorders.

MATERIALS AND METHODS

This study was approved by the Ethical Review Committee of The Royal (Dick) School of Veterinary Studies and Roslin Institute, The University of Edinburgh on the 16th February 2012. The heads of 54 horses, similar in size to Thoroughbred heads, were obtained from a rendering plant between October 2012 and March 2013. They originated from horses with unknown histories that had died or were euthanized on humane grounds due to disease. The heads were resected at the level of the atlas and then frozen, usually on the day of death.

Diagnostic Imaging

After they were thawed, six computed radiographic projections were obtained from each head to allow examination of the cheek teeth (Agfa CR 25 digitizer NX8000 HP7900 Raid Server, Agfa Healthcare UK Ltd., Brentford, Middlesex, UK) including: lateral, dorsoventral, two latero 45° dorsal–lateroventral oblique of the maxillary arcades, and two latero 45° ventral–laterodorsal oblique of the mandibular arcades.

Transverse CT images of the heads, positioned on their mandibles, were then acquired with a multislice CT scanner (Siemens, Volume Zoom, Germany) in a helical scan mode using a 512 × 512 matrix, 120 kV, 300 mA, focal spot 1.2, at a slice thickness of 3 and 1.5 mm; images were saved in DICOM format. Radiographic and CT images were evaluated by two observers using dedicated software Osirix® (www.osirix-viewer.com), and a consensus was reached between them. Bone windows (H70) with corresponding window width of 4,000 HU and window level of 1,000 HU were used throughout the evaluation of the CT images. Based on visual examination of incisors and dental imaging examinations, the 26 heads were determined to have a mean age of 16 years (range 5–20 years). Based on imaging findings, followed by a visual dental examination with the jaws disarticulated, 26 heads containing 30 cheek teeth (26 maxillary and 4 mandibular) that were considered abnormal on imaging and/or clinical examination were selected for the study. The 30 abnormal teeth were extracted along with their attached alveoli when possible, using a stainless steel osteotome and mallet. Eight maxillary cheek teeth that were normal on gross examination and on imaging, including four with attached alveoli, were extracted from these heads to serve as controls.

Comparison of Head Dimensions with Those of Horses of Known Breed

To compare the head sizes in this study population with head sizes of a known breed, CT images of 12 Thoroughbreds of known age [0–5 years old ($N = 4$); 6–15 years old ($N = 4$); and >16 years old ($N = 4$)] were measured to obtain their head dimensions. These Thoroughbreds had undergone CT head imaging for clinical reasons other than sinonasal disorders.

Head Linear Dimensions and Volumes

Head "length" (i.e., distance from the caudal aspect of the orbit to the nasoincisive notch) was measured from CT sagittal reconstructions; head "width" (width of the hard palate at the level of Triadan 06) was measured from CT dorsal reconstructions, and head "height" (distance from the hard palate to the dorsal aspect of the maxillary bone at the level of the orbit) was measured using CT sagittal reconstructions. These three measurements were multiplied together to produce a measurement of head "volume" (17).

Evaluation of CT Images

CT evaluation included the assessment of the pulp horns including for the presence of gas-attenuating structures. To accurately identify the presence of gas, a point-shape region of interest (ROI) tool was placed in a consistent manner over the gas-attenuating structures within the pulp horn, and the HU value was generated as shown in **Figure 9**. The ROI size was identical for all abnormal pulps. Density values between −900 and −1,000 HU were considered to represent gas. CT assessment also included examination of the calcified apical tissues, identification of gas in the apical periodontal membranes, and evaluation of the periapical alveolar bone changes including for the presence of lysis and thickening.

Gross Anatomical Examination

Each extracted abnormal and control tooth was photographed on all sides and grossly examined, before being transversely sectioned into four equal parts, i.e., occlusal, two mid-crown and apical aspects, using a 1 mm thick lapidary blade. A 5 mm thick section was cut from each of the above portions, then visually examined and photographed on both sides. These thin sections were fixed in formalin before decalcification, histological processing, and examination.

Histological Processing and Examination

The dental sections were decalcified and embedded in paraffin wax, and 4 μm thick sections were cut and stained with hematoxylin and eosin as described (9). All abnormal and control teeth and their histological slides were anonymized, relabeled, and examined by two observers. Histological examination of each of the four sections of each tooth documented findings in: pulp; primary, secondary, and tertiary dentine (if present); infundibulae (in maxillary cheek teeth); peripheral cementum; periodontal ligament; and alveolar bone. Recorded pulpar changes included the presence of intrapulpar bacteria, infiltrates of neutrophils, lymphocytes and/or plasma cells, necrotic or "faded pulp" (9), and pulp stones. All enamel was lost during decalcification.

Statistical Analyses of Head Sizes

A paired *T*-test was used to assess for differences in dimensions between the cadaver heads used in this study and the 12 control Thoroughbred horses. No significant difference was found between length ($p = 0.196$), width ($p = 0.942$), height ($p = 0.086$), or volumes ($p = 0.829$) of the two groups of heads.

RESULTS

Since gross pathological and histological changes are the gold standard for confirming the presence of dental disease, the pathological findings are presented first here, in contrast to the sequence of the actual study where imaging was initially performed.

Thirty abnormal cheek teeth were identified including 26 maxillary teeth: Triadan 06 ($N = 6$); 07 ($N = 1$); 08 ($N = 4$); 09 ($N = 7$); 10 ($N = 3$); 11 ($N = 2$); and 12 (supernumerary teeth) ($N = 3$), and 4 mandibular teeth: Triadan 08 ($N = 1$); 09 ($N = 2$); and 11 ($N = 1$).

Gross Pathological Findings in Extracted Teeth

Alveolar Bone

Alveolar bone surrounding the dental reserve crown and apex remained intact around 21 teeth (all with apical infection) but became detached from the other 9 teeth during extraction or histological processing. Gross examination of the external aspects of the dental alveoli was unrewarding due to iatrogenic chisel damage from the extraction process.

Pulp

Gross pulpar abnormalities including discolored, absent, or necrotic pulp were present in 23 of 28 teeth (81.5%), all which were later histologically confirmed to have pulpar/apical disease (see Histological Findings). Intrapulpar food material was present in 8/28 (28.6%) teeth (**Figures 1A–C**). The eight control teeth, one supernumerary, and the dysplastic tooth had no gross pulpar abnormalities.

Dentine

Gross dentinal changes, mainly the presence of circumpulpar dentinal staining and irregular dentinal–pulpar margins, were grossly identified around 1 or more pulp horns in 18/28 teeth (64.3%) (**Figures 1**, **4B** and **7**). A grossly appreciable communication was identified between a carious infundibulum and infected pulp horns in one maxillary tooth.

Periodontal Changes

Generalized periodontal thickening or fibrous soft tissue swellings of the periapical region were grossly identified in 25/28 teeth (89.3%) with apical infection. Limited, subgingival periodontal changes were visible in one dysplastic tooth without endodontic disease, likely due to malformation of the junction between the periodontal ligament and the alveolar bone.

Cementum

Proliferative calcified apical changes, including thickened, irregularly shaped roots and/or more generalized apical hypercementosis, were grossly identified in 24/28 teeth (85.7%) with apical infection. Limited peripheral cemental destructive changes were present near the gingival margin in the dysplastic cheek tooth.

Infundibulae

Gross and deep caries with discolored enamel (grade 2 caries) was identified in the infundibulae of 7/26 maxillary cheek teeth (26.9%), with as noted a pulpar–infundibular connection in one tooth.

In summary, of the 28 teeth later confirmed histologically to have pulpar/apical infection, 23 had gross pulpar abnormalities, 26 had apical calcified tissue changes, and 26 had periapical periodontal changes. Gross changes in external shape and of internal architecture (on cut section) were present in all three supernumerary (two with intercurrent apical infection and one endodontically normal) and the dysplastic tooth. Limited periodontal and peripheral cemental thickening were present in the dysplastic tooth. No gross changes were identified in the eight control teeth.

Histological Findings

Alveolar Bone

In the four control maxillary cheek teeth with attached alveolar bone, the peripheral cemental profile was smooth histologically and supported by a band of well-vascularized periodontal ligament of uniform thickness, in turn bordered more peripherally by anastomosing trabeculae of alveolar bone. The main bony trabeculae were oriented parallel to the circumference of the tooth and were interspersed with marrow fat (**Figures 2** and **3**). No osteoclastic activity was detected in the alveolar bone of any control teeth.

The 21 apically infected teeth with attached dental alveolus had changes in the alveolar bone that were not present in the control teeth. For the purposes of this study, these changes were regarded as abnormal. The changes were marked in 16 teeth and less severe in five. They were characterized by multifocal disruption of the normal trabecular pattern of the alveolar bone, which was usually associated with expansion/thickening of the periodontal ligament. Entrapped within this stroma were variably sized, irregular islands of disorganized alveolar bone, many of which had scalloped profiles associated with numerous osteoclasts occupying Howship's lacunae (**Figures 4A**, **6A** and **6B**). There were also areas of increased cellularity composed of densely packed spindle cells consistent with fibroplasia (**Figure 6B**).

In the alveolar bone of the five teeth with milder changes, there was mild scalloping of the alveolar bone, mild osteoclast activity, and slightly increased thickening of the periodontal ligament. In three of these five cases, there was slight sclerosis of the periapical alveolar bone on both radiographic and CT imaging.

Periodontal Ligament

In addition to the aforementioned thickening of the periodontal ligament associated with alveolar bone changes in all

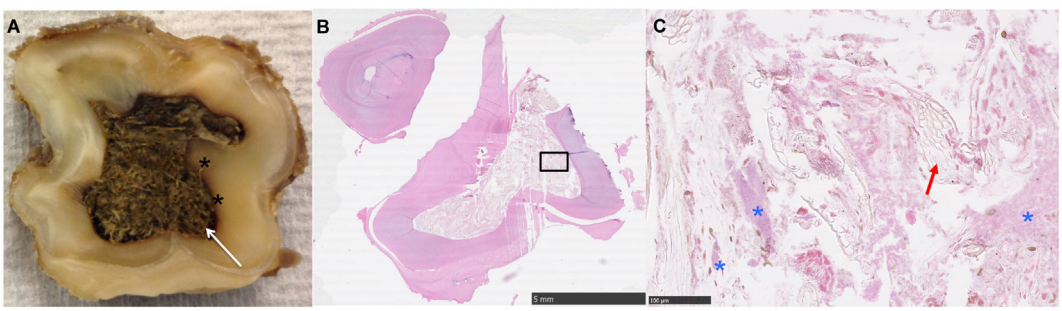

FIGURE 1 | **(A)** Transverse section near the apical level of an apically infected Triadan 208: note the large amount of plant material within the common pulp cavity (white arrow) and staining of the adjacent dentine (*). **(B,C)** Histological image of transverse section of apex (HE): note the large pulp cavity containing plant material (red arrow) and bacteria (*).

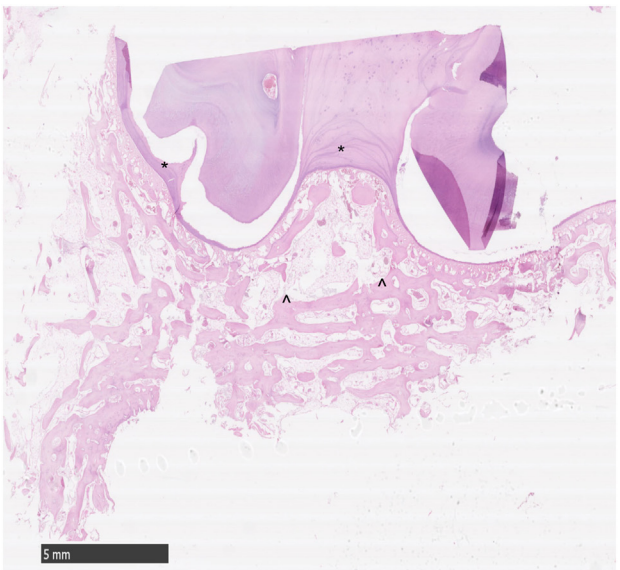

FIGURE 2 | Histological transverse section of normal alveolar bone. HE. Note the smoothly outlined peripheral cemental profile (*) that is bordered more peripherally by anastomosing trabeculae of alveolar bone. The main bony trabeculae are oriented parallel to the profile of the circumference of the tooth (^) and are interspersed with marrow fat. No osteoclastic activity is apparent.

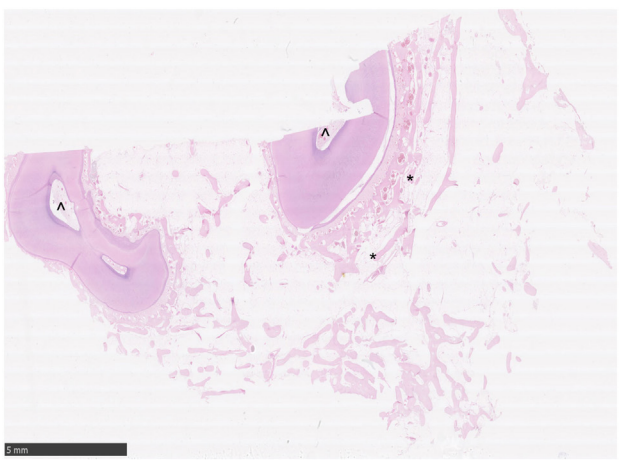

FIGURE 3 | Histological transverse section of normal alveolar bone. HE. Note the alveolar bony trabeculae oriented parallel to the profile of the circumference of the tooth (*) and interspersed with marrow fat. No osteoclastic activity is apparent. Note the normal pulp stroma with blood vessels (^).

21 alveoli, further histological abnormalities were noted in the periodontal ligament that remained attached to 18/28 apically infected teeth (64.3%). These changes included the presence of hemorrhage/fibrin (N = 12/28) (43%), infiltration with bacteria/neutrophils (N = 9/28), plasma cells (N = 3/28), and lymphocytes (N = 1/28).

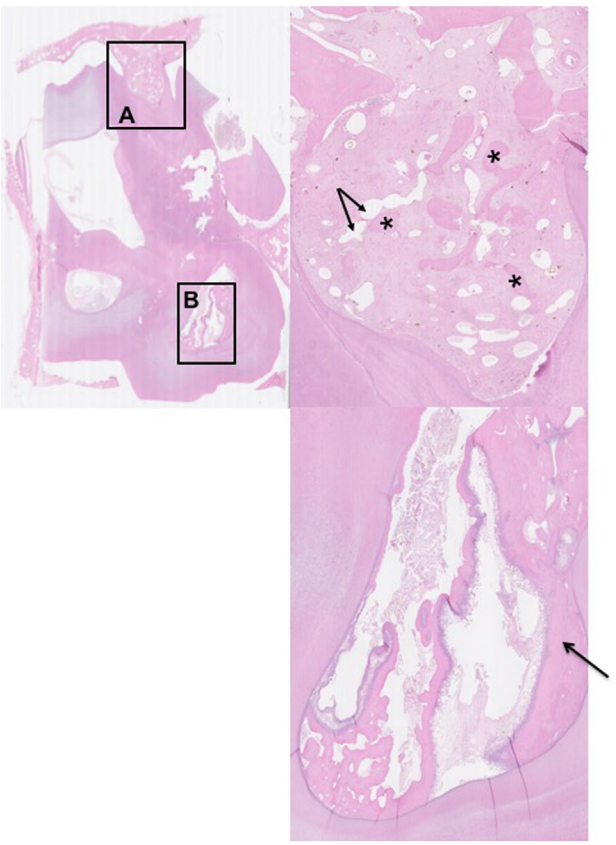

FIGURE 4 | Histological transverse section of the apex of Triadan 110 including of distorted alveolar bone. HE. There is focal disruption and disorganization of the normal trabecular pattern of the alveolar bone with thickening of the surrounding periodontal ligament. The thickened periodontal ligament and disorganized islands of alveolar bone form a protruding "tongue" that focally displaces the peripheral cementum. **(A)** The thickened periodontal ligament is composed of increased amounts of mature collagen-containing enlarged, irregular islands of disorganized alveolar bone (*) and vascular structures (arrows). **(B)** Pulp containing debris and irregular secondary dentine: note the marked lysis within irregular secondary dentine (black arrow).

Pulp

Pulpar changes were histologically present in all 28 teeth diagnosed with pulpar/apical infection, and such histological evidence was the main criterion for diagnosing these teeth with pulpar/apical infection. These changes involved 96 of the 152 pulps (mean 3.6 affected pulps/tooth, range 1–5) in the 28 teeth, with every pulp diseased in 3/28 teeth.

Histological pulpar abnormalities included what we termed "faded pulp" in 20/28 (71.4%) teeth. This feature was characterized by a pulp stroma that was much paler than that of normal viable pulps, with loss of nuclear detail in stromal fibroblasts, loss of normal vasculature and, sometimes, the accumulation of loose dentinal debris at the pulp periphery (9). Also recognized were the presence of intrapulpar bacteria and neutrophils (N = 19/28), food material (N = 8), and pulp necrosis (N = 1). Pulp stones (N = 1–5) were present within the pulp and secondary dentine

in 8/28 apically infected and in 4/8 control teeth. All pulps in the eight control teeth, one supernumerary tooth and the dysplastic tooth were histologically normal.

Dentine

Histological changes were present in dentine surrounding infected pulps in 7/28 (25%) infected teeth, including dentinal lysis at the pulp periphery ($N = 5$) and irregular pulpar margins ($N = 2$). Five of the seven teeth with histological pulpar changes showed gross dentinal abnormalities. Tertiary dentine was not identified in any teeth.

Peripheral Cementum

Histological abnormalities were present in the peripheral periapical cementum in 15/28 apically infected teeth, including cemental lysis and caries-like destruction ($N = 5$), plaque/biofilm formation ($N = 13$), and intra-cemental abscess formation and bacteria ($N = 5$).

Infundibulae

Histological infundibular changes were found in 9/26 (34.6%) maxillary cheek teeth including the accumulation of plant material, bacteria, debris, and carious infundibular cementum.

The final pathological diagnoses were apical infection ($N = 28$) including in two supernumerary teeth; a further (uninfected) supernumerary tooth and a dysplastic tooth.

CT Findings (Pre-Extraction at 1.5 and 3 mm Intervals)

No pulpar or periapical abnormalities were detected in one supernumerary tooth, the dysplastic tooth, or the eight control teeth. In addition, one tooth with pulpar discoloration and histological evidence of neutrophil/bacterial pulpar infiltration did not have any CT imaging evidence of apical infection.

The main CT findings in the 28 teeth diagnosed with apical infection included: gas within pulps ($N = 19/28$) (67.9%); irregular pulp horn margins ($N = 16$); increased pulpar volume ($N = 7$) [total of 19/28 teeth (67.9%) with pulpar changes]; widened periodontal space ($N = 5$); gas within periapical tissues ($N = 2$); root clubbing ($N = 20$), root fragmentation ($N = 7$); periapical halo ($N = 4$); periapical bone changes including peripheral sclerosis ($N = 20$); alveolar bone thickening ($n = 3$); resorption/lysis more axially ($N = 8$), and infundibular changes (other than central cemental hypoplasia) ($N = 12$). The three supernumerary and the dysplastic tooth all had abnormal internal architecture of their calcified dental tissues.

In all 16 teeth with severe histological alveolar bone changes, perialveolar bone changes were visible on CT, but only 4 of these 16 cases had identifiable periapical alveolar changes radiographically.

CT Findings (Post-Extraction 0.5 mm Intervals)

Following extraction, CT imaging of the 28 teeth diagnosed with apical infection at 0.5 mm slice thickness also showed convincing evidence of apical infection on CT imaging in 27/28 teeth, including the presence of intrapulpar gas in 17/27 teeth (2 teeth with gas in pulps on pre-extraction CTs sustained iatrogenic fractures to the roots of the affected pulp horns during extraction with exposure of the affected pulp and loss of intrapulpar gas); increased pulpar volume in 7/27 teeth and irregular pulp horn margins in 14/27 teeth [total of 21/28 (75%) with pulpar changes]. Pre- and post-extraction CT imaging changes in infundibulae and roots were similar.

Radiography

Radiographic abnormalities strongly indicative of apical infection were found in 14 of the 28 apically infected teeth (50%), including root blunting (clubbing) ($N = 14/27$) and alveolar bone sclerosis ($N = 8/27$) (**Figure 8**), with no convincing radiographic changes present in 13 teeth (**Figure 9**).

DISCUSSION

Liuti et al. (9) have recently shown CT to be highly sensitive (97%) in detecting maxillary cheek teeth periapical infection, as assessed by gross pathological and histological evaluation of teeth diagnosed with apical infections by CT and subsequently extracted on clinical grounds. A similar sensitivity (96.4%) was found in this study during which CT imaging of cadaver-sourced maxillary and mandibular teeth identified 27 of 28 teeth with pathological evidence of apical infection. This study recorded a single false negative case (1/28) on CT imaging, in contrast to Liuti et al. (9) where a single false positive case (1/32) was recorded on CT imaging.

A significant amount of dental imaging information is also gained from assessment of the periodontal ligament and alveolus of a suspect tooth. In clinical cases, the periodontal ligaments can only be pathologically examined in areas that (very variably) remain attached to the extracted tooth. In addition, some periodontal pathological changes, such as hemorrhage and fibrin, may be iatrogenic due to the *in vivo* extraction process (9). It is interesting that in the current *ex vivo* study where iatrogenic extraction-related periodontal fibrin deposition or intra-periodontal hemorrhage could not occur, hemorrhage and/or fibrin were still present in the periodontal membranes of 43% (12/28) apically infected teeth. This is in contrast to the 59% (19/32) periodontal hemorrhage/fibrin deposition from teeth extracted *in vivo* (9), where the higher prevalence of intra-periodontal changes was likely due to iatrogenic extraction damage.

Alveolar bone cannot be pathologically examined in clinical cases, so it is not possible to compare imaging and pathological alveolar bone findings in such cases. The use of diseased teeth from fresh cadaver heads in this study allowed most of the periodontal ligament to be removed along with adjacent alveolar bone in 70% (21/30) of teeth. This facilitated pathological assessment of alveolar bone when present and, as noted, allowed a more complete assessment of the periodontal ligaments that additionally, were free of iatrogenic extraction-related inflammatory changes.

Alveolar bone was histologically abnormal around all 21 apically infected teeth where it remained attached. Changes included extensive osteoclastic activity and marked disruption of the trabecular alveolar bone with its replacement by a collagenous

stroma, the latter leading to apparent thickening of the periodontal membranes on CT imaging.

Normal alveolar bone constantly remodels to accommodate the changing size and shape of erupting brachydont teeth (18), and this phenomenon is more pronounced in hypsodont teeth that have more prolonged eruption. However, the above-noted changes in the periapical alveolar bone of the infected teeth greatly differed from those in the alveolar bone of the control teeth alveoli.

Buhler et al. (14) reported alveolar bone sclerosis as a CT finding with equine periapical infection. In this study, sclerosis was detected with CT imaging, especially on the abaxial aspect of the periapical alveolar bone in 20/28 (71.4%) cases of apical infection, with thickening of this bone less commonly recognized (3/28). By contrast, alveolar bone resorption or lysis was recognized on CT imaging, especially on the axial aspect of alveolar bone in 28.6% (8/28) of cases, sometimes immediately adjacent to areas of sclerosis (**Figures 5** and **7**).

Radiographically, alveolar bone sclerosis has been described as an imaging feature dental apical infection (6) and was detected in 8/28 apically infected cases in this study, 4 of which contained alveolar bone changes histologically.

Apically infected teeth always have one or more infected pulps (that precedes the periodontal infection) (19). All 28 apically infected teeth in this study had pulpar abnormalities confirmed microscopically, while 68% had grossly evident pulpar abnormalities. Subsequent progressive bacterial destruction of the surrounding dentine creates larger pulp horns that also may develop irregular pulpo-dentinal margins (9, 14). Such pulp horn widening or irregular margins were detected by CT in 19 out of 28 (67.9%) apically infected cheek teeth in this study.

Other CT changes associated with apical infection, including clubbing (hypercementosis), fragmentation, and/or lysis of roots, were present in 27/28 (96.4%) of the cases. Changes to the apical calcified tissues (mainly increased deposition of cementum around roots) were more obvious grossly and were present in 26/28 (92.8%) teeth while histological changes (including erosion, necrosis, and biofilm/plaque deposition) were present in 15/28 (53.6%). This discrepancy between gross and histological findings may be due to loss of some roots during decalcification and histological processing (9). It has been reported (20) that peripheral cemental changes in apically infected mandibular cheek teeth were subtle and included cemental discoloration or loss, or increased cemental deposition.

Casey et al. showed that CT and pathological findings in formalin-preserved, apically infected cheek teeth correspond well with respect to mineralized dental tissue changes or the presence of food material in the pulp canals (20). However, pulpar changes that were evident grossly and histologically were not detectable on CT (20). By contrast, *in vivo* CT studies on clinical cases of apical infection (9, 13, 14, 16) have found CT to be very effective for identifying dental soft tissue (pulpar and periodontal) changes in diseased teeth, and particularly for recognizing gas in pulpar and periapical periodontal infections.

The production of gas by anaerobic bacteria, such as *Clostridium perfringens* (the cause of gas gangrene) where infected wounds become grossly emphysematous, is well recognized. Likewise, the presence of gas-attenuating areas in the pulp and/or periapical soft tissues of apically infected cheek teeth could be attributed to gas production by anaerobic bacteria (whose metabolism involves gas production). Such infection could occur following blood or lymphatic borne (anachoretic) or direct routes of apical infection from the oral cavity, including dental fractures, infundibular caries, or deep periodontal disease (periodontal–endodontic lesion) (21).

With severe (grade 3) infundibular caries with subsequent erosion of cementum, enamel and dentine, and pulpar invasion, or with infundibular caries-related sagittal fractures and subsequent

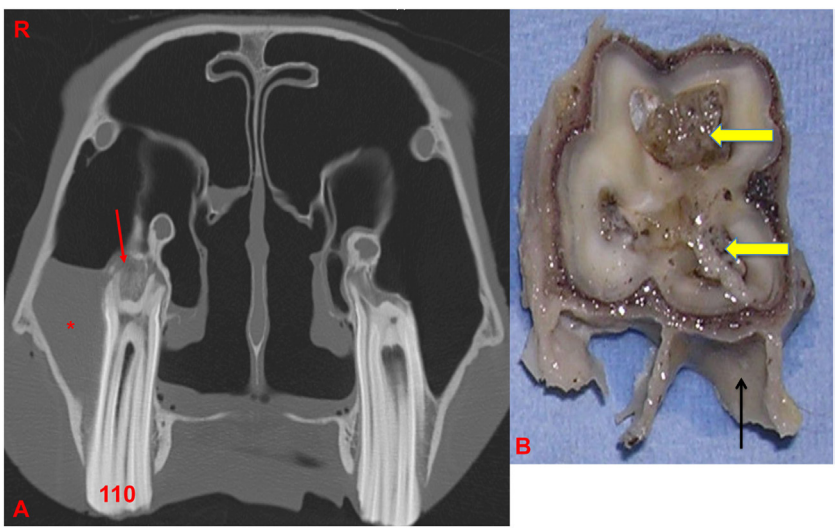

FIGURE 5 | **(A)** Transverse CT image at the level of 110: note the thickening, sclerosis, and also, erosion of the alveolar bone (red arrow) with apical clubbing. A moderate amount of fluid (*) is present within the caudal maxillary sinus. **(B)** Transverse section of 110 at the level of the apex: note the large and discolored pulps (arrows) and adjacent dentine: alveolar bone is present in this section (black arrow). R, right.

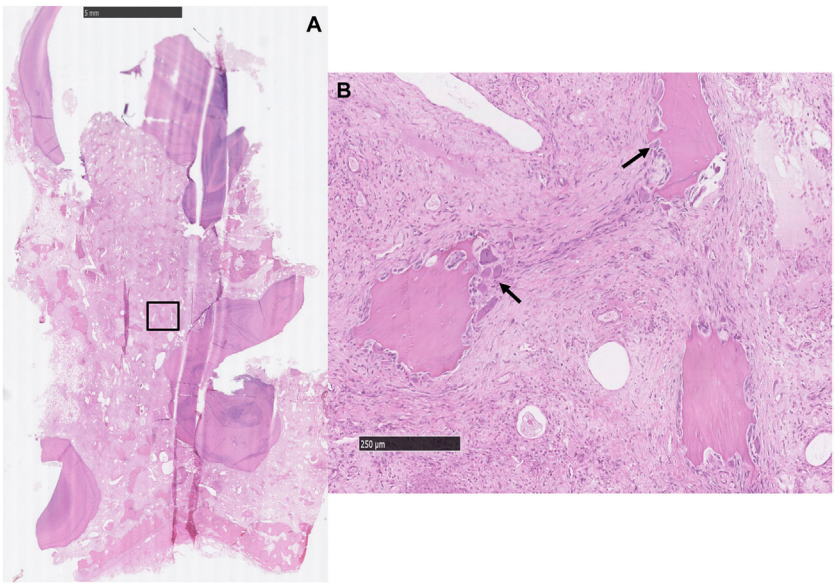

FIGURE 6 | **(A)** Histological transverse section of the periapical aspect of an apically infected tooth where the soft tissue between the roots is expanded by a large amount of collagen-containing, entrapped, variably sized, irregular islands of alveolar bone [inset **(B)**]. HE. **(B)** The stroma contains entrapped islands of alveolar bone with scalloped borders and numerous osteoclasts (black arrows) occupying bays (Howship's lacunae). There is also moderate to marked fibroplasia in the intervening stroma. HE.

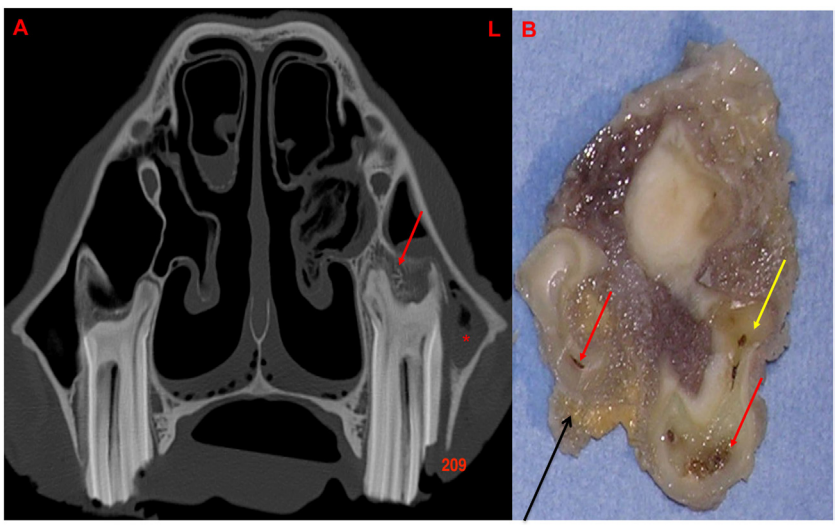

FIGURE 7 | **(A)** Transverse CT image at the level of 209 with a lateral idiopathic "slab" fracture (through first and second pulp horns): note the thickening, sclerosis, and also erosion of the alveolar bone (red arrow) with apical clubbing. A moderate amount of fluid (*) is present within the rostral maxillary sinus. **(B)** Transverse section of 209 at the level of the apex: note the large and discolored pulps (red arrow) and discolored dentine (yellow arrow): alveolar bone is present in this section (black arrow). L, left.

apical infection (21–24), the presence of gas-attenuating areas within the infected pulp or periapical areas could additionally be attributed to the movement of gas (including air) from within the affected infundibulae to the pulp. With idiopathic fractures of the clinical crown and secondary apical infection (25, 26), air from oral cavity could also contribute to gas attenuation of infected pulpar/periapical tissues.

Casey et al. (20) compared post-extraction CT images of formalin-preserved mandibular cheek teeth with their gross pathological and histological but did not detect gas attenuation of infected pulps.

It is possible that the prolonged storage of teeth by Casey et al. (20) in formalin solution before CT may have affected the stability or preservation of intrapulpar gas, although apically infected

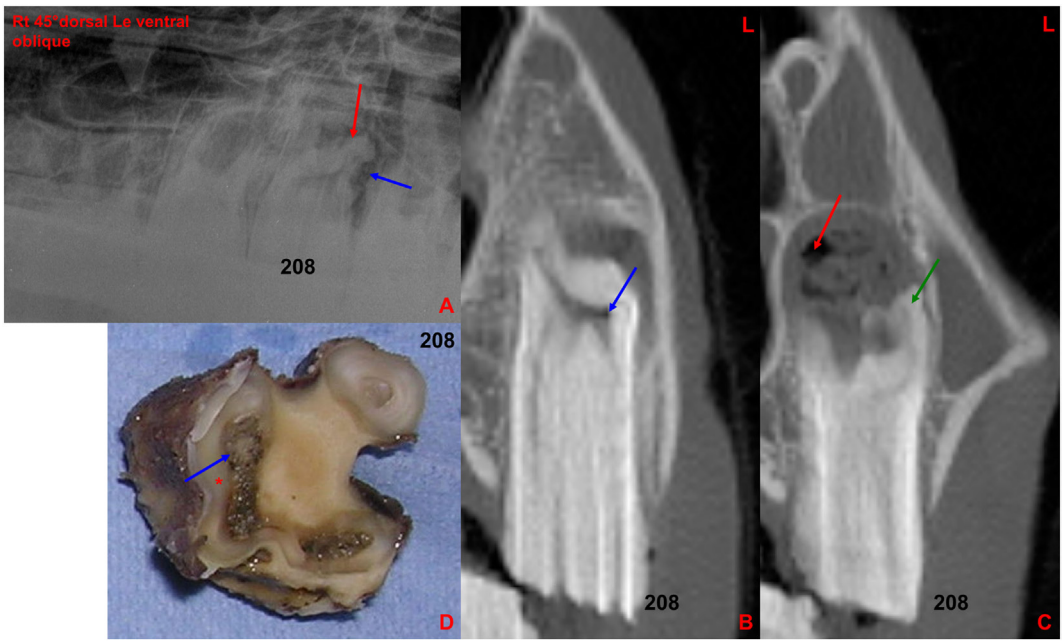

FIGURE 8 | **(A)** Right 30°dorsal left ventral oblique radiographic projection of the rostral maxillary cheek teeth: note the marked clubbing of the caudo-buccal 208 tooth root (red arrow) with an irregular surrounding lucency (blue arrow), both indicative of apical infection. **(B)** Transverse CT image at the level of 208: note small gas-attenuating structures (blue arrow) within the buccal aspect of the common pulp chamber. **(C)** Transverse CT image at the level of 208 [more caudally located than image **(B)**]: note the increased size of the periapical space, clubbing of a buccal root (green arrow) and multiple gas pockets (red arrow) mixed with soft tissue attenuating structures in the perialveolar space. **(D)** Transverse section of the above extracted 208 at the apical level: note the large and discolored necrotic common pulp (blue arrow) and adjacent dentine (*). L, left.

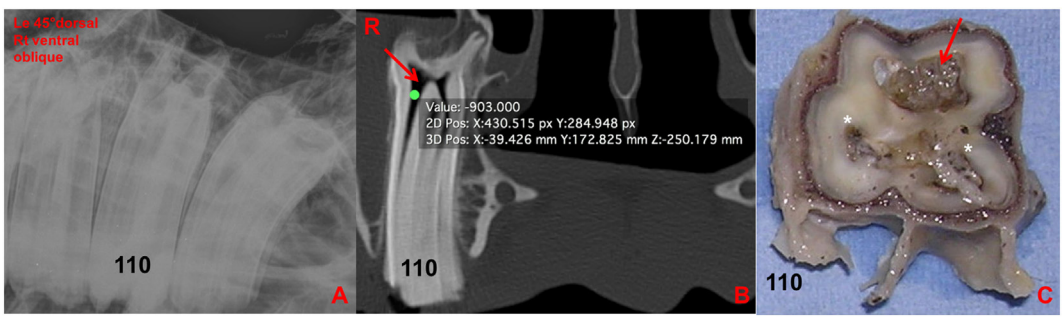

FIGURE 9 | **(A)** Left 30°dorsal right ventral oblique radiographic projection at the level of 110. No clinically significant abnormalities were detected in this radiograph. **(B)** Transverse CT image at the level of 110: note the large amount of gas-attenuating structures (red arrow) within the common pulp chamber and pulp horns (−903 HU). **(C)** Transverse section of 110 at the level of the apex: note the discolored large common pulp chamber of the buccal pulp horns (red arrow) and the other two discolored pulp horns and adjacent dentine (*). R, right.

teeth stored in formalin in this institute for over 4 years have still contained intrapulpar gas (authors' personal observations). In this study, intrapulpar gas was recognized on CT in 19/28 (67.9%) of infected teeth, while an *in vivo* study showed intrapulpar gas in 100% of apically infected teeth (9). The lower prevalence of intrapulpar gas in this study may be related to freezing of the heads before imaging examinations that could have affected the later distribution and/or recognition of intrapulpar gas on CT imaging.

Using the HU values from CT images is an established methodology to identify small gas cavities in tissue; vacuum phenomenon in the intervertebral disks has been described on CT as an accumulation of gas (principally nitrogen) in the vertebral column with a range of density between −900 and −980 HU (27).

None of the infected teeth had advanced gross destructive changes or extensive proliferative cemental apical deposits, i.e., all appeared to be low-grade chronic pulpar/apical infections and this may explain the poor sensitivity of radiography in diagnosing these infections at this early stage. In a similar study (9), the current authors found that only 13% of apically infected teeth had grossly appreciable abscesses of their apices, while 67% of apically infected teeth had some remaining viable pulps,

supporting the presence of a chronic low-grade infection of the periapical region in that study. In this study, a higher proportion of teeth, i.e., (89%) 25/28, had some remaining viable pulps.

Radiography detected changes including tooth root clubbing (52%) and periapical sclerosis (29.6%) in teeth with histologically confirmed apical infection. Overall, radiography detected changes that were considered sufficient to recommend extraction in 14/28 (50%) of the current cases, similar to the findings of Liuti et al. (9) where 17/30 (53%) of teeth contained what could be termed definitive evidence of apical infection, albeit at an early stage of infection. With progression of these apical infections, radiography would likely become more sensitive in detecting the pulpar/apical infection.

Infundibular caries can cause midline sagittal fractures of affected teeth (25, 26), and extension of infundibular caries can also cause maxillary cheek teeth pulpar/apical infection (21, 24) as was found in one tooth in this study. In this study, histological evidence of infundibular caries was present in 37.5% of all maxillary cheek teeth, with a poor correlation between pathological and CT findings. Anatomical (28) and imaging (15) studies of cheek teeth infundibulae in clinically normal horses showed that 88–90% of infundibulae are incompletely filled with morphologically normal cementum, with these defects preferentially affecting the Triadan 09 position in older horses. Suske et al. (24) found infundibular cemental hypoplasia in 51% of normal cheek teeth and in 72% of cheek teeth affected by periapical and endodontic infections, fractures, or periodontal disease. In fact, infundibular cemental hypoplasia and secondary infundibular cemental caries are so common that interpretation of infundibular images is problematic (9). Unless there is a midline sagittal infundibular caries-related fracture or evidence of extension of infundibular caries to enamel or dentine, such lesions are generally considered to be clinically insignificant at that time, although they may later progress to cause fracture and/or pulpitis/apical infection.

Apically infected teeth have by definition, changes in their periodontal ligaments, especially around the apex, and periodontal lesions were grossly identified in 89% (25/28) of apically infected teeth in this study. However, periodontal lesions were histologically detectable in only 64.2% (18/28) of these 28 teeth. The absence of this finding in the other 10 teeth is likely due to failure to capture localized periapical periodontal lesions in sections, loss of apical tissues during histological preparation or possibly due to the pulpitis not extending to the periapical periodontal tissues in some very early pulpar infections. There was a good correlation in this study between the histological findings and radiographic, CT and gross periodontal findings. However, it can be difficult to differentiate grossly between preexisting changes and extraction-induced changes in the periodontal ligament. In this study, this was not of concern because the alveolar bone and periodontal ligament were removed with the tooth after death.

Inflammatory cells were only present in a small number of periodontal tissues from these teeth and they mainly had a perivascular distribution, suggesting hematogenous origin rather than direct extension from an apical lesion. Gross examination excluded a descending periodontal route of infection for the two infected supernumerary teeth. Such a route can come into play in some supernumerary/dysplastic teeth that are not well seated into their alveoli (29), as was the case for the dysplastic tooth in this study.

In this study, pulp stones were found both free in the pulp and embedded in the secondary dentine, both in abnormal (16/30) and control teeth (4/8) similar to the findings of Liuti et al. (9). For this reason, their presence was not considered as an abnormality.

This study has shown an inexplicably high prevalence (51.9%) of pulpar/apical infection in 54 heads obtained from a rendering plant. Unfortunately, no clinical histories were available for any of these cases, and this extraordinarily high prevalence of dental disease may be a reflection of the study population. These were all ill horses that had died from disease or were euthanized on humane grounds. It would appear that none was euthanized on the grounds of old age since the mean age was 12 years (5–20 years). No heads contained evidence of significant decomposition and, in all 26 horses with the 28 apically infected teeth, just 4.5% (28/627) of the cheek teeth had imaging or gross pathological evidence of apical infection. In addition, in 89% (25/28) of the apically infected teeth, some pulp horns were grossly and histologically normal, thus confirming that postmortem changes did not cause the observed pathological changes.

The true prevalence of clinical equine cheek teeth endodontic/periapical disease in the general equine population is unknown but, as adjudged by the caseload of this equine hospital, cases with external signs of apical infection such as mandibular or maxillary swellings, sinus tracts or dental sinusitis, it is likely to be less than 2%. However, occlusal pulpar exposure (indicating some prior pulpar insult) is sometimes clinically apparent in teeth without clinical signs of apical infection. In addition, some cheek teeth with "idiopathic fractures" (1) have a reduced secondary dentinal thickness, which is also evidence of prior pulpar disease (25). Consequently, pulpitis and non-clinically detected periapical infection may be more common than currently realized, especially in systemically ill horses, although it may only affect some of the pulp horns of a single cheek tooth in most horses.

CONCLUSION

Changes highly indicative of apical infection were identified on CT imaging in 96.4% and radiographically in 50% of pathologically confirmed apically infected cheek teeth. Alveolar bone changes were histologically present in all 21 examined alveoli, and all 16 alveoli with marked alveolar bone changes had detectable CT alveolar changes. This study confirms the superior accuracy of CT compared with radiography in detecting equine cheek tooth apical infection and showed excellent correlation between both dental and alveolar CT imaging and pathological findings.

ETHICS STATEMENT

This study was approved by the Ethical Review Committee of The Royal (Dick) School of Veterinary Studies, Roslin Institute, The University of Edinburgh on the 16th February 2012.

AUTHOR CONTRIBUTIONS

TL contributed to study design and execution, data analysis and interpretation, and manuscript preparation. SS contributed to study execution and interpretation and manuscript preparation. PD contributed to study design and execution, data analysis, and manuscript preparation. All the authors approved the final manuscript.

ACKNOWLEDGMENTS

The authors would like to thank Mr. Neil McIntyre and Craig Pennycook for their technical assistance.

FUNDING

This study was funded by University of Edinburgh.

REFERENCES

1. Dixon PM, Tremaine WH, Pickles K, Kuhns L, Hawe C, McCann J, et al. Equine dental disease part 4: a long-term study of 400 cases: apical infection of cheek teeth. *Equine Vet J* (2000) 32:182–94. doi:10.2746/042516400777612099
2. Dixon PM, Parkin TD, Collins N, Hawkes C, Townsend N, Tremaine WH, et al. Equine paranasal sinus disease: a long-term study of 200 cases (1997–2009): treatments and long-term results of treatments. *Equine Vet J* (2012) 44:272–6. doi:10.1111/j.2042-3306.2011.00427.x
3. Gibbs C, Lane JG. Radiographic examination of the facial, nasal and paranasal sinus regions of the horse. II. Radiological findings. *Equine Vet J* (1987) 33:49–58.
4. Weller R, Livesey L, Maierl J, Nuss K, Bowen IM, Cauvin ER, et al. Comparison of radiography and scintigraphy in the diagnosis of dental disorders in the horse. *Equine Vet J* (2001) 33:49–58. doi:10.2746/042516401776767458
5. Barakzai S, Tremaine H, Dixon PM. Use of scintigraphy for diagnosis of equine paranasal sinus disorders. *Vet Surg* (2006) 35:94–101. doi:10.1111/j.1532-950X.2005.00118.x
6. Townsend NB, Hawkes CS, Rex R, Boden LA, Barakzai SZ. Investigation of the sensitivity and specificity of radiological signs for the diagnosis of periapical infection of equine cheek teeth. *Equine Vet J* (2011) 43:170–8. doi:10.1111/j.2042-3306.2010.00148.x
7. Isgren CM, Townsend NB. The use of radiography for diagnosis of apical infection of equine cheek teeth. *Equine Vet Edu* (2015) 28:448–54. doi:10.1111/eve.12385
8. Du Toit N. Does radiography help or hinder in apical infection? *Equine Vet Edu* (2016) 28:470–1. doi:10.1111/eve.12339
9. Liuti T, Smith S, Dixon PM. Radiographic, computed tomographic, gross pathological and histological findings with suspected apical infection in 32 equine maxillary cheek teeth (2012-2015). *Equine Vet J* (2017) 50(1):41–7. doi:10.111/evj.12729
10. Gerlach K, Ludewig E, Brehm W, Gerhards H, Delling U. Magnetic resonance imaging of pulp in normal and diseased equine cheek teeth. *Vet Radiol Ultrasound* (2013) 54:48–53. doi:10.1111/j.1740-8261.2012.01971.x
11. Henninger W, Frame M, Willmann M, Simhofer H, Malleczek D, Kneissl S, et al. CT features of alveolitis and sinusitis in horses. *Vet Radiol Ultrasound* (2003) 44:269–76. doi:10.1111/j.1740-8261.2003.tb00454.x
12. Solano M, Brawer RS. CT of the equine head: technical considerations, anatomical guide, and skeletal disease. *Clin Tech Equine Prac* (2004) 3:374–88. doi:10.1053/j.ctep.2005.02.016
13. Veraa S, Voorhout G, Klein WR. Computed tomography of the upper cheek-teeth in horses with infundibular changes and apical infection. *Equine Vet J* (2009) 41:872–6. doi:10.2746/042516409X452143
14. Buhler M, Furst A, Lewis FI, Kummer M, Ohlerth S. Computed tomographic features of apical infection of equine maxillary cheek teeth: a retrospective study of 49 horses. *Equine Vet J* (2014) 46:468–73. doi:10.1111/evj.12174
15. Windley Z, Weller R, Tremaine WH, Perkins JD. Two-dimensional and three-dimensional computer tomographic anatomy of the enamel, infundibulae and pulp of 126 equine cheek-teeth. Part 1: findings in teeth without macroscopic occlusal or computer tomographic lesions. *Equine Vet J* (2009) 41:433–40. doi:10.2746/042516409X390214
16. Windley Z, Weller R, Tremaine WH, Perkins JD. Two-dimensional and three-dimensional computer tomographic anatomy of the enamel, infundibulae and pulp of 126 equine cheek-teeth. Part 2: findings in teeth with macroscopic occlusal or computer tomographic lesions. *Equine Vet J* (2009) 41:441–7. doi:10.2746/042516409X391033
17. Liuti T, Reardon R, Smith S, Dixon PM. An anatomical study of the dorsal and ventral nasal conchal bullae in normal horses: computed tomographic anatomical and morphometric findings. *Equine Vet J* (2016) 48:749–55. doi:10.1111/evj.12516
18. Nanci A. *Bone in Ten Cate's Oral Histology*. 7th ed. Nanci A, editor. St. Louis, MO: Mosby Elsevier (2008). p. 108–40.
19. Nair PNR. Pathogenesis of apical periodontitis and the causes of endodontic failures. *Crit Rev Oral Biol Med* (2004) 15(6):348–81. doi:10.1177/154411130401500604
20. Casey MB, Person GR, Perkins JD, Tremaine WH. Gross, computed tomographic and histological findings in mandibular cheek teeth extracted from horses with clinical signs of pulpitis due to apical infection. *Equine Vet J* (2015) 47:557–67. doi:10.1111/evj.12315
21. Dacre I, Kempson S, Dixon PM. Pathological studies of cheek teeth apical infection in the horse: 5. Aetiopathological findings in 57 apically infected maxillary cheek teeth and histological and ultrastructural findings. *Vet J* (2008) 3:352–63. doi:10.1016/j.tvjl.2008.09.024
22. Lundstörm TS, Dahlen GG, Wattle OS. Caries in the infundibulum of the second upper premolar tooth in the horse. *Acta Vet Scand* (2007) 49:10. doi:10.1186/1751-0147-49-10
23. Dixon PM, Savill D, Horbyl A, Reardon RJ, Liuti T. Critical evaluation of ex vivo restoration of carious equine maxillary cheek teeth infundibulae following high-pressure gas and micro-particle abrasion. *Vet J* (2014) 3:368–74. doi:10.1016/j.tvjl.2014.04.004
24. Suske A, Poschke A, Muller P, Wober S, Staszyk C. Infundibula of equine maxillary cheek teeth: part 2: morphological variations and pathological changes. *Vet J* (2016) 209:66–73. doi:10.1016/j.tvjl.2015.11.023
25. Dacre I, Kempson S, Dixon PM. Equine Idiopathic cheek teeth fracture. Part 1: pathological studies on 35 fractured cheek teeth. *Equine Vet J* (2007) 4:310–8. doi:10.2746/042516407X182721
26. Dixon PM, Barakzai SZ, Collins NM. Equine Idiopathic cheek teeth fracture. Part 3: a hospital-based survey of 68 referred horses (1995-2005). *Equine Vet J* (2007) 4:327–32. doi:10.2746/042516407X182983
27. Schwarz T, Owen MR, Long S, Sullivan M. Vacuum disk and facet phenomenon in a dog with cauda equine syndrome. *J Am Vet Med Assoc* (2000) 6:862–4. doi:10.2460/javma.2000.217.862
28. Fitzgibbon CM, Du Toit N, Dixon PM. Anatomical studies of maxillary cheek teeth infundibula in clinically normal horses. *Equine Vet J* (2010) 1:37–43. doi:10.2746/042516409X474761
29. Dixon PM, Easley J, Ekmann A. Supernumerary teeth in the horse. *Clin Tech Equ Prac* (2005) 2:155–61. doi:10.1053/j.ctep.2005.04.007

Conflict of Interest Statement: The authors declare that the research was conducted in the absence of any commercial or financial relationship that could be constructed as a potential conflict of interest.

6.2 Conclusion

Buhler et al (2014) detected sclerosis of the alveolar bone in apically infected cheek teeth with the use of CT. In the current study, CT detected sclerosis mainly on the abaxial aspect of the periapical alveolar bone, while bone resorption and lysis were found on the axial aspect of the alveolar bone. Histology primarily showed lytic changes within the alveolar bone, characterised by disruption, loss and disorganization of the normal bony trabecular pattern. These were accompanied by increased numbers of osteoclasts compared to normal alveolar bone, indicative of resorption. This bone resorption was associated with thickening of the periodontal ligament, which contained an increased amount of mature collagen.

Radiographically, alveolar bone sclerosis has been described as a feature of dental apical infection (Townsend et al 2011) and in this study periapical alveolar sclerosis was radiographically detected in 8/28 apically infected cases.

CT imaging changes highly indicative of apical infection were identified in 96.4% of pathologically confirmed, apically infected cheek teeth, compared to only 50% of cheek teeth that were assessed radiographically. Alveolar bone changes were histologically present in all 21 examined alveoli while all 16 alveoli with marked alveolar bone changes had detectable alveolar bone changes on CT. This study confirms the superior accuracy of CT compared with radiography in detecting equine cheek teeth apical infection and showed excellent correlation between both dental and alveolar CT imaging and pathological findings. This also appears to be the first study to histologically examine the alveolar bone of apically infected teeth; in particular using histology to confirm axial lysis and remodelling that contributes to

the enlarged periodontal space detected around affected teeth.

The authors compared the head size used in this study with head sizes of known Thoroughbred horses in order to assess for major difference between the two populations. Unfortunately, the text noted the use of a paired t test in this comparison, but in reality a t-test was used ie two independent groups were compared.

CHAPTER 7: Summary and Conclusions

The literature on equine sinonasal and dental disease is extensive with many clinical publications on these often chronic, clinically significant disorders (McGorum et al 1992, Tremaine and Dixon 2001 a,b, Dixon and Dacre 2005, Dacre et al 2008 c,d, O'Leary and Dixon 2011, Dixon et al a,b 2012).

For many years, radiography has been the imaging modality of choice for evaluating dental structures and sinonasal compartments of horses with suspected maxillary cheek teeth apical infections. However, due to the numerous superimposed, often complex anatomical structures, conventional radiography has been shown to have poor sensitivity (50-69%) in detecting cheek teeth apical infections (Gibbs 1974, Gibbs and Lane 1987, Lane et al 1987), while digital radiography has been somewhat better with a sensitivity of 76-80% (Townsend et al 2011). Scintigraphy has 56% sensitivity in detecting apical infection and 79% sensitivity for dental related sinusitis (Weller et al 2001, Barakzai et al 2006).

The last decade has seen an increasing use of advanced imaging modalities, such as CT and to a lesser extent MRI, in anatomical studies and clinically in the diagnosis and treatment of equine sinonasal and dental disorders. Most of the relatively limited literature assessing CT imaging of equine sinonasal disorders has been based on studies performed on cadaver skulls or on horses examined under general anaesthesia.

In the first part of this study, emphasis was given to the use of CT for the evaluation of sinonasal structures and maxillary cheek teeth in normal horses of different age groups. Morphological assessments, including linear and volumetric measurements

of the sinonasal region and maxillary cheek teeth, were performed to increase our anatomical knowledge of these structures, with the aim of improving our diagnostic capabilities, surgical treatments and, ultimately, the prognosis for such disorders.

Sixty normal equine cadaver heads were selected and divided into three age groups. Each head was subjected to radiography and CT imaging, then, using a band saw, sectioned transversely into 5-6 slices and evaluated for anatomical abnormalities.

Multiple morphological measurements were performed and linear and volumetric measurements and shapes of the dorsal and ventral nasal conchal bullae in horses of different ages were assessed. This study found new important information regarding the dimensions and positions of the dorsal and ventral conchal bullae; information, which will improve treatment of disorders of this poorly, defined anatomical area (Dixon et al 2015).

CT images were also used to evaluate several poorly or undescribed sinonasal anatomical features including the position of the cheek teeth in relation to the various sinus compartments; age-related rostral drift of the maxillary cheek teeth; volume of the sinus compartments; position of the infraorbital canal in relation to the alveoli; and age-related changes in the length of the reserve dental crown.

The results showed that the Triadan 09 alveolus is located in the CMS in 2/15 (13%) of the youngest group horses and that the Triadan 10 alveolus is fully positioned in the RMS in 53% of all cases (32/60 heads), in contrast to expectations, since the literature indicates that the Triadan 09 lies fully within the RMS and that the Triadan 10 lies fully within the CMS. Some of this variation is likely due to the site and degree of caudo-medial obliquity of the maxillary septum.

Therefore, the assessment of the intra-sinus position of each tooth has to be assessed over the full width of each alveolus.

In all horses older than two years of age there was complete separation of the infraorbital canal (IOC) from the apices of all the maxillary cheek teeth, despite root elongation with cementum following eruption (Sisson and Grossman 1953, Dixon et al 2011). This finding indicates the risk of infraorbital nerve damage during dental surgery (particularly of the RMS) in horses less than 2 years old.

This study is the first to objectively describe and quantify the dental drift of equine cheek teeth. In particular, the caudal aspect of the maxillary Triadan 11 undergoes a dramatic change in position as the more horizontal aspect of this curved tooth erupts, thus shortening the tooth, and as the teeth simultaneously drift rostrally in the maxillary sinuses.

The maxillary cheek teeth drifted rostrally more than 25mm between the youngest and older groups, yet the most problematic cheek teeth diastemata are circa 2mm wide occlusally..This study highlights that absence of normal dental drift is involved in the aetiology of this disease which affects 50% of UK horses(Walker et al 2012). Further studies on larger numbers of horses of known ages and breeds, including of caudal drift would clarify this area further and might help in our understanding of the pathogenesis of equine cheek teeth diastemata, including the spontaneous resolution sometimes observed.

Equine dental reserve crown length decreases with age due to occlusal wear, but this prolonged eruption has not been well quantified to date in the literature. In this study,

the reserve crown length decreased from a mean of 4.7 cm (adjusted length 19.7% of head height) of all 12 teeth in the youngest (aged <6y.o.) horses to a mean of 2.9 cm (adjusted length 10.5%) in the oldest group (aged >15y.o.), with the 06s and 09s having the shortest reserve crowns.

The volumes of the equine sinus compartments, which has only been recorded in

Warmblood horses using a different technique (Brinkschulte et al 2013) to the current technique, were assessed to help evaluate differences in size between age groups and to better define the size of the different sinuses in Thoroughbred-sized horses for treatment planning. As expected, no significant differences were found between left and right individual sinus compartment volumes. However significant age-related increases in sinus compartment volumes were observed for the DCS, VCS, CMS, RMS and SP, with most changes attributable to dental eruption and increasing head size. No age-related volume differences were found for the small ES and large FS. The volume of the ES and FS sinus compartments are unaffected by dental eruption, but growth in head size would influence the dimensions of all sinus compartments.

Some novel information of equine skull shape was obtained by use of Procrustes analysis in horses of different ages. This study showed the feasibility of using this technique on readily obtainable equine head CTs. This study showed differences in landmark variability between young and old horses, in particular highlighting the importance of allometry (growth of different areas at different rates) between the different age groups. Future geometric morphometric studies could investigate changes in equine skulls of known age, breed and gender and relate these to their

genotype in order to characterize breed-related disorders affecting teeth and sinonasal compartments. For example, miniature horses are predisposed to dental overcrowding due to their small skull and large teeth conformation, predisposing them to severe dental and sino-nasal problems.

As noted above, cheek teeth diastemata, the most common, painful equine dental disease affecting 50% of UK horses (Walker et al 2012), is believed to be due to an imbalance between jaw size, cheek tooth size and orientation and dental drift. Examination of this disorder using geometric morphometric analysis could help, to better define the morphological characteristics of this disease.

In the second part of the study, 32 maxillary cheek teeth diagnosed to have apical infection were extracted from horses presented to our hospital with nasal discharge and facial swelling. All affected horses underwent clinical examination, radiography, standing CT followed by oral extraction of diseased teeth under sedation. Each tooth was grossly evaluated, imaged by CT at thinner slices, sectioned and then histologically examined. The pre-extraction radiographic and CT imaging findings were compared to the gross and histological findings of the extracted teeth to evaluate the sensitivity of CT in detecting apical infection in maxillary cheek teeth. Results of this study found a 97% sensitivity of CT in detecting maxillary cheek teeth apical infection, in comparison to 53 % sensitivity by radiography, indicating that CT is an accurate tool for identifying diseased teeth and improving treatment planning and prognosis.

The gross and histological examinations of the apically infected cheek teeth performed in conjunction with Dr Smith have added considerably to the body of

knowledge on this poorly studied area, in particular showing that all pulp horns are not affected with apical infections and that most infections are chronic low-grade infections rather than the commonly described apical abscessation.

In the third part of the study, 30 teeth and their alveoli were extracted from equine cadaver heads and, similar to above, radiographic, CT and gross examinations of the equine heads were performed. On the basis of these findings, 30 abnormal teeth were extracted and examined grossly and histologically and a comparison made between radiographic and CT imaging findings, and gross and histological findings. Twenty-one of these 30 extracted teeth had some alveolar bone attached, allowing comparison of imaging and pathological alveolar bone findings, and helping to validate further the accuracy of imaging in detecting diseased teeth and abnormal alveolar bone

CT imaging changes highly indicative of apical infection were identified in 96.4% of pathologically confirmed, apically infected cheek teeth, compared to only 50% that were assessed radiographically.

This study also showed that alveolar bone sclerosis was detected by CT mainly in the abaxial aspect of the periapical alveolar bone, while bone resorption and lysis were detected mainly in the axial aspect of the alveolar bone. Histologically, disruption and disorganization of the normal trabecular pattern of the alveolar bone and its replacement with collagen was detected, explaining the widened periodontal space around infected teeth that is a commonly imaged.

This ex vivo study, similar to the previous in vivo study, confirms the superior accuracy of CT compared with radiography in detecting equine cheek tooth apical

infection and shows excellent correlation between both dental and alveolar CT imaging and pathological findings and added further information on the pathological changes in apical infection, uniquely on the alveolar bone changes also.

Conclusion

This study has provided a detailed descriptive morphological evaluation of the normal equine paranasal sinuses, nasal conchal bullae and maxillary cheek teeth, including linear and volumetric quantification. It is anticipated that this new information will improve the diagnoses, surgical treatments, and ultimately the prognosis, of horses affected with sinonasal and cheek teeth disorders, especially those affected by dental sinusitis.

This study is the first to objectively assess the accuracy of radiographic and CT imaging in the detection of apical infection and alveolar bone changes in dental sinusitis, with CT shown to be 97% sensitive in diagnosing maxillary cheek teeth apical infection.

The use of standing equine head CT imaging has been a great advance in equine clinical practice, since it reduces the costs and risks of general anesthesia, allowing this modality to be more widely used. CT imaging allows visualization of abnormalities not identified on clinical examination, endoscopy or radiography, thus improving diagnosis and treatment of such cases. The findings of this study will hopefully enhance its value and diagnostic reputation even further.

Bibliography

Arencibia A, Vázquez J.M, Jaber R, Gil F, Ramiírez J.A, Rivero M, González N. and Wisner E.R. (2000). Magnetic resonance Imaging and cross sectional anatomy of the normal equine sinuses and nasal passages. Veterinary Radiology & Ultrasound, 41; 313–319

Barakzai S, Dixon P.M. (2003). A study of open-mouthed oblique radiographic projections for evaluating lesion of the erupted (clinical) crown. Equine Veterinary Education, 15; 143-148

Barakzai S, Tremaine W.H, Dixon P.M. (2006). Use of Scintigraphy for the Diagnosis of Equine Paranasal Sinus Disorders. Veterinary Surgery, 35; 94–101

Bignon O, Baylac M, Vigne J.D, Eisenmann V (2005). Geometric morphometric and the population diversity of Late Glacial horses in Wester Europe (Equus caballus arcelini): phylogeographic and anthropological implication. Journal of Archeological Science 32; 375-391

Bookstein (1987). Describing a craniofacial anomaly: finite elements and the biometrics of landmark locations. American Journal of Physical Anthropology, 74; 495-509

Bookstein F.L (1984). A statistical method for biological shape comparisons. Journal of Theoretical Biology 107; 475-520

Bookstein F.L (1986). Size and shape spaces for landmark data in two dimensions. Statistical Science 1; 181-222

Bookstein F.L (1991). Introduction; In Morphometric tools for landmark data. Geometry and Biology. Cambridge University Press;1- 4

Brinkschulte M, Bienert -Zeit A, Lüpke M, Hellige M, Ohnesorge B, Staszyk C. (2014). The sinonasal communication in the horse: examinations using computerized three-dimensional reformatted renderings of computed-tomography datasets. BMC Veterinary Research, 10:72

Brinkschulte M, Bienert-Zeit A, Lupke M, Hellige M, Staszyk C, Ohnesorge B. (2013). Using semi-automated segmetantion of computed tomography dataset for three-dimensional visualization and volume measurments of equine paranasal sinuses. Veterinary Radiology & Ultrasound, 54; 582-590

Buhler M, Furst A, Lewis F.I, Kummer M, Ohlerth S. (2014). Computed tomographic features of apical infection of equine maxillary cheek teeth; a retrospective study of 49 horses. Equine Veterinary Journal, 46; 468-473

Carter R.A, Raymond J.G, Burton Staniar W, Cubitt T.A, Harris P.A (2009). Apparent adiposity assessed by standardised scoring system and morphometric measurements in horses and ponies. Veterinary Journal 179; 204-210

Cavalleri J.M, Metzger J, Hellige M, Lampe V, Stuckenschneider K, Tipold A, Beineke A, Becker K, Disti O, Feige K (2013). Morphometric magnetic resonance imaging and genetic testing in cerebellar abiotrophy in Arabian horses. BMC Veterinary Research 23; 105

Cervantesa I, Baumung R, Molina A, Druml T, Gutierrez J.P, Solkner J, Valera M (2009). Size and shape analysis of morphofunctional traits in the Spanish arab horse. Livestock Science 125; 43-49

Dacre I.T, Kempson S, Dixon P.M. (2008 a). Pathological studies of cheek teeth apical infections in the horse: 1. Normal endodontic anatomy and dentinal structure of equine cheek teeth. The Veterinary Journal, 178; 311-320

Dacre I.T, Shaw D.J, Dixon P.M. (2008 b). Pathological studies of cheek teeth apical infections in the horse: 3. Quantitative measurements of dentine in apically infected cheek teeth. The Veterinary Journal, 178; 333–340

Dacre I.T, Kempson S, Dixon P.M. (2008 c). Pathological studies of cheek teeth apical infections in the horse: 4. Aetiopathological findings in 41 apically infected mandibular cheek teeth. The Veterinary Journal, 178; 341-351

Dacre I.T, Kempson S, Dixon P.M. (2008 d). Pathological studies of cheek teeth apical infections in the horse: 5. Aetiopathological findings in 57 apically infected maxillary cheek teeth and histological and ultrastructural findings. The Veterinary Journal, 178; 352–363

Dane M.T, Bell C, Carmalt J.L. (2010). A description of the relationship between the nasomaxillary aperture and the paranasal sinus system of horses. The Veterinary Journal, 186; 216-220

De Bowes, R.M. and Gaughan, E.M. (1998). Congenital dental disease of horses. Veterinary Clinic North America Equine Practice 14; 273-289.

Dixon P.M, Dacre I.T. (2005). A review of equine dental disorders. The Veterinary Journal, 169; 165–187

Dixon P.M, Parkin T.D, Collins N, Hawkes C, Townsend N, Tremaine W.H, Fisher G, Ealey R. and Barakzai S.Z. (2012 a). Equine paranasal sinus disease - a long-term study of 200 cases (1997–2009): Ancillary diagnostic findings and involvement of the various sinus compartments. Equine Veterinary Journal, 44; 267-71

Dixon P.M, Ceen, S, Barnett T, O'Leary J.M, Parkin T.D, Barakzai S. (2014). A long-term study on the clinical effects of mechanical widening of cheek teeth diastemata for treatment of periodontitis in 202 horses (2008–2011). Equine Veterinary Journal, 46; 76-80

Dixon P.M, Parkin T.D, Collins N, Hawkes C, Townsend N, Tremaine W.H, Fisher G, Ealey R. and Barakzai S.Z. (2012 b). Equine paranasal sinus disease: A long-term study of 200 cases (1997–2009): Treatments and long-term results of treatments. Equine Veterinary Journal, 44; 272-6

Dixon P.M. and Head K. W. (1999). Equine Nasal and Paranasal Sinus Tumours: Part 2: A Contribution of 28 Case Reports. The Veterinary Journal, 157; 279–294

Dixon P.M, Froydenlund T, Liuti T, Kane-Smith J, Horbal A, Reardon R.J. (2015). Empyema of the nasal conchal bulla as a cause of chronic unilateral nasal discharge in the horse: 10 cases (2013-2014). Equine Veterinary Journal, 47; 445–9

Dixon P.M, Hawkes C, Townsend N. Complications of equine oral surgery (2008). Veterinary Clinical North America Equine Practice; 24; 499–514

Dixon, P.M, Du Toit, N. and Dacre, I.T. (2011). Equine dental pathology. In: Equine Dentistry, 3rd edn., Eds: J. Easley, P. Dixon and J. Schumacher, Elsevier, Saunders, Edinburgh. pp 129

Dixon P.M, Parkin T.D, Collins N, Hawkes C, Townsend N.B, Fisher G, Ealey R, Barakzai S.Z (2011). Historical and clinical features of 200 cases of equine sinus disease. Veterinary Record, 169; 439.

Drake A.B, Klingenberg C.P, (2008). The pace of morphological change: historical transformation of skull shape in St.Bernard dogs. Proceeding of the Royal Society 275: 71-76

Drake A.B, Coquerelle M, Kosintsev P.A, Bachura O.P, Sablin M,Gusev A.V, Fleming L.S, Losey R.J (2017). Three-dimensional geometric morphometric analysis of fossil canid mandibles and skulls. Scientific reports 7 DOI:10.1038/s41598-017-10232-1

Dyce K.M, Sack O.W, Wensing C.J.G. (2010). The head and ventral neck of the horse In: Textbook of veterinary anatomy. 4th edn. Edinburgh: Elsevier, Saunders: 479–509

Easley J, Dixon P.M, Reardon R.J.M. (2016). Orthodontic correction of overjet/overbite (‘parrot mouth’) in 73 foals (1999-2013). Equine Veterinary Journal 48; 565-572

Gibbs C, Lane J.G (1987). Radiographic examination of the facial, nasal, and paranasal sinus region of the horse: II. Radiological findings. Equine Veterinary Journal, 19; 474-482

Gibbs C. (1974). The Equine Skull: its radiological investigation" Veterinary Radiology & Ultrasound, 15; 70-78

Glat PM, Freund RM, Spencer JA, Levine J, Noz M, Bookstein FL, McCarthy JG, Cutting CB (1996). A classification of plagiocephaly utilizing a three-dimensional computer analysis of cranial base landmarks. Annals of Plastic Surgery 36; 469-74

Greet T.R. (1981). Nasal aspergillosis in three horses. Veterinary Record, 109; 487-489

Good P (2000). Permutation tests: a practical guide to resempling methods for testing hypothesis 2nd edn Springer New York; 1-12 Journal of Human Evolution 46; 679-97

Hawkes C. S, Easley J., Barakzai S. Z. And Dixon P. M. (2008). Treatment of oromaxillary fistulae in nine standing horses (2002–2006). Equine Veterinary Journal, 40; 546-551

Head K.W. and Dixon P.M. (1999). Equine Nasal and Paranasal Sinus Tumours. Part 1: Review of the Literature and Tumour Classification. The Veterinary Journal, 157; 261–278

Henninger W, Frame M, Willmann M, Simhofer H, Malleczek D, Kneissl S. and Mayrhofer E. (2003). CT features of alveolitis and sinusitis in horses. Veterinary Radiology & Ultrasound 44; 69–276

Huggons N, Bell R.J.W, Puchalski S.M. (2011). Radiography and computed tomography in the diagnosis of nonneoplastic equine mandibular disease. Veterinary Radiology & Ultrasound, 52; 53–60

Jones R.S. (2001). Comparative mortality in anaesthesia. British Journal Anaesthesia, 87; 813-5

Joyce J.R, Pierce K.R, Romane W.M, Baker J.M. (1971). Clinical study of nutritional secondary hyperparathyroidism in horses. Journal of American Veterinary Medicine Association 158; 2033-42

Klingenberg C.P (2011). MorphoJ: an integrated software package for geometric morphometrics. Molecular ecology Resources, 11; 353-357

Komosa M, Molinski K, Godynicki S (2006). The variability of cranial morphology in modern horses. Zoological Science 23; 289-98

Kopke, S., Angrisani, N. and Staszyk, C. (2012). The dental cavities of equine cheek teeth: three-dimensional reconstructions based on high resolution micro-computed tomography. BMC Veterinary Research, 8; 173.

Lane J.G, Gibbs C, Meynink S.E, Steele F.C. (1987). Radiographic examination of the facial, nasal, and paranasal sinus region of the horse: I. Indication and procedure in 235 cases. Equine Veterinary Journal, 19; 466-473

Lane J.G, Longstaffe J.A, Gibbs C. (1987). Equine paranasal sinus cyst: a report of 15 cases. Equine Veterinary Journal, 19; 537-544

Liuti T, Reardon R, Smith S, Dixon P.M (2016). An anatomical study of the dorsal and ventral nasal conchal bullae in normal horses: Computed Tomographic anatomical and morphometric findings. Equine Veterinary Journal 48; 749-755

Manso-Diaz G, Dyson SJ, Dennis R, Garcia-Lopez JM, Biggi M, Garcia-Real MI, San Roman F, Taeymans O. (2015). Magnetic resonance imaging characteristics of equine head disorders; 84 cases (2000-2013). Veterinary Radiology & Ultrasound, 56; 176-87

Mcgorum B, Dixon P.M, Lawson G.H.K. (1992). A review of ten cases of equine mycotic rhinitis. Equine Veterinary Education, 4(1); 8-12

Mitteroecker P, Guz P, Bernhard M, Schaefer K, Bookstein F.L (2004). Comparison of cranial ontogenic trajectories among great apes and humans. Journal of Human Evolution, 46; 679-97

Mitteroecker P, Gunz P (2009). Advances in Geometric Morphometrics. Evolutionary Biology 36: 235-247

Morrow K.L, Park RD, Spurgeon T.L, Stashak T.S, Arceneaux B. (2000). Computed Tomography imaging of the equine head. Veterinary Radiology & Ultrasound, 41; 491-497

Muylle, S, Simoens P, Lauwers H (1999). Age-relate morphometry of equine incisors. Zentralblatt Fur Veterinarmedizin. Reihe A 46; 633-43

O'Leary J.M, Dixon P.M. (2011). A review of equine paranasal sinusitis. Aetiopathogenesis, clinical signs and ancillary diagnostic technique. Equine Veterinary Education, 23; 148-159

Okumura M, Araujo A.G.M (2014). Long-term cultural stability in hunter–gatherers: a case study using traditional and geometric morphometric analysis of

lithic stemmed bifacial points from Southern Brazil. Journal of Archeological Science 45; 59-71

Pease A.P. (2007). The Equine Head, In: Textbook of Veterinary Diagnostic Radiology, Thrall fifth Edition, Elsevier,160-177

Perkins J.D, Windley Z, Dixon P.M, Smith M, Barakzai S.Z. (2009). Sinoscopic treatment of rostral maxillary and ventral conchal sinusitis in 60 horses. Veterinary Surgery, 38; 613-9

Probst A, Henninger W. and Willmann M. (2005). Communications of normal nasal and paranasal cavities in computed tomography of horses. Veterinary Radiology & Ultrasound, 46; 44–48

Polly P.D, Stayton C.T, Dumont E.R, Pierce S.E, Rayfield E.P, Angielczyk R &K (2016). Combining geometric morphometric and finite element analysis with evolutionary modeling: towards a synthesis. Journal of Vertebrate Paleontology 36: 4

Ramzan P.H (2009). Oral endoscopy as an aid to diagnosis of equine cheek tooth infections in the absence of gross oral pathological changes: 17 cases. Equine Veterinary Journal, 41; 101-6

Ramzan P.H, Dallas R.S, Palmer L (2011). Extraction of fractured cheek teeth under oral endoscopic guidance in standing horses. Veterinary Surgery, 40; 586-9

Ramzan P.H, Palmer L. (2010). Occlusal fissure of the equine cheek tooth: prevalence, location and association with disease in 91 horses referred for dental investigation. Equine Veterinary Journal, 42;124-128

Saunders J, Windley Z. (2011). Equine sinonasal and dental. In: Veterinary Computed Tomography, Tobias Schwarz and Jimmy Saunders, Ed Wiley-Brackwell 1st edition, 427-442

Seetah K, Cucchi T, Dobney K, Barker G, (2014). A geometric morphometric re-evaluation of the use of dental form to explore differences in horse (Equus caballus) population and its potential zooarchaeological application. Journal of Archaeological Science 41; 904-910

Shaw D.J, Dacre I.T, Dixon P.M. (2008). Pathological studies of cheek teeth apical infections in the horse: 2. Quantitative measurements in normal equine dentine. The Veterinary Journal, 178; 321–332

Simhofer H, Griss R, Zetner K.(2008). The use of oral endoscopy for detection of cheek teeth abnormalities in 300 horses. The Veterinary Journal, 178; 396–404

Sisson, S. Grossman, J.D. (1953) The Respiratory System, In: The anatomy of the domestic animals. Ed Sisson S and Grossman JD 4th edition, pp 517-546 W B Saunders Company Philadelphia

Smallwood J.E, Wood B.C, Taylor W.C and Tate L.P Jr. (2002). Anatomic reference for computed tomography of the head of the foal. Veterinary Radiology & Ultrasound, 43; 99–117

Solano M, Brawer R.S. (2004). CT of the Equine Head: Technical Considerations, Anatomical Guide, and Selected Diseases. Clinical Techniques in Equine Practice, 3; 374–88.

Suske A, Poschke A, Muller P, Wober S, Staszyk C. (2016b). Infundibula of equine maxillary check teeth. Part 2: Morphological variations and pathological changes. The Veterinary Journal, 209; 66-73

Suske A, Poschke A, Schrock P, Kirschner S, Brockmann M, Staszyk C. (2016a). Infundibula of equine maxillary check teeth. Part 1: development, blood supply and infundibular cementogenesis. The Veterinary Journal, 209; 57-65

Tatarniuk D.M, Bell C, Carmalt J.L. (2010). A description of the relationship between the nasomaxillary aperture and the paranasal sinus system of horses. The Veterinary Journal, 186; 216–220

Tessier C, Bruhschwein A, Lang J, Konar M, Wilke M, Brehm W, Kircher P. (2013). Magnetic Resonance Imaging features of sinonasal disorders in horses. Veterinary Radiology & Ultrasound, 54; 54-60

Townsend N. B., Hawkes C. S., Rex R., Boden L. A, Barakzai S. Z. (2011). Investigation of the sensitivity and specificity of radiological signs for diagnosis of periapical infection of equine cheek teeth" Equine Veterinary Journal, 43; 170-178

Tremaine W.H and Dixon P.M. (2001a). A long-term study of 277 cases of equine sinonasal disease. Part 1: Details of horses, historical, clinical and ancillary diagnostic findings. Equine Veterinary Journal, 33; 274-282

Tremaine W.H and Dixon P.M. (2001b). A long-term study of 277 cases of equine sinonasal disease. Part 2: Treatments and results of treatments. Equine Veterinary Journal, 33; 283-289

Tremaine W.H, Clarke C.J and Dixon P.M (1993). Histopathological findings in

equine sinonasal disorders. Equine Veterinary Journal, 31; 296-303

Tremaine W.H. Complications associated with dental and paranasal sinus surgery:

Published in IVIS with the permission of the AAEP, 2006.

Trotter G.W. (1993). Paranasal sinuses. In Veterinary Clinics of North America: Equine Practice 9 (1)

Tucker R, Windley Z, Abernethy A.D, Witte T.H, Fiske-Jackson A.R, Turner S, Smith L.J, Perkins J.D. (2015). Radiographic, computed tomographic and surgical anatomy of the equine sphenopalatine sinus in normal and diseased horses. Equine Veterinary Journal, 48; 578-584

Veitschegger K, Wilson L.A.B, Nussberger B, Camenisch G, Keller L.F, Wroe S, Sanchez-Villagra M.R (2018). Resurrecting Darwin's Niata- anatomical, biomechanical, genetic, and morphometric studies of morphological novelty in cattle. Scientific Reports 8: 9-129

Veraa S, Voohout G, Klein W.R. (2009). Computed Tomography of the upper cheek teeth in horses with infundibular changes and apical infection. Equine Veterinary Journal, 42; 872-876

Vidic B (1968). The variation in length of the pterygoid process as a function of the variations of the sphenoid angle. The anatomical record 160; 527-530

Zelditch M.L (2004). Introduction: In Geometric morphometric for Biologist, Elsevier Ltd, 1-8

Wagner A.E. (2008). Complication in equine anaesthesia. Veterinary Clinic North American Equine Practice, 24; 735-52

Walker H, Chinn E, Holmes S, Barwise-Munroe L, Robertson V, Mould R, Bradley S, Shaw D.J, and Dixon P.M.(2012). Study of the prevalence and some clinical characteristics of equine cheek teeth diastemata in 471 horses examined in a UK first opinion equine practice (2008–2009). Veterinary Record, 171, 44

Webster M, Sheet H.D (2010). A practical introduction to landmark-based geometric morphometrics. The paleontological Society Papers 16; 163-188

Weller R, Livesey L, Maierl J, Nuss J.K, Bowen I.M, Cauvin E.R, Weaver, M, Schumacher J, May S.A. (2001). Comparison of radiography and scintigraphy in the diagnosis of dental disorders in the horse. Equine Veterinary Journal 33; 49-58

Windley Z, Weller R., Tremaine W. H. and Perkins J.D. (2009a). Two- and three-dimensional computed tomographic anatomy of the enamel, infundibulae and pulp of 126 equine cheek teeth. Part 1: Findings in teeth without macroscopic occlusal or computed tomographic lesions. Equine Veterinary Journal, 41; 433-440

Windley Z, Weller R, Tremaine W. H. and Perkins J. D. (2009b). Two-and three-dimensional computed tomographic anatomy of the enamel, infundibulae and pulp of 126 equine cheek teeth. Part 2: Findings in teeth with macroscopic occlusal or computed tomographic lesions. Equine Veterinary Journal, 41; 441-447

Woodford N.S. and Lane J.G. (2006). Long-term retrospective study of 52 horses with sinonasal cyst. Equine Veterinary Journal, 38; 198-202

Wyn-Jones G. (1985). Interpreting radiographs 6: Radiology of the equine head (Part 2). Equine Veterinary Journal, 17; 417-2

APPENDIX

Chapter	<5	6-15	>16
2	15	21	24
3	13	21	26
4	15	21	24

The reason for having different group number is related to 2 different stages of data collection; during data collection for chapter 2, I decided to include two horses <5 years of age and removing 2 horses from the group >16, in order to keep the overall amount equal to 60 horses. The aim was to see if more variability was seen within the young group. Statistical analysis for each chapter was done based on the amount of horses for each category.